STUDIES ON QUENCH CHARACTERISTICS OF SUPERCONDUCTING MAGNETS OF SST-1

By

AASHOO N. SHARMA

Enrolment Number PHYS06201004002

Institute for Plasma Research, Gandhinagar, India

A thesis submitted to the

Board of Studies in Physical Sciences

In partial fulfilment of requirements

for the Degree of

DOCTOR OF PHILOSOPHY

of

HOMI BHABHA NATIONAL INSTITUTE

February 2015

HOMI BHABHA NATIONAL INSTITUTE

Recommendations of the Viva Voce Committee

As members of the Viva Voce Committee, we certify that we have read the dissertation prepared by Aashoo N. Sharma entitled "Studies on Quench Characteristics of Superconducting Magnets of SST-1" and recommend that it may be accepted as fulfilling the thesis requirement for the award of Degree of Doctor of Philosophy.

Chairman: Prof. Abhijit Sen Date: 07/09/2015

Guide / Convener: Dr. Subrata Pradhan Date: 07/09/2015

Technical Advisor: Dr Jean Luc Duchateau Date: 07/09/2015

Member: Dr. R. Srinivasan Date: 07/09/2015

Member: Dr. D. Raju Date: 07/09/2015

Member: Dr. S. V. Kulkarni Date: 07/09/2015

Final approval and acceptance of this thesis is contingent upon the candidate's submission of the final copies of the thesis to HBNI.

I hereby certify that I have read this thesis prepared under my direction and recommend that it may be accepted as fulfilling the thesis requirement.

Date: 07/09/2015

S Pradhan

Place: Gandhinagar Guide: Dr. Subrata Pradhan

STATEMENT BY AUTHOR

This dissertation has been submitted in partial fulfilment of requirements for an advanced degree at Homi Bhabha National Institute (HBNI) and is deposited in the Library to be made available to borrowers under rules of the HBNI. Brief quotations from this dissertation are allowable without special permission, provided that accurate acknowledgement of source is made. Requests for permission for extended quotation from or reproduction of this manuscript in whole or in part may be granted by the Competent Authority of HBNI when in his or her judgment the proposed use of the material is in the interests of scholarship. In all other instances, however, permission must be obtained from the author.

Ashu Sharma

Aashoo Sharma

DECLARATION

I, hereby declare that the investigation presented in the thesis has been carried out by me. The work is original and has not been submitted earlier as a whole or in part for a degree / diploma at this or any other Institution / University.

Aashoo Sharma

List of Publications arising from the thesis

Published in referred journals

1. Thermo-hydraulic and quench propagation characteristics of SST-1 TF coil, A.N. Sharma, S. Pradhan, J.L. Duchateau, Y. Khristi, U. Prasad, K. Doshi, Fusion Engineering and Design, Volume 89, Issue 2, February 2014, Pages 115–121

Accepted for publication in referred journals

1. Quench characterization and thermo-hydraulic analysis of SST-1 TF Magnet Busbar, A. N. Sharma, S. Pradhan, J. L. Duchateau, Y. Khristi, U. Prasad, K. Doshi, P. Varmora, V. L. Tanna, D. Patel, A. Panchal, in Fusion Engineering & Design, Vol. 90, January 2015, Pages 67–72
2. Cryogenic Acceptance Tests of SST-1 Superconducting Coils, A. N. Sharma, U. Prasad, K. Doshi, P. Varmora, Y. Khristi, D. Patel, A. Panchal, S. J. Jadeja, V. L. Tanna, Z. Khan, D. Sharma, S. Pradhan, in IEEE Trans of Applied Superconductivity Vol. 25, no.2, pp.1-7, April 2015
3. "Quench detection of SST-1 TF coils by helium flow and pressure measurement" A. N. Sharma, S. Pradhan, U. Prasad, P. Varmora, Y. Khristi, K. Doshi, D. Patel in Journal of fusion energy, April 2015, Vol. 34, Issue 2, pp 331-338

Other Publications (Research report in IPR):

1. IPR/RR-651/2014 "Thermo-hydraulic analysis of quenches with slow propagating speeds" A. N. Sharma, S. Pradhan, Y. Khristi, U. Prasad, K. Doshi, P. Varmora, V. L. Tanna, D. Patel, A. Panchal

Ashu Sharma

Aashoo Sharma

DEDICATED TO MY BIG FAMILY

AND SAIBABA

ACKNOWLEDGEMENT

I was always very excited to anticipate writing this section of the thesis, in which the author can write things not related to the subject and without following the so called guidelines of 'how to write a thesis'. I am finally happy to see this day.

I am thankful to my guide Dr. Subrata Pradhan for conceptualizing this work under IPR - CEA collaboration during 2006 to 2009. He played an instrumental role in registering me with HBNI for the Ph. D. programme and in coordination of all HBNI progress reviews. He ensured that I continued doing this work despite our heavy involvement in SST-1 refurbishment activities. Without his constant persuasion, this work would not have been possible.

Dr. Jean Luc Duchateau of CEA Cadarache played a crucial role in this wok as he introduced me to Gandalf code and quench thermo-hydraulics during my visit to CEA in 2006. He made me battle-ready for this work and gave many valuable inputs for writing this thesis.

I am also thankful to my doctoral committee Chairman Prof. Abhijit Sen, and committee members Dr. R. Srinivasan, Dr. D. Raju and Dr. S. V. Kulkarni for their valuable suggestions to improve the quality of this work.

Thank you Papaji (Prof. N. K. Sharma) and Mummiji (Mrs. Sudha Sharma) for your constant encouragement and regular reminders to finish this thesis at the earliest date possible. I dedicate this work to both of you and to my big extended family comprising Bade Bhaiyya (Mr. Kumar Gandharva), Dada (Mr. Utpal), Bhabhi (Mrs. Seema), Preeti, Indraneel, Meenakshi, Rahul, Priyanka, father and mother in laws (Mr. Dev Kumar and Mrs. Beena), niece Sanatkumar, Yaduraj, Mayank, Kartikeya, Aarav and Advait.

My never complaining and caring wife Preeti deserves special thanks. She carried out lot of my social and personal responsibilities while I was busy with this work. My sons, Yaduraj and Kartikeya, never knew that I was diverting time meant for them to this work, but I will now compensate for it.

My IPR colleagues Upendra, Dipak, Pankaj, Yohan, Dr. Vipul Tanna and Dr. Ziauddin Khan deserve a special mention for being available for various technical discussions in laboratory and non-technical ones at the famous “kaka’s chai ki tapree”. I am thankful to Patty Grosso for proofreading the thesis and giving her valuable grammatical suggestions.

“Above all, thank you BABA for your blessings, I can’t do anything without it”

CONTENTS

SYNOPSIS

Steady-state Superconducting Tokamak (SST-1) is a medium scale experimental device at the Institute for Plasma Research (Gandhinagar, India) employing superconducting Toroidal and Poloidal Field Magnets [2.1]. SST-1 has dual objectives of studying the physics of plasma processes in a tokamak under steady-state conditions, as well as to learn various technologies associated with the steady-state operation of the tokamak. The superconducting Toroidal Field (TF) and Poloidal Field (PF) magnet system in SST-1 uses multi-filamentary multiple stabilized NbTi/Cu based high current carrying, high field cable-in-conduit conductor (CICC) as the base conductor [2.2] [2.4].

Quench in a superconducting magnet is best described as a transition of a portion of its superconducting winding pack to normal conducting state. In case of quench in magnets like SST-1 TF coil, the joule heating in the quenched section of the magnet winding pack can lead to a very high rise in temperature as a result of the large transport current densities in the magnet and the low specific heat of material present inside the winding pack at low temperature [3.3]. Such uncontrolled rise in temperature can lead to permanent damage to the conductor and insulation inside the winding pack. A properly designed quench detection and protection system detects quench at an early stage of development and extracts the magnet energy into an external resistor known as dump resistor [3.4].

Voltage measurements are commonly used to detect the superconductor to normal transition and are the fastest method of detecting quench in superconducting magnets [4.6]. In tokamak magnets, such measurements are influenced by the inductive voltages arising from the current changes in the magnet itself and/or from current changes in other inductively coupled coils. Inductive voltage cancellation scheme is an important aspect of quench detection circuit design [4.1] [4.2]. Other important design parameters are the selection of threshold voltage and time taken to declare that the magnet has quenched, as well as to send a trigger to activate the quench protection system [4.3] [4.4]. Design of a fail-safe, state-of-the-art quench detection and protection system for SST-1 TF magnet system was one of the objectives of this thesis work. The quench detection and subsequent protection schemes are fully customized for SST-1 tokamak operational requirements [4.7], [4.9], [4.10].

Understanding the quench behaviour of CICCs is an extremely important issue for reliable superconducting magnet design and operation. The simulation of quench and its different aspects like quench initiation, quench propagation and quench protection threshold limits are crucial for magnet safety during operation. This is even more important for large magnets for fusion machines, due to the very high energy content in them [5.17]. While the analytical tools are handy for adiabatic estimations (worst case scenarios), numerical simulation becomes important for large magnets as adiabatic estimations lead to over-designed magnets and can be bulky and costly. These codes are additionally useful in analysing the reason of magnet quench [5.1]. This knowledge is often useful to make required modifications in the magnet system to avoid quench. Although commercial and non-commercial codes are available for quench simulation, as each CICC has its unique characteristics depending on the intended operational scenarios, suitable input data and subroutines are required to be made to accurately model individual CICCs [6.2]. Application of a commercial quench simulation code, Gandalf, towards study of quench behaviour of assembled SST-1 magnets was another motivation of this thesis work. Dedicated experiments have been carried out to determine the experimental friction factor of SST-1 CICC as a function of Reynolds number. The code was used to simulate TF coil quench observed in coil test campaigns [5.18]. This code was further extended to simulate quenches observed in TF busbar sections which were extremely slow-propagating in nature. The thermo-hydraulic analyses of TF magnet system busbar and some CICC design cases have also been studied [6.3].

Quenches can also be redundantly detected by monitoring non-electrical signals like mass flow rate and pressure. Any significant change in the steady-state operational values of these signals can indicate a fault condition, like quench, inside the magnet. These are inherently slow signals and are expected to give slow response to the quench process, but can be used as secondary quench detectors. This redundancy could be very useful in case of major malfunction or failure of primary quench detector [8.12]. This has been of interest to magnet designers for a very long time [8.9]. However, the experimental database and guidelines to design such a system was not available and have not been reported to our knowledge. Vast databases of behaviour of these signals during quenches observed in SST-1 coil test experiments have been analysed and subsequently a guideline for detecting quenches in SST-1 TF magnets with this method has been proposed [8.13]. A hardware design was also proposed for this quench detector as a part of this thesis work. In the following text, summary of main chapters have been outlined.

[1] Fusion and Superconductivity

Basic concepts of superconductivity and the role of superconducting magnets in fusion machines are discussed. Basic concepts of quench in superconducting magnets, quench detection in magnet and quench protection aspects are discussed in this section.

[2] SST-1 Tokamak

Steady State Superconducting Tokamak, SST-1, is a medium-size superconducting tokamak commissioned and under operation in India. SST-1 had been designed to address physics and technological issues relevant to steady-state operation of fusion machines. This section gives details of the SST-1 tokamak and its major subsystem like magnets, cryostat, vacuum system, cryogenics system, heating systems etc.

[3] Analytical study of SST-1 CICC

Adiabatic model of SST-1 CICC for estimation of the hotspot temperature (maximum temperature rise inside the winding pack following a quench) has been developed using analytical method. This model has been used for first order estimation of maximum temperature in CICC after quench initiation and current dumping and for designing of quench protection of SST-1 magnet system.

[4] Design of TF coil quench detection circuit

A fail-proof electronic circuit was developed for quench detection of SST-1 TF coil. Simple voltage difference scheme was adopted to cancel the inductive voltages. Other main features of this circuit are in-built redundancy in channels to avoid loss of data, galvanic isolation (3.5 kV), low-pass filter, precise adjustable voltage reference (± 20 ppm) and precise and adjustable time reference settings (± 1 ms). Apart from quench detection, it also transmits analog voltage across magnet sections to data acquisition system during the magnet operation.

[5] TF coil quench simulation

SST-1 Toroidal Field coils were individually tested cooled to 5 K with nominal currents in a dedicated campaign spanning from June 10, 2010 till January 24, 2011. The electromagnetic, thermal hydraulic and mechanical performances of each TF magnet have been qualified at its nominal operating conditions. Quench in TF coil #15 at 9000A during the coil test experiment was analysed to understand the thermal hydraulic and quench propagation characteristics of the SST-1 TF magnets. GANDALF, which is a one-dimensional finite elements code for simulation of the quench and stability of CICC based magnets, was used for quench simulation studies of TF coil #15. The code's input parameters, like CICC specifications and the operating conditions were generated from the details of SST-1 model coil test experiments. Gandalf subroutine for superconducting properties was modified to obtain the experimentally reported critical current density of 2853 A/mm^2 at 5 T, 4.2 K. A dedicated experiment was done to study the behaviour of SST-1 CICC friction factor under different mass flow rates and a suitable correlation for it was selected and implemented in the code. A simplified cryogenic plant model was implemented using the FLOWER subroutine of Gandalf. Quench propagation velocity and normal zone voltage development were simulated and compared with the experimental results. A predictive quench propagation analysis of sixteen assembled TF magnets system has also been done using the code.

[6] Quench characterization and thermo-hydraulic simulation of TF magnet busbar

Very low quench propagation speed was observed in superconducting busbar in single coil test experiments. Quench evolution in these sections was analysed and simulated using Gandalf code. A safe quench threshold voltage level has been recommended for SST-1 TF magnet busbar. Heat load acting on SST-1 TF magnet system busbar had been estimated. Using this estimation, appropriate mass flow rate has been proposed which would provide a safe operational temperature margin.

[7] CICC design study

In a CICC, `Copper to Superconductor ratio' is an important design parameter. Copper fraction is useful in the reduction of maximum hotspot temperature during quench and the amount of Superconductor gives higher temperature margin and stability against external disturbances. Total amount of copper and superconductor is also limited by the available space in the CICC. A parametric study has been done to see the effect of Copper to Superconductor ratio on the stability and quench protection of a selected representative CICC.

[8] Quench detection of TF coils by helium flow and pressure measurement

A flow measurement system has been developed for SST-1 magnet system using the in-house designed Venturi meters. This system has been successfully used for helium flow measurement during the TF coil test experiments and on the assembled TF magnet system of during engineering commissioning and plasma experiment phase of SST-1. A secondary quench detection system based on flow and pressure measurement has been conceptualized for SST-1 TF magnet system. The flow and pressure trends during quenches observed in single coil test experiments have been used to quantify the quench detection system logic. A schematic is also proposed for development of suitable hardware for this secondary quench detection system. It could act as a redundant quench detector in case of failure of primary detector.

[9] Summary

The work done under this thesis work is summarized in this chapter. Important findings, new developments and the future possible work are also described in this chapter.

List of figures

List of tables

1. Fusion and Superconductivity

"*The seas of this planet contain 100,000,000,000,000,000 tons of hydrogen and 20,000,000,000,000 tons of deuterium. Soon we will learn to use these simplest of all atoms to yield unlimited power.*" - Arthur C. Clark (c. 1960)

1.1 Controlled Nuclear Fusion: an exciting alternate source of energy

Oil, gas and coal are three major non-renewable global sources of energy for mankind. Due to increase in the world's energy consumption and limited amount of available reserves of these energy sources, there is major thrust worldwide to develop clean and sustainable sources of energy. Nuclear fusion is a promising candidate for such an energy source.

Nuclear fusion is a process in which two or more atoms fuse together to form a heavier atom accompanied by the release of energy. Fusion reaction of two isotopes of hydrogen, namely deuterium (*D*) and tritium (*T*) is shown here as an example. It produces 17.6 MeV of energy (14.1 MeV neutron + 3.5 MeV alpha particle)

$$D + T \rightarrow {}^{4}He + n \tag{1.1}$$

By gross estimation, a large power station generating 1500 megawatts of electricity would consume approximately 600 g of tritium and 400 g of deuterium each day. While deuterium is easily extractable from sea water, tritium breeding can be done from lithium, easily available in nature. So fusion is considered as a source of unlimited energy, if we can overcome the scientific and technological challenges of achieving fusion.

In the core of Sun, temperature is about 15,000,000 °C, so hydrogen atoms are in a constant state of agitation and collide at very great speeds. The natural electrostatic repulsion between the positive charges of their nuclei is overcome, and the atoms fuse producing helium. But without the benefit of gravitational forces at work in our Universe, achieving fusion on earth will be extremely difficult. The most favourable fusion reaction, as believed by fusion community is D-T fusion reaction discussed earlier, followed by D - D, D - ^{4}He reactions. Even for a significant rate of D-T fusion reaction, the temperature required to overcome the coulomb forces is 5 x 10^7 K. For other fusion reactions, even higher temperatures are required. The gas at such high temperature becomes a neutral mixture of positively charged ions and electrons and is called as Plasma, the so called fourth state of matter.

Due to very high temperatures, confinement of fusion plasma is very challenging. Plasma confinement and heating to thermonuclear temperatures in a Tokamak has been very successful so far, in demonstration of thermonuclear fusion. The concept of tokamak was invented by Russian physicists Igor Tamm and Andrei Sakharov in the 1950s. The Joint European Torus (JET) tokamak in Culham, U.K was the first tokamak in the world to demonstrate the thermonuclear fusion by producing 16 megawatts of fusion power. It has proved the technical feasibility of fusion using deuterium and tritium.

International Thermonuclear Experimental Reactor (ITER), the biggest experimental fusion reactor in the world based on the tokamak concept, is presently under construction [1.1]. It is located in the south of France and being made under the collaboration between seven partners China, the European Union, India, Japan, Korea, Russia and the United States. It is designed to produce 500 MW of power from an input of 50 MW. The technologies developed for ITER project will be useful for the development of a future demonstration nuclear fusion power plant DEMO [1.2].

Fusion research is actively pursued in India since late 1987. At present in India, there are three functional tokamaks, Aditya, SINP tokamak and SST-1. While Aditya and SINP tokamaks are pulsed machines with copper magnets (so-called first generation machine), SST-1 (Steady-state Superconducting Tokamak -1) is an advanced device designed to study long steady-state plasma operations, which is an essential aspect of fusion plasma. More details about SST-1 are given in chapter 2. As mentioned earlier, India is an active partner in the International Thermonuclear Experimental Reactor (ITER) project. The scientific and technological know-how and the trained manpower generated from all these projects will be useful to develop nuclear fusion power plants in India.

1.2 Basic concepts of Tokamak

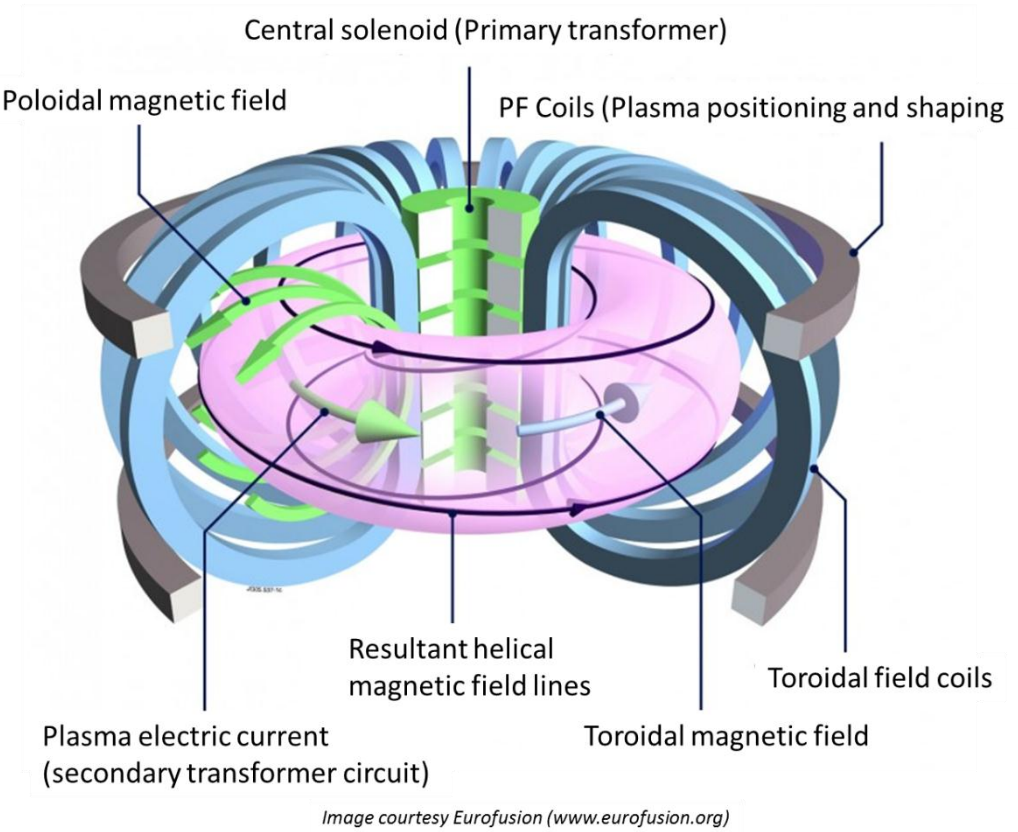

Figure 1.1: Magnetic confinement of plasma in tokamak

Plasma is a macroscopically neutral mixture of positively charged ions and electrons. For thermonuclear fusion to occur, it is to be heated to very high temperatures of millions of degrees. At such high temperatures, it is impossible to confine plasma in a physical enclosure, as it will erode the enclosure material. This will damage the enclosure and will cool down the plasma temperature. In a tokamak, closed magnetic field lines are used to confine plasma. When charged particles are moving along the magnetic field they spiral around the magnetic field lines due to Lorentz force. This prevents their collision from the enclosure and allows usage of different heating mechanism to heat plasma to required temperature [1.3].

The main tokamak components of tokamak are shown in figure 1.1 and its various functions are as follows:

Vacuum vessel: The plasma is contained in a toroidal chamber called vacuum vessel (VV) (not shown in figure 1.1). The vacuum is maintained inside VV by external pumps. Several openings are available on VV for installation of plasma heating systems and for different diagnostics to measure various plasma parameters.

TF and PF coil system: Toroidal field (TF) coils generate the field along the toroidal direction. The combination of toroidal field and the field from plasma current produces helical field lines. Plasma particles gyrate along these closed field lines. Poloidal field (PF) coils generate magnetic field for plasma position control and shaping.

Central Solenoid (TR): Plasma current is induced by a transformer, with the central solenoid coil acting as the primary winding and the plasma as the secondary winding. The heating provided by the plasma current (known as ohmic heating) is to be supplemented with other heating methods like radio frequency heating and neutral beam heating to achieve the temperatures required to make fusion occur.

1.3 Necessity of superconducting magnets

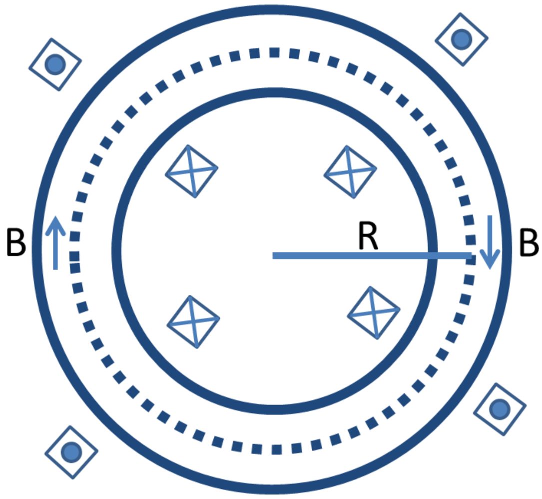

Figure 1.2: Toroidal magnetic in tokamak

The value of toroidal magnetic field at the major radius R (centre of plasma volume), as shown in figure 1.2, plays a crucial role in increasing efficiency of fusion reactions, power output and reducing the size of machine (and hence the cost) [1.4]. The highest possible toroidal magnetic field value at the centre of plasma volume is the desire of tokamak designers.

It was realized very long ago that superconducting magnets are essential for obtaining practical electrical power from magnetically confined fusion [1.5]. Advantages of using superconducting magnets to produce the required magnetic field can be easily understood by taking the example of ITER Magnet system.

The electrical power requirement estimated for ITER magnets with a copper conductor is about 2.2 GW as compared to the 20 MW required for the cryogenic refrigeration with the present configuration with superconducting magnets [1.6]. The input power required for TF magnet system alone is much higher than the 500 MW power planned to be generated in ITER.

Additionally copper-based machine are essentially pulsed machines, due to magnet heating and the nature of electrical high power sources, generally used to charge such huge resistive magnets. Contrary to this, fusion reactors must operate in steady-state mode to generate and supply energy to electrical grids. Due to these reasons, all the present major tokamaks like SST-1, KSTAR, EAST and Tore Supra, as well as the future planned ones like JT60-SA and ITER make use of superconducting magnets.

1.4 Superconductivity

Superconductivity: In 1911, Dutch physicist Heike Kammerlingh Onnes discovered that when mercury is cooled below 4.19 K, its resistivity suddenly drops to an unmeasurably low value (~ 10^{-25} Ω.m). This behaviour was also found in other metals like lead and tin. This new state was called as 'Superconducting' and the material showing this behaviour as 'Superconductor'. The temperature at which this transition from normal to superconducting state occurs is called as critical temperature 'T_c'.

In 1934, Meissner and Ochsenfeld discovered that type I superconductors show perfect diamagnetic behaviour, which is absence of magnetic induction within the bulk of superconductor under B_{c1}. The screening super-currents flowing in a thin layer of samples prevents the external magnetic field from entering the bulk by producing the cancelling magnetic field. Above B_{c1}, the magnetic field enters the bulk and superconducting state is destroyed. This field is called as critical magnetic field. Another important characteristic of superconductors which interests the magnet designer is its current carrying capability. The maximum possible current density within a superconducting material without destroying its superconductivity is known as critical current density 'J_c'.

For every superconductor, there exists a critical surface bounded by these three parameters, as shown in figure 1.3. Superconducting state prevails everywhere below this surface and normal resistivity state everywhere outside it.

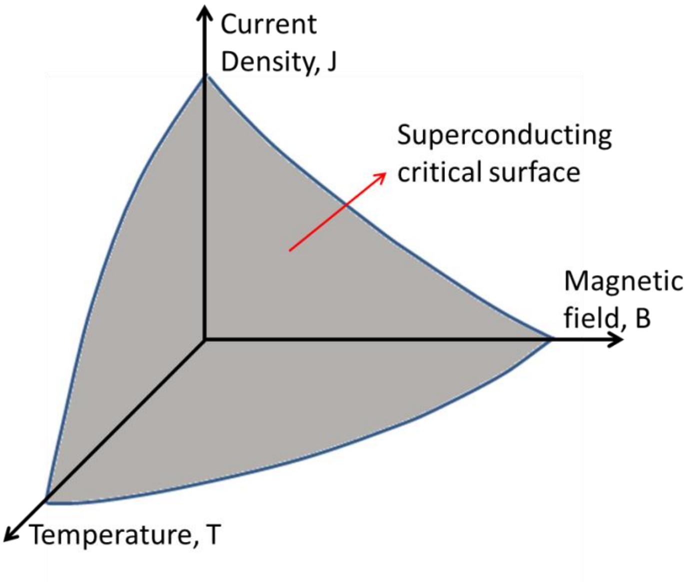

Figure 1.3: Critical surface of superconductor

1.5 Fusion Magnet relevant superconductors

The magnet-grade superconductor is required to have high current-carrying capability with a high critical field. The material should also be readily available commercially and its critical temperature should also be lower than readily available cryogens like liquid helium, liquid hydrogen and liquid nitrogen.

Type I superconducting materials such as pure mercury, lead, tin have very low critical field of about 0.1 T. These pure metals are not suitable for magnet applications. Type II superconductors like NbTi, Nb3Sn, Nb3Al, Nb3Ge, MgB2, BSCCO, and YBCO can be used for high magnetic field applications. Unlike type I, type II are characterised by complete magnetic flux expulsion up to lower critical field Bc1 and incomplete magnetic flux expulsion up to a higher critical field Bc2 as shown in figure 1.4, where M is the intensity of magnetization and B is the applied magnetic field. In type II conductors, superconductivity is lost only when the applied magnetic field is higher than Bc2.

Magnetic field penetrates type II conductors in the form of vortices. Each vortex carries a magnetic flux equal to superconducting magnetic flux quantum Φ_0

$$\emptyset_0 = \frac{h}{2e} \approx 2.07 \times 10^{-15} \quad (Wb) \qquad (1.2)$$

Where 'h' is Planck constant 6.6262 x 10^{-34} J-s and e is the charge of electron 1.60219 x 10^{-19} C. When these vortices move in the bulk of superconductor under the combined influence of external current and magnetic field, an electrical field is generated leading to losses. Metallurgists have perfected pinning of these vortices by flux pinning, in which these vortices interact with increased crystal lattice defects within the material and are unable to move. This enables achievement of very high critical current density for some type II superconductors.

NbTi and Nb3Sn are two dominant commercial magnet grade superconductors for fabrication of high field fusion magnets. NbTi can be typically manufactured by cold drawing and one or more precipitation heat treatments. It can be used only for field applications below 10 T. Nb3Sn is an intermetallic compound produced mainly by bronze process and internal tin process [1.7]. Multifilamentary composites of Nb3Sn are suitable to produce magnets with field strength above 10 T and up to 21 T. These two superconductors are also widely used in other high field applications like magnetic resonance imaging, nuclear magnetic resonance and accelerator magnets. There are few other superconducting materials like Nb3Al which could challenge Nb3Sn because of better mechanical properties but are not commercially developed. There is another category of superconductor known as high temperature superconductor like MgB2 (Tc ~ 39 K), YBCO (Tc ~ 90 K) BSSCO (Tc ~ 110 K). These materials also exhibit excellent properties for making fusion magnets but the fact that they are ceramics makes their development costly and it is difficult to use them in large size fusion magnets. But these materials are very useful for making current leads for fusion magnets and help in important cryogenic savings during operation of the magnets.

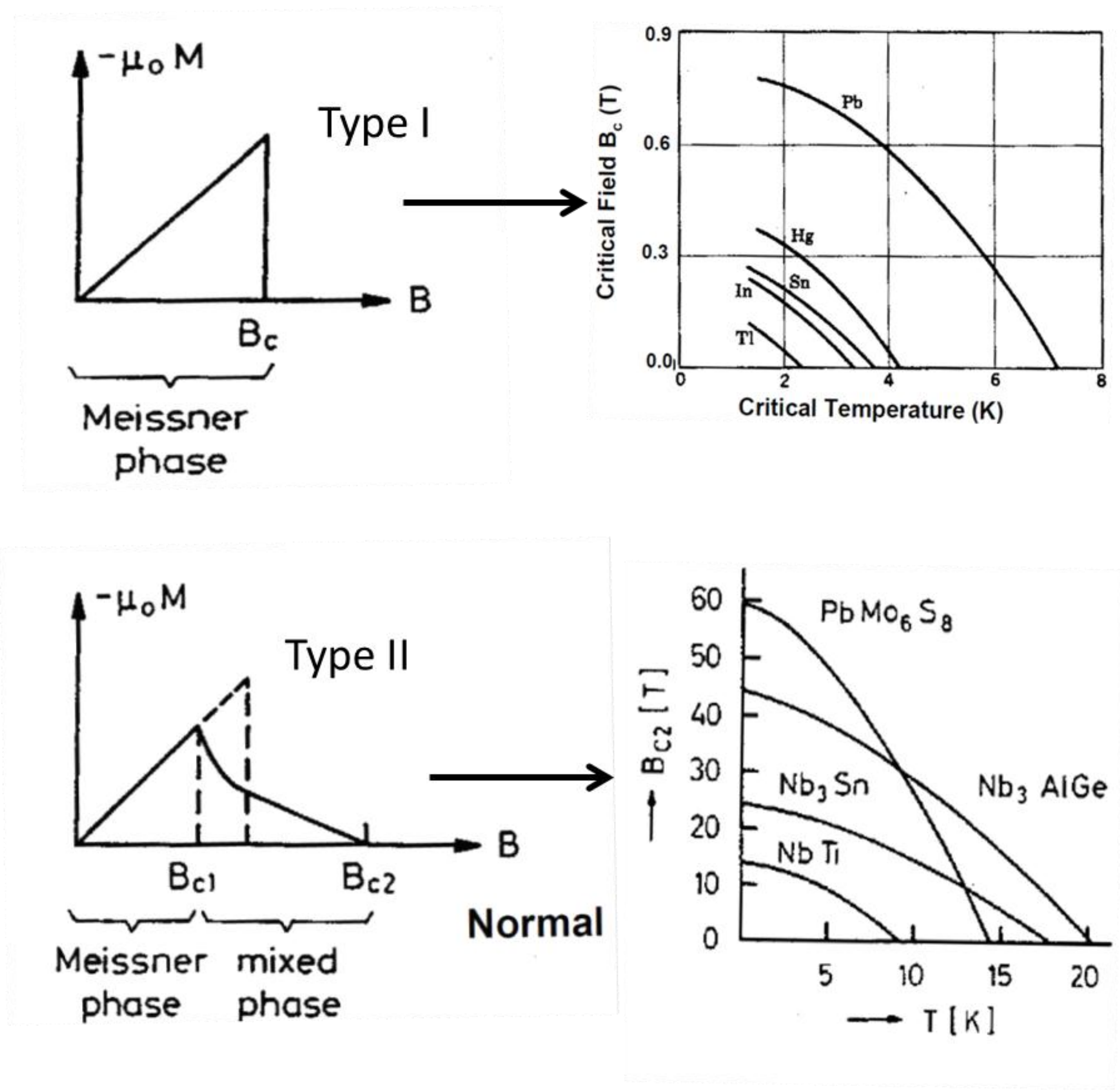

Figure 1.4: Type I and Type II superconductors

1.6 Technological challenges in fabrication and operation of superconducting magnets

The basic function of the superconducting magnets in a tokamak is to generate the required magnetic field, with required spatial and temporal variation. Tokamak being a complex electro-magnetic, thermo-mechanical environment, design and operation of its magnet system is a challenging task. Some of these aspects are discussed here

Design of cable: Choice of superconductor material, choice of percentage of cable constituents like superconductor, stabilizer and coolant, conductor jacket material and section estimation are some of the driving factors for suitable cable design for fusion magnets.

Coil design: Shape of coil, choice of electrical insulation, coil casing material and section estimation to bear the electromagnetic and thermal loads during coil operation, ease of fabrication and shape optimization to accommodate several other components of tokamak are some of the driving factors for suitable coil design for fusion magnets.

Operational reliability: Magnet must be designed to remain superconducting under the expected normal operational scenarios of the tokamak. In an off-normal event, if the magnet looses superconductivity (Quench), a suitable protection system must be designed and implemented to ensure the safety of the magnet and the machine.

Study of quench behaviour of SST-1 TF magnet system and design of quench detection and protection system is the main subject of this thesis work.

2. SST-1: India's first superconducting tokamak

Steady-state Superconducting Tokamak, SST-1, is a medium size steady-state device designed to the study of very long pulse (1000 s), elongated single null and, double null divertor plasmas in hydrogen [2.1]. SST-1 had been designed to address physics and technological issues relevant to steady-state operation of fusion machines. Some of the key physics issues that will be addressed in SST-1 machine are energy, impurity and particle confinement studies in long pulse discharges, controlled removal of heat and particles from the divertor region, maintenance of good confinement and stability, control of resistive wall modes in the advanced high beta regimes. Technologically, SST-1 aims at operating the superconducting magnet system (SCMS) comprised of TF coils in steady-state operation, PF coils operation with fast current ramp-up and down for plasma shaping, establishing feedback mechanisms to stabilize highly elongated and triangular plasmas, sustaining currents of about 330 kA by auxiliary heating and active steady-state heat removal at first wall with heat flux of the order of 1 MW / m^2. This chapter gives details of this machine.

2.1 Steady-state Superconducting Tokamak SST-1

SST-1 has a major radius of 1.1 m, a minor radius of 0.2 m, a toroidal field of 3.0 T at the plasma centre and plasma current up to 220 kA. Plasmas with elongation in the range of 1.7-1.9, triangularity in the range of 0.4-0.7 with plasma reduced internal inductance in the range of 0.75-1.4 and poloidal beta in the range 0.01-0.85 have been envisaged for this machine. Auxiliary current drive is based on a Lower Hybrid Current Drive, Ion Cyclotron Resonance Heating, Electron Cyclotron Resonance Heating and Neutral Beam Injection. A cut section

3D view, 2D cross-sectional view of SST-1 tokamak, along with the major machine parameters are shown in figure 2.1. Major systems of SST-1 tokamak are described in following sections.

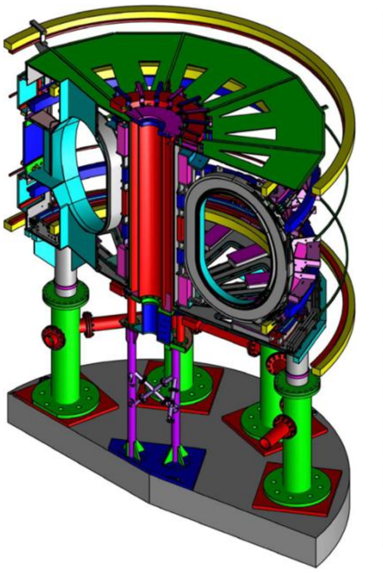

MACHINE PARAMETERS	
MAJOR RADIUS	1.1 m
MINOR RADIUS	0.2 m
ELONGATION	1.7 - 2
TRIANGULARITY	0.4 - 0.7
TOROIDAL FIELD	3 T
PLASMA CURRENT	220 kA
ASPECT RATIO	5.2
SAFETY FACTOR	3
AVERAGE DENSITY	1 x 10^{13} cm^{-3}
AVERAGE TEMP.	1.5 keV
PLASMA SPECIES	HYDROGEN
PULSE LENGTH	1000 s
CONFIGURATION	Single and Double Null
HEATING & CURRENT DRIVE	
LOWER HYBRID	1.0 MW
NEUTRAL BEAM	0.8 MW
ICRH	1.0 MW
FUELLING	Gas Puffing

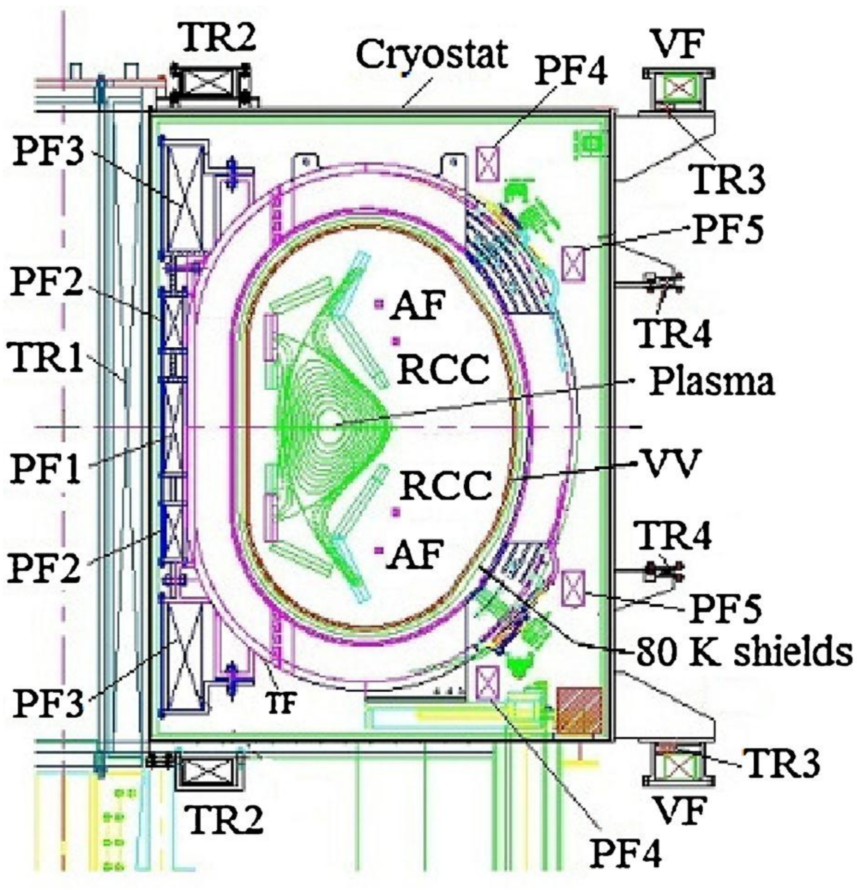

Figure 2.1: SST-1 3D and 2D cross-section and major parameters

2.1.1 *Magnet system*

The magnet system of SST-1 comprises superconducting and resistive magnets. All TF magnets and nine PF magnets are superconducting [2.2]. All other magnets are water cooled copper conductor-based.

TF Magnet system

The TF magnet system consists of 16 superconducting, modified `D' shaped coils arranged symmetrically around the major axis and spaced 22.5 degrees apart. The TF system is designed to produce 3.0 T magnetic flux density at plasma axis with ripple < 2% within the plasma volume. The base conductor for these magnets is an NbTi based CICC [2.3].

The TF coil casings are wedge shaped at the inner legs and form a cylindrical vault structure when all the 16 coils are assembled together. The outer vault is formed by connecting inter coil structures between the TF coils. These vaults resist all the in-plane and out of plane forces expected on the TF magnet system during SST-1 operation.

Poloidal Field Magnets System

The SST-1 PF magnet system has nine superconducting coils (PF1-5) and two resistive coils PF6 [2.4]. These coils allow for a variety of plasma equilibria with wide range of elongation and triangularity. Feasibility of limiter operation during plasma current ramp-up, double and single null operation at plasma current of 220 kA, double null operation at plasma current of 330 kA and various start-up scenario were the design drivers for PF system. A free boundary, axi-symmetric, ideal MHD equilibrium model-based code was used for the locating and the sizing of the PF system. The SC PF magnets are wound from the same CICC as that was used for TF magnets and have a maximum nominal operational current rating of 10 kA. All superconducting PF coils are supported on the TF casings. PF6 coils to be used for radial position control, in addition to equilibrium and shaping, are located inside the vacuum vessel.

Central solenoid:

The central solenoid system is composed of a main transformer (TR1) and three pairs of compensating coils (TR2, TF3 and TR4). This magnet system is used for plasma start-up and initial current ramp-up. These coils are made from oxygen free high conductivity (OFHC) copper conductor with a central channel for cooling with water. It has a stored magnetic flux of 1.4 Wb. It is designed to produce circular plasma with 100 kA current for duration of one second.

Other coils:

In addition to above mentioned coils, a pair of copper conductor based vertical field coils will keep the plasma in equilibrium during the initial phase. In addition, there is a pair of active feedback coils placed inside the vacuum vessel to provide feedback for plasma position control.

2.1.2 Cryogenic System

A helium refrigerator/liquefier (HRL) with @1 kW capacity (400 W refrigeration and 200 l/h liquefaction) at 4.5 K has been designed, procured, installed and commissioned to meet the operational requirement of the SCMS [2.5, 2.6]. SCMS will be cooled with 4.5 K at 0.4 MPa supercritical helium (SHe). The current leads will be cooled with liquid helium at 4.2 K, 0.12 MPa.

The main components of the HRL are the compressors with oil removal system, an on-line purifier, a cold box, a main control dewar (MCD) and the warm gas management system. There are 3 numbers of compressors, each with a flow rate of 70 g/s with 1.4 MPa outlet pressure. Three medium pressure 1.4 MPa storage tanks made of carbon steel & painted inside with anti-rust epoxy, each with 68 m^3 inner volume, are used as buffer tanks during the operation of HRL. One stainless steel storage tank is exclusively used to store the helium gas coming from the magnet quench. Two storage tanks, at 15 MPa, each of 25 m^3 inner volume are used for the inventory of the helium gas. These tanks are also used to store helium gas coming from various applications using the recovery system comprising of a recovery compressor of capacity 100 Nm^3/h and two gas bags each of 40 m^3 capacity.

The HRL has 7 heat exchangers and three turbines, where, first two turbines are connected in series. A cold circulator (CC) capable of providing 300 g/s flow rate at 0.4 MPa has been placed on the downstream of the third turbine. Further downstream of the CC, the Integrated flow distribution and control (IFDC) system is used to distribute the required flow to the SCMS.

The MCD of 2500 l capacity is also used to house the heat exchanger, which absorbs the transient heat load arising from the SCMS, during PF ramp up-down as well as plasma discharge. The HRL has different operating modes like controlled cool down & warm up of the SCMS, maintaining SCMS at 4.5K during tokamak operation, safe handling of the SCMS quench, higher SHe flow rate at higher pressure drop in the SCMS, absorption of high transient heat loads of the SCMS, compressor power saving for lower cooling requirements in standby mode, and operation without liquid nitrogen.

A liquid nitrogen (LN_2) management system has been designed, fabricated, installed and commissioned to take care of the LN_2 requirement. The system consists of 3 LN_2 storage tanks with 300 m long super-insulated vacuum transfer lines, followed by a phase separator before LN_2 is distributed to sub-systems. All the cryogenic systems have been automated with a Supervisory Control and Data Acquisition system on Programmable Logic Controller. A P&ID diagram of SCMS cooling system is shown in figure 2.2.

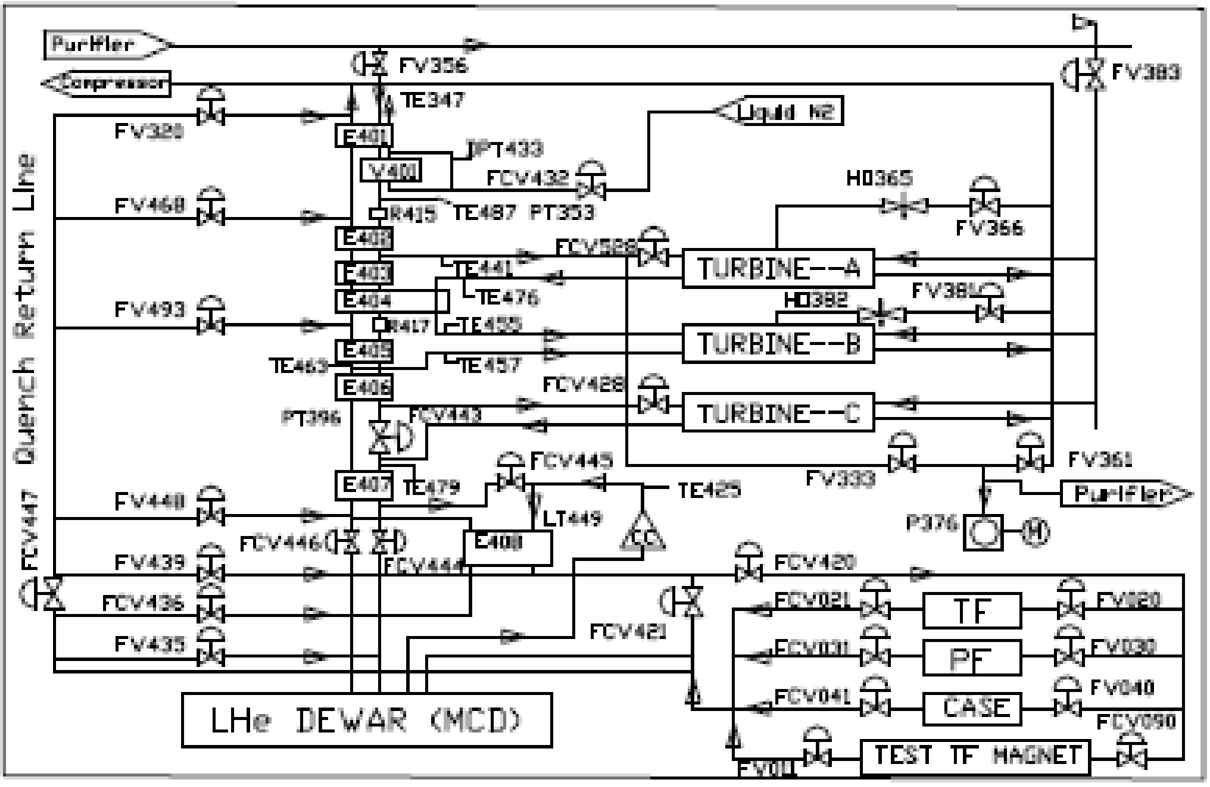

Figure 2.2: SST-1 SCMS cooling scheme

2.1.3 Vacuum Vessel, Cryostat and Pumping System

The vacuum vessel is ultra-high vacuum, fully welded SS304L chamber made from sixteen modules, each module consisting of a vessel sector, an interconnecting ring and three ports [2.7]. The ring sector sits in the bore of TF coil, while the vessel sector with ports is located between two TF coils. It has a height of 1.62 m, the mid-plane width of 1.07 m, a total volume of 16 m^3 and a surface area of 75 m^2.

The cryostat, is a high vacuum chamber, encloses the vacuum vessel and the SC magnets. It is a sixteen-sided polygon chamber made of SS304L with a volume of 35 m^3 and surface area of 59 m^2. The base pressure inside the cryostat will be maintained at less than $1x10^{-5}$ torr to minimize residual gas conduction losses on the SCMS. LN2 panels are placed between all surfaces having temperature higher than 85 K and surfaces at 4.5 K to reduce the radiation loads on SC magnets and cold mass support system. The total surface area of these panels is 126 m^2. These are single-sided embossed bubble panels. The cooling method is based on the latent heat of vaporization. During normal operations 10,000 l/s pumping speed is required to achieve base pressure of less than $1\text{x}10^{-8}$ torr in the vacuum vessel. Two turbo-molecular (TM) pumps, each of 5000 l/s speed, would be used for this purpose. Two closed cycle cryo pumps will be used during wall conditioning of vacuum vessel. The main gas load from vacuum vessel is during steady-state plasma operation. Sixteen numbers of TM pumps, each with a pumping speed of 5000 l/s at 10^{-3} torr for hydrogen, are to be connected to sixteen pumping lines on the vacuum vessel. The net speed of each pumping line is estimated to be 3900 l/s. The net pumping speed provided for cryostat using two TM pumps is 10000 l/s. Vacuum vessel and cryostat will be pumped down from atmospheric pressure to 10^{-3} torr using two separate root pumps of 2000 m^3/hr capacity. A vacuum vessel sector along with different attached components is shown in figure 2.3.

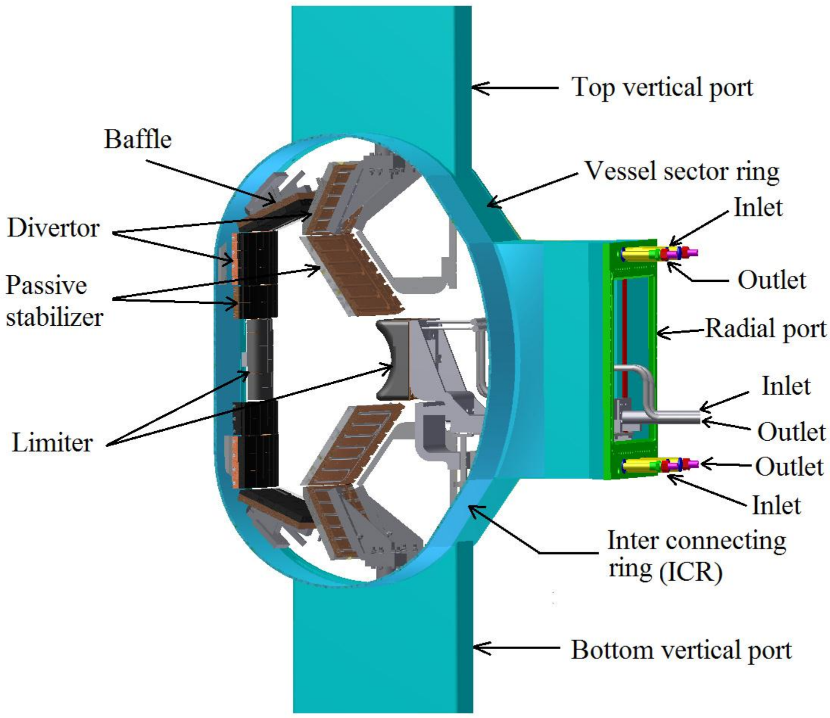

Figure 2.3: SST-1 Vacuum vessel sector

2.1.4 Plasma Facing Components (PFC)

The PFC of SST-1 comprise of divertor & baffles, poloidal limiters and passive stabilizers [2.8]. The normal incident peak heat flux on inboard and outboard strike point is 1.6 MW/m^2 and 5.6 MW/m^2 respectively. The poloidal inclination of the outboard divertor plates is adjusted so as to have the average heat flux at the strike point to be less than the allowed limit of 0.6 MW/m^2. The target points of inboard as well as outboard divertor plates have been chosen at a distance as large as practicable from the null point. A baffle has been incorporated in the design so as to form a closed divertor configuration that helps in increasing the neutral pressure in the divertor region. A pair of poloidal limiters is provided to assist plasma breakdown, current ramp-up and current ramp-down and for the protection of RF antennae and other in-vessel components during normal operation and during VDEs and disruptions. The outboard limiters are made movable to protect RF antennae. On the inboard side, a safety limiter is placed 30 mm away from the separatrix. Passive stabilizers comprised of conducting structures surrounding the plasma are provided to reduce the growth rate of the vertical instability. The stabilizers are located close to the plasma to have greater mutual coupling with it when the plasma moves from its equilibrium position. The top and the bottom stabilizers are connected in saddle configuration with a current bridge at the location of this break. The passive stabilizers are designed to handle heat fluxes of 0.25 MW/m^2. Isostatically pressed fine-grain graphite is chosen as the base line armour material for PFC of SST-1 tokamak. The PFCs are actively cooled so as to keep the temperature of the plasma facing surfaces less than 1000 °C. The PFCs are also designed for baking up to 350 °C.

2.1.5 High Power Radio Frequency Systems

SST-1 has three different high-power radio frequency systems to additionally heat and non-inductively drive plasma current to sustain the plasma in steady-state for a 1000 s duration [2.9].

Electron Cyclotron Resonance Heating system is based on a 200 kW, continuous-wave gyrotron at 82.6 GHz. Beam launching systems have been designed, fabricated and tested for microwave compatibility for radial and top launch. The system would be used for initial breakdown and heating of the plasma. Localized current drive would also form a part of experimentation.

Lower hybrid current drive system is being prepared at 3.7 GHz. The system is based on two 500 kW, continuous wave Klystrons with four outputs. Power at these arms is further divided successively to sixty four channels which then finally deliver the power to a grill type window positioned at the equatorial plane on a radial port at the low field side of SST-1.

Ion Cyclotron Resonance Frequency system would operate in a range between 22 to 91 MHz to accommodate various heating schemes at 1.5 T and at 3.0 T operation of SST-1. The same system would also be used for initial breakdown and wall conditioning experiments. Fast wave current drive in the centre of the plasma is also planned at a later stage. A multi-stage 1.5 MW continuous wave radio frequency system is being built to meet these goals. All the system components require active cooling.

2.1.6 Auxiliary Heating System: Neutral beam injection (NBI)

The power required in NBI in the low and high-density phases for SST-1 machine is 0.5 and 1.7 MW, respectively. This requirement will be fulfilled by tangential injection of the beam, corresponding to maximum absorption at 0.98 m radius of tangency in the plasma. Hydrogen or Deuterium beam will be used at 30 - 80 keV. The injection is expected to raise the ion temperature to ~ 1 keV, contribute to a fuelling of ~ 4 torr l/s, impart a toroidal momentum of ~ 100 km/s, and drive a current of ~ 40 kA at the core of the plasma. The power will be delivered from a single beam line and the dynamic range of voltage will be accommodated in a single source.

2.1.7 Diagnostics for SST-1 Tokamak

Various diagnostics will be used in SST – 1 to measure parameters like plasma current, position, shape, density, electron and ion temperatures in the core, edge and divertor regions, impurity concentrations, radiated power and surface temperatures of various PFCs and limiters. Other diagnostics include FIR interferometer, Thomson scattering, ECE, charge exchange, thermography, soft and hard x-ray monitoring, visible and VUV spectroscopy.

2.1.8 SST-1 CONTROL AND DATA ACQUISITION SYSTEM

All the essential subsystems of SST-1 will be monitored through a central machine control. Various subsystems of SST-1 operate in heterogonous platforms such as VME, PXI, and SCADA etc. This diversity issue was addressed with a GPS-based time synchronization system in a master slave configuration, as shown in figure 2.4. The reference time for all synchronous and asynchronous events for the plasma shots are being derived from a precision crystal oven oscillator. A terabyte-level data storage system has also been implemented for data handling and manipulation purposes. An electronic log book system has been introduced aimed at logging all the experiments and campaigns also.

SST-1 Data Acquisition (DAQ) System is focused at establishing the communication interfaces between the front end signal conditioning and electronics, data acquisition and controls for automated information exchanges during the SST-1 operation under the overall

Central Control. A dedicated Network Attached Data Storage Server has been implemented to store the diagnostics data for post-shot analyses.

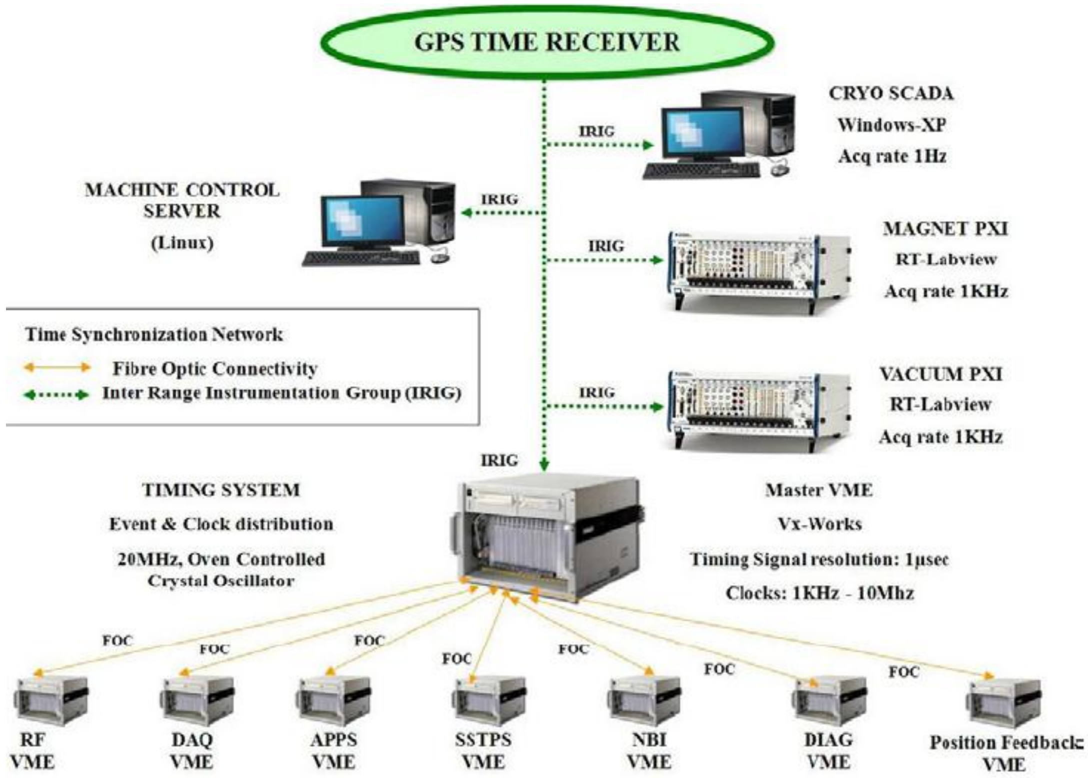

Figure 2.4: SST-1 control system architecture

2.2 Present status of SST-1

Steady-state Superconducting Tokamak (SST-1) has been commissioned after the successful experimental and engineering validations of its critical sub-systems. During the 'engineering validation phase' of SST-1, the cryostat was demonstrated to be leak tight to superconducting magnets system operations in all operational scenarios, the 80 K thermal shield was demonstrated to be uniformly cooled without regions of 'thermal runaway and hotspots', the superconducting Toroidal Field magnets were demonstrated to be cooled to their nominal operational conditions and charged up to 1.5 T of field at the major radius. A successful plasma breakdown in SST-1 assisted with electron cyclotron pre-ionization in second harmonic mode was obtained in June 2013, thus marking the 'First Plasma' in SST-1.

Subsequent to the first plasma, successful repeatable plasma start-ups with E ~ 0.4 V/m, plasma currents in excess of 70 kA for 400 ms assisted with ECH pre-ionization at a field of 1.5 T have been so far achieved. Lengthening the plasma pulse duration with LHCD, confinement and transport in SST-1 plasmas and MHD activities typical to large aspect ratio SST-1 discharges are presently being investigated in SST-1. In parallel, SST-1 has uniquely demonstrated reliable cryo-stable high field operation of TF magnets in two-phase cooling mode, operation of vapour-cooled current leads with cold gas instead of liquid helium and DC joint resistances below 1 nΩ in superconducting magnet winding packs. SST-1 is also continually getting upgraded with First Wall integration, superconducting central solenoid installation, over loaded MgB2-brass based current leads etc. being scheduled by first half of 2015 [2.10].

3. Analytical study of quench protection of SST-1 TF magnets

Quench in a Superconducting magnet is transition of a section of its winding from superconducting state to normal conducting state. In fusion magnets, due to the large current densities and low specific heat of material at low temperature, joule heating in the quench section can lead to very high temperature rise and damage to the conductor and insulation. So generally for such large magnet systems protection, as soon as quench is detected in a magnet, its current is reduced to zero with a suitable dump time constant by introduction of external dump resistor in series with the coil. Selection of this dump time constant (dump resistor) is a fine balance of allowable temperature rise at the location of quench initiation, and the terminal voltage development due to this dump resistor. It is possible to make a conservative calculation by assuming complete adiabatic boundary conditions. These simple formulae are useful in the design of magnet protection system as it allows easy and quick estimates of these parameters and are fairly accurate. In this chapter, basic concepts of quench, related properties of superconductors, the basics of quench protection and the estimations for SST-1 TF quench protection are discussed.

3.1 SST-1 TF coil CICC

SST-1 TF coils are made using NbTi-based CICC with copper as stabilizer material [2.3]. CICC cross section and some important features are shown in figure 3.1. It has 135 NbTi/Cu strands of 0.86 mm diameter cabled in 4 cabling stages of 3 x 3 x 3 x 5 as shown in figure 3.1. Twist pitch for each stage is 40 mm, 75 mm, 130 mm and 290 mm respectively. Twist directions, in all stages, are anti-clockwise (Z) and the twist pitches may vary within ±10% of the specified nominal values. Each strand has about 1224 ± 30 hexagonal NbTi filaments embedded in copper stabilizer with copper to superconductor ratio of > 4.9:1. The last stage bundled cable was wrapped with 25 micron SS 304 foil with 50% overlap. The conduit material is SS304L and is 1.5 mm thick. It also acts as a load-bearing structure inside the winding pack where the operating stresses may be as high as 300 MPa at cryogenic temperature. The cable outer cross section is 14.8 x 14.8 mm^2. The void fraction in the cable space, for supercritical helium flow is 40 ± 2%. The cable nominal operating current is 10 kA at 4.5 K and 5 T. The critical current is 36 kA at 4.2 K, 5 T. The measured critical current density of strands is 2853 A/mm^2 at 5 T [3.1].

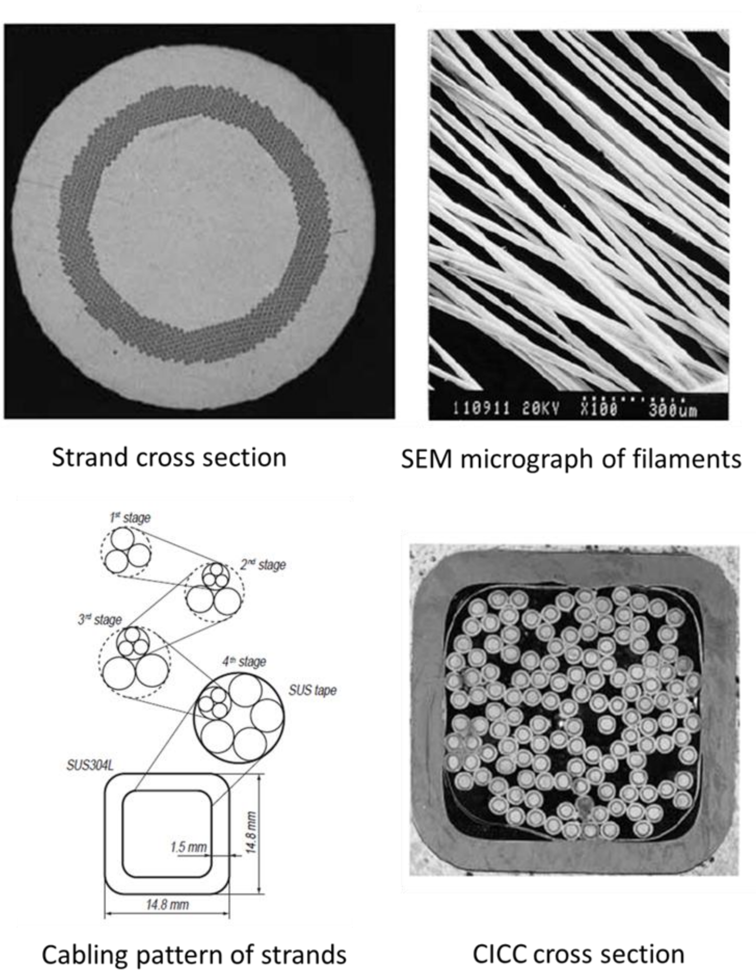

Figure 3.1: Constituents of SST-1 CICC

3.2 Basic concepts of quench

As discussed earlier, superconducting state of material is characterized by the critical surface in *B-J-T* space bounded by material specific B_c, J_c and T_c. If during operation of superconducting magnet any of these limits are violated, transition from superconducting state to normal state occurs. This transition is called as quench.

Quench in a composite conductor like that of SST-1 superconducting strands having a stabilizer matrix of high-purity low-resistance copper around the superconductor has different characteristics as compared to the superconducting strands without the stabilizer matrix. This difference mainly comes from the sharing of current between superconductor and the stabilizer matrix when the strand temperature is above the so-called current sharing temperature T_{cs} and less than its critical temperature T_c. Above T_c the current in the superconductor section is almost zero and the entire current flows through the stabilizer matrix due to its very low resistance as compared to resistance of superconductor above T_c. For a superconducting material a limit in current density can be defined which is J_{noncu} which is a function of the operating magnetic field B_{op} and temperature T_{op}. This limit is defined when an electric field of 10 μV/m is measured across the conductor. The current-sharing temperature T_{cs} is defined as:

$$J_{noncu}(B_{op}, T_{cs}) = \frac{I}{S_{noncu}} \qquad (3.1)$$

where I is the current in the superconductor and S_{noncu} is the cross section area of superconductor (NbTi in the case of SST-1).

The quench development in a composite conductor can be described by following one dimensional differential equation

$$C_{avg}(T)\frac{\partial T}{\partial t} = \frac{\partial}{\partial x}\left(k_{avg}(T)\frac{\partial T}{\partial x}\right) + \rho_m(T)J_{cd}J_m(T) + g_{dist}(t) - \frac{hP}{A}(T - T_b) \qquad (3.2)$$

Where T = conductor temperature, t = time, x = spatial coordinate, $C_{avg}(T)$ = average volumetric heat capacity (over matrix and superconductor). The first term on the right-hand side represents thermal conduction along the strand with $k_{avg}(T)$ as the average volumetric average thermal conductivity. The term $\rho_m(T).J_{cd}J_m(T)$ represents the Joule heat generation $G(T)$. When the conductor is superconducting, this term is zero. $\rho_m(T)$ is the electrical resistivity of the matrix and J_{cd} is the overall conductor current density defined as the transport current I_t divided by the cross-sectional area of the conductor A. $J_m(T)$ is the matrix current density and is determined by the critical properties of the superconductor which are, in turn, a function of temperature. The term g_{dist} represents external heat sources which will be discussed in next section. The last term represents convective cooling with heat transfer coefficient h, wetted perimeter P and T_b is the helium bath temperature.

The current sharing depends on the behaviour of critical current I_c of the given superconductor as a function of temperature. This behaviour is represented in figure 3.2, assuming for simplification a linear dependence I_c on temperature at constant magnetic field.

As seen in the figure 3.2, when the temperature is less than the current sharing temperature T_{cs} the conductor will be fully superconducting and there will be no joule heat generation since no part of transport current I_t is flowing through the matrix (0. Above T_{cs} the current through the superconductor I_{sc} decreases and the excess current I_m flows through the matrix. As the temperature increases above T_{cs}, I_{sc} decreases further and I_m increases. Above T_c virtually the entire transport current flows through the matrix.

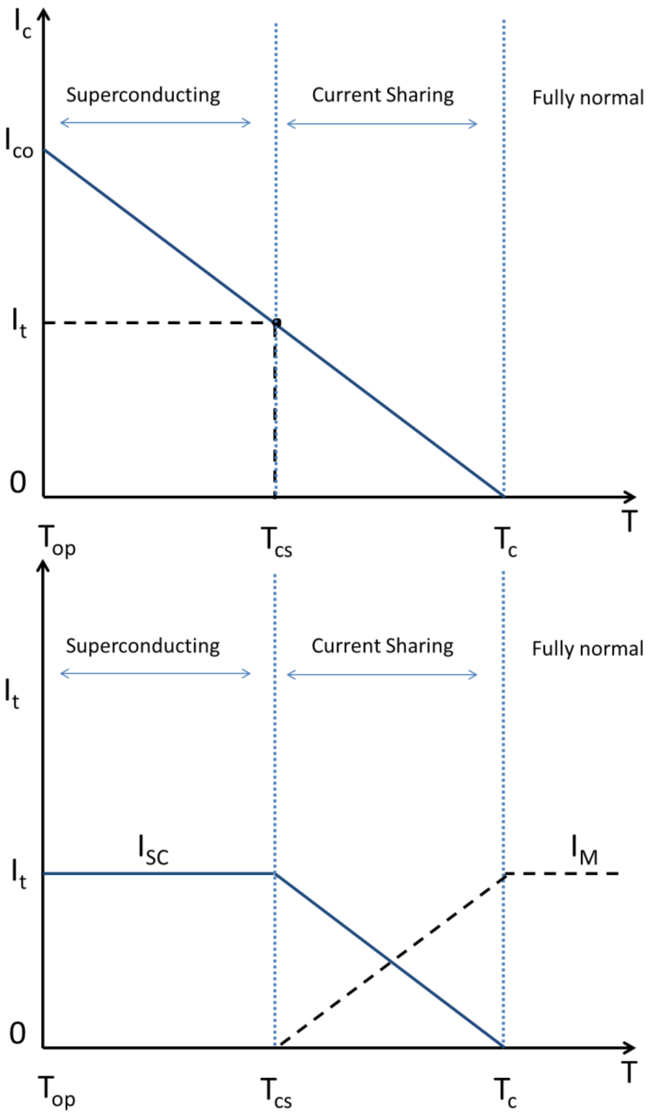

Figure 3.2: Critical current dependence on temperature at constant magnetic field

The heat generation term *G(T)* directly depends on this current sharing and it can be represented as follows (where f is the ratio of cross-sectional areas of matrix to the conductor, A_m / A)

$$G(T) = \begin{cases} 0 & T < T_{cs} \\ \frac{\rho_m(T) J_{cd}^2}{f} \times \frac{T - T_{cs}}{T_c - T_{cs}} & T_{cs} \le T \le T_c \\ \frac{\rho_m(T) J_{cd}^2}{f} & T \ge T_c \end{cases} \qquad (3.3)$$

Fitting formulae are available to obtain the critical surface $J_c(B, T)$ which enable accurate estimation of J_c as a function of temperature and magnetic fit as described in more detail in chapter 5 of the thesis. The critical current density for SST-1 CICC as a function of temperature and magnetic field is shown in figure 3.3.

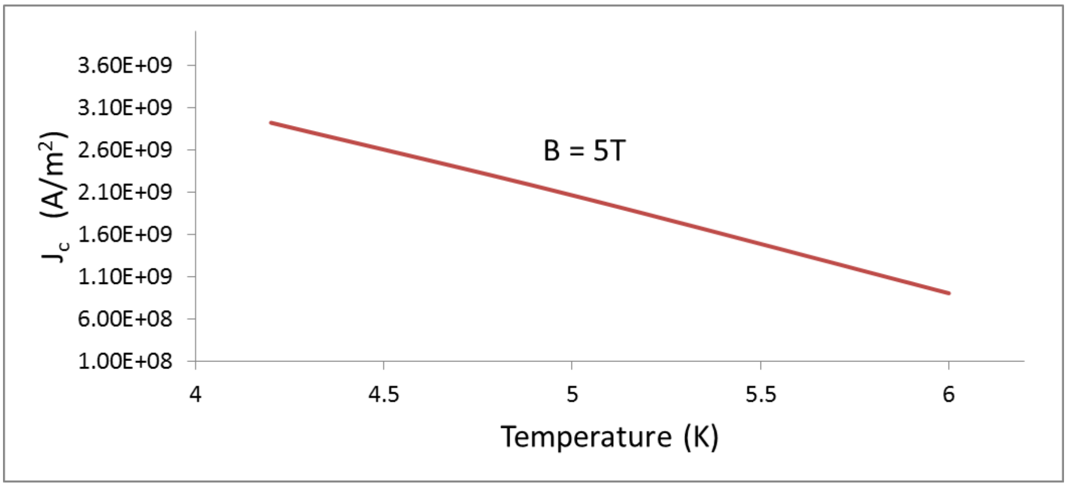

Figure 3.3: SST-1 strand critical current density dependence on temperature and magnetic field

If the magnet is operating at a temperature T_{op}, temperature margin available for magnet operation can be calculated as

$$T_{margin} = T_{cs} - T_{op} \qquad (3.4)$$

If the magnet operating temperature exceeds the available temperature margin, joule heating is initiated in it. This initiates joule heating in the stabilizer section which then heats up the nearby sections of superconductor and supports further increasing quenched lengths of the conductor. This is known as quench propagation and the rate of increase of this quenched length is known as quench velocity generally expressed in the unit of m/s. This relatively simple model of quench propagation as described in equation 3.2 is dominated by thermal conduction of materials involved and is applicable for adiabatic windings. In CICC-based magnets quench propagation is dominated by helium thermodynamics, apart from the contribution of thermal conduction. Joule heating raises the helium temperature and locally helium pressure increases significantly from the initial value depending on the nature of disturbance. This pressure rise is limited by the expansion of helium. The expansion of helium is restrained by inertia and by the turbulent friction with the CICC jacket and the strands. This partially restrained system, along with the joule heating rate, determines the rates of pressure rise and the thermal expulsion. The heated helium is expelled towards both ends of CICC, which heats up the other still superconducting sections of CICC and determines the rate of quench propagation [3.2]. Quench propagation in CICC will be further discussed in chapter 5 of this thesis.

3.3 Disturbance spectrum

In a tokamak environment, there are many possible sources which can deposit energy in a section of superconducting magnets which may quench it, if the temperature rise from this disturbance is more than the available temperature margin. These disturbances are generally categorized as transient and continuous disturbances depending on their time scale, and as point or distributed depending on the affected length of the conductor [3.3]. In practice, a combination of all types disturbances is generally present. For example, steady heat loads from joints can be categorized as continuous point disturbances. Distributed continuous disturbances are caused by heat conduction or radiation from surrounding warm structures. Examples of distributed transient disturbances are AC losses, nuclear or electromagnetic radiation and plasma disruption etc. The point transient disturbances are generally thought to be of mechanical origin, i.e. sudden strand movements due to the Lorentz forces acting on the conductor. For every tokamak magnet CICC is designed with sufficient temperature margin to take care of the expected spectrum of all such disturbances without getting quenched.

3.4 Possible effects following a quench

In case of a quench, current flowing through the superconductor is transferred to the copper section of the superconducting strands and joule heating starts in the strands. This joule heating is tremendous due to the facts that these magnets are generally operated at very high current densities. Also the materials have very low specific heat at low temperatures as compared to their room temperature values. Entire stored energy of the magnet (½ LI^2) will be dissipated in the quenched section of magnet, if proper quench protections steps are not taken after detection of the quench. These can lead to insulation damages, conductor melting and arcing etc. rendering the magnet unusable. So detection of quench and suitable protection within reasonable time of occurrence of quench is an essential aspect of ensuring magnet safety during operation.

3.5 Quench protection method

The quench protection method is usually very specific to the magnet design. Depending on its energy content, it is decided if some inbuilt quench protection is possible to protect the magnet or if an active protection is required [3.4]. In built quench protection schemes generally involve installation of diodes, resistors or a combination of both to bypass or share the magnet current of the quenched region allowing the reduction of joule heating. Quench heaters are also used sometimes to quickly spread the quench region to equally dissipate the magnet energy in the entire magnet rather than a localised quench region. This helps in reducing the localised high temperature in the quenched region.

In fusion-grade magnets, due to very high energy contents, an active quench protection method is used which involves introduction of an external resistor very high as compared to resistance of the quenched region. Most of the magnet energy is dissipated in this external resistor thus high temperature rise within magnet is avoided. This method is shown schematically in figure 3.4. As seen in the figure, an external resistor R_{dump} is installed in parallel to the magnet having self-inductance L and connected to power supply P.S. When quench develops in the magnet, schematically shown as R_{quench}, the quench detection circuit (discussed in chapter 4) opens the switch S. As the $R_{dump} >> R_{quench}$, most of the magnet energy is dissipated in the dump resistor physically located outside the cryostat. The magnet current decays exponentially with the L/R dump time constant. Selection of this dump time constant depends on two parameters; the allowable temperature rise and voltage developed across the magnet following dumping.

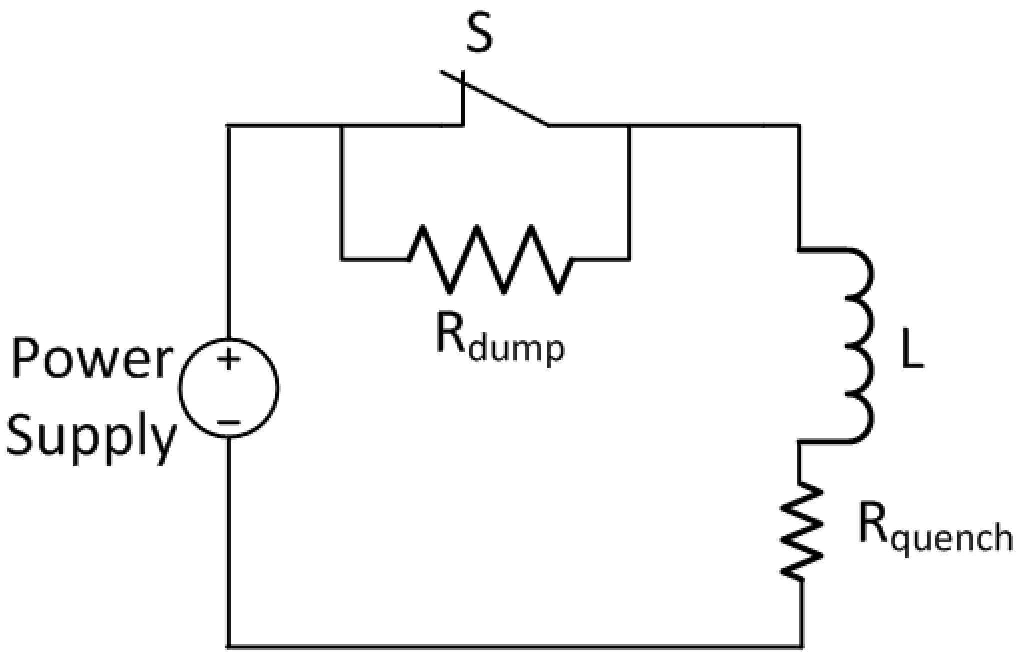

Figure 3.4: Active quench protection using external dump resistor

When the magnet current is decaying, the quenched region of the magnet continues to heat up. The point where quench had originated always achieves the highest temperature rise as it is subjected to joule heating for the longest time. This point is generally referred to as hotspot and its temperature as the hotspot temperature. As the temperature rise is not uniform within the magnet, differential thermal stresses may develop within the magnet leading to shear stresses in the magnet damaging the magnet insulation. In CICC-based magnets, it can lead to high pressure due to coolant heating and can damage the CICC as well. Usual allowable temperature rise is 150 K in fusion magnets as up to this temperature the differential thermal stresses are within the acceptable limits. As soon as the dump resistor is introduced in the magnet circuit, peak dump voltages appear across the winding. The insulation of the magnet must be rated to withstand the peak dump voltage.

3.6 Selection of dump resistor

As the dump resistor is introduced in the magnet circuit, the magnet current I decays exponentially as follow

$$I(t) = I_{op} e^{\frac{-t}{\tau}} \qquad (3.5)$$

where $I(t)$ is instantaneous current at time 't', I_{op} is initial operating current and $\tau = L/R_{dump}$ is the dump time constant. The magnet current decays to almost zero in time equal to five times the dump time constant.

The dump voltage appearing across the magnet terminals following the current dump can be estimated as follows

$$V_{dump} = I_{op} \times R_{dump} \qquad (3.6)$$

We can analyse from these two equations 3.5 and 3.6 that if we want to increase the rate of magnet current decay, we should select a low dump time constant, which means a higher dump resistor should be selected for a fixed inductance L of the magnet. And if we select a higher dump resistor, higher dump voltage will appear across the magnet. So dump resistor selection involves balancing these two requirements. While estimation of dump voltage is easy, the estimation of temperature rise at hotspot during the current decay process requires consideration of temperature dependent material properties namely specific heat and resistivity for all the conductor constituents.

Assumption of local adiabaticity is a useful method used for estimation of hotspot temperature [3.5]. It considers the worst case situation where the entire heat generated by joule heating is absorbed by the conductor constituents and no helium cooling or heat conduction is present. For a unit volume of winding, we can write

$$j^2 \rho \, dt = \gamma \, C \, dT \qquad (3.7)$$

where t = time, T = temperature, $j(t)$ = current density, $\rho(T)$ = resistivity, γ = density, $C(T)$ = specific heat [Note: all quantities are averaged over winding cross section]

Rearranging the terms, we get for the temperature rise during current decay process as

$$\int_0^{\infty} j^2 \, dt = \int_{T_{op}}^{T_{max}} \frac{\gamma \, C}{\rho} \, dT \qquad (3.8)$$

Right hand side of equation 3.6 depends only on material properties. We can define a function $U(T_{max})$ as

$$U \, (Tmax) = \int_{T_{op}}^{T_{max}} \frac{\gamma \, C}{\rho} \, dT \qquad (3.9)$$

Using equation 3.5 of exponential current decay we can write

$$J_{op}^2 \, \frac{\tau}{2} = U \, (T_{max}) \qquad (3.10)$$

This equation 3.10 can be used to estimate maximum hotspot temperature following the decay of current from initial current density of J_{op} with a dump time constant of τ. As discussed in section 3.7 in real applications, there is always a delay of quench detection time and the power supply switch opening before the current decay is initiated, so equation 3.8 is modified to

$$J_{op}^2\,(delay + \frac{\tau}{2}) = U\,(T_{max}) \qquad (3.11)$$

We will now apply this to estimate the hotspot temperature for SST-1 magnet system.

For SST-1 CICC, cross-sectional areas of different components are as follows

NbTi = 1.33×10^{-5} m^2

Cu = 6.51×10^{-5} m^2

SS = 7.98×10^{-5} m^2

Copper properties for residual resistivity ratio (RRR) value of 100 at magnetic field of 5.1 T (peak field on SST-1 TF magnet at 10000 A) were taken. SST-1 CICC jacket material is SS 304L. The estimated thermal diffusion time constant for steel CICC jacket is about 8.5 ms [3.4]. This is much less compared to the order of quench decay time constant of tens of seconds, so jacket contribution has been considered in this calculation. Using the material database, the area averages effective ρ, γ and C values at temperatures from 4 K to 300 K were obtained for SS, Cu and NbTi. A matlab program was used to do the integration to obtain $U(T_{max})$ values at different temperature from 4 K to 300 K. This is plotted in figure 3.5.

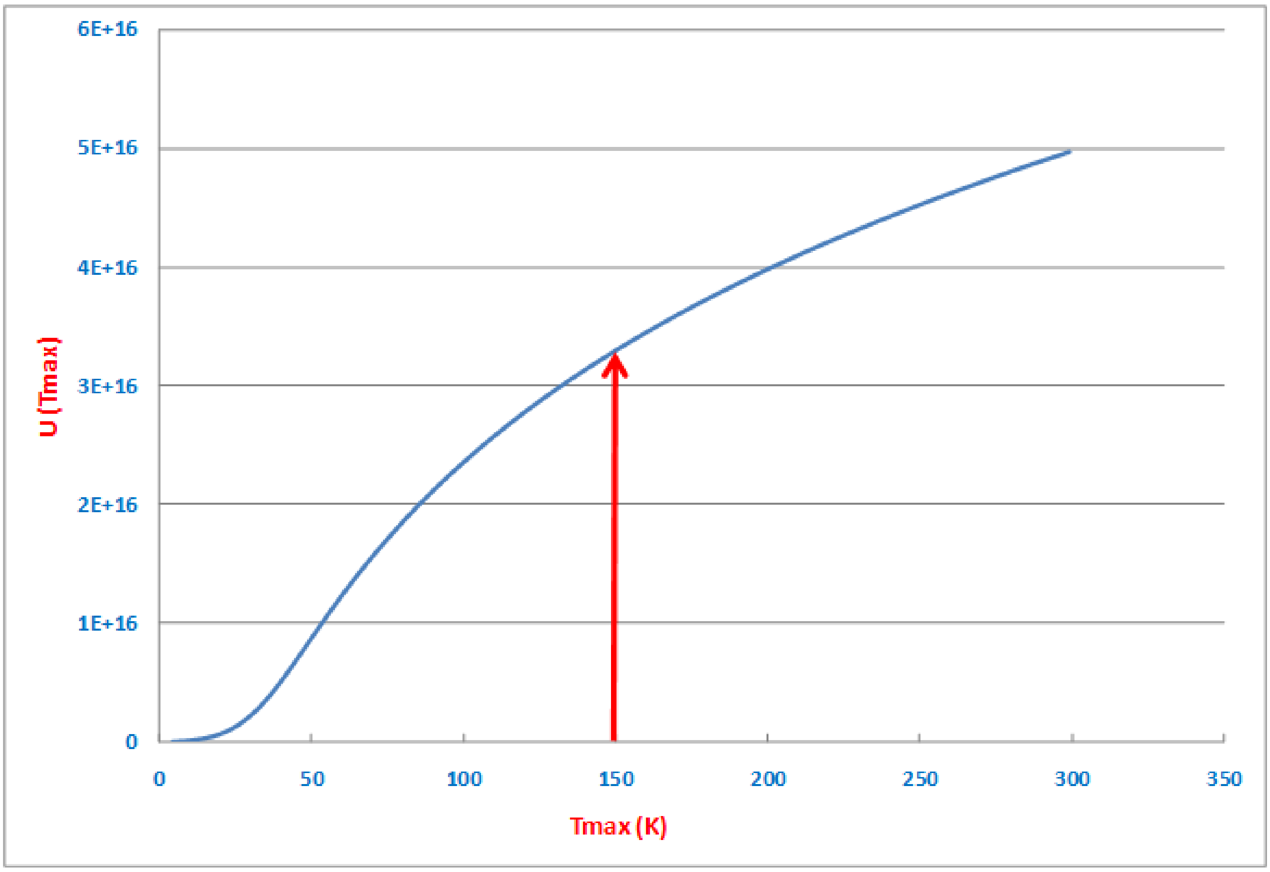

Figure 3.5: $U(T_{max})$ function for SST-1 CICC

If we want to limit the hotspot temperature to 150 K, we have

$$U(T_{max}) = 3.3 \times 10^{16} \ (A^2 \ s \ m^{-4})$$

For TF magnets I = 10000 A, using SST-1 CICC cross section we have

$$J_{op}^2 = 1.63 \times 10^{16} \ A^2 \ m^{-4}$$

So we get

$$delay + \frac{\tau}{2} = 8.26 \ s$$

If a *delay* of 0.26 s is considered, then we get τ = 16 s. This can be interpreted as follows; if we dump the SST-1 TF magnets operating at 10000 A with a dump time constant of 16 s, the maximum hotspot temperature will be limited to 150 K.

For SST-1 we have selected the dump time constant of 12 s to further reduce the hotspot temperature. The corresponding hotspot maximum temperature is about 115 K.

SST-1 TF magnet inductance is 1.128 H. So the required dump resistor value for dump time constant of 12 s comes out to be 94 mΩ. The corresponding maximum dump voltage is 940 V. As this voltage is much below the SST-1 TF magnet insulation voltage ratings of 2000 V, this dump resistor value was acceptable. An air-cooled, SS alloy-based dump resistor was selected for this purpose and installed in the quench protection system of SST-1 TF magnet system [3.6].

3.7 Typical temporal evolutions of quench voltages

A typical temporal evolution of voltages across a magnet, when a normal zone (quenched region) generates and propagates followed by the magnet current dump after quench detection, is shown in figure 3.6. The current and voltage values are arbitrary.

The initial time t_p is the propagation time. During this time normal zone is generated and propagated till the voltage across the magnet reaches the voltage $V_{th,}$ called as threshold voltage value. This confirms the generation of unrecoverable normal zone in the magnet.

The time t_h is the threshold time. In a tokamak, voltage across the magnet may be either from the real normal zone development or from the inductive noise getting coupled onto this magnet from other magnets or other subsystems. So t_h time period is selected to be more than the expected time periods of these disturbances. If voltage across the magnet remains at the threshold voltage level or becomes higher than the threshold voltage level, then it is considered to be a real quench and the protection measures are initiated.

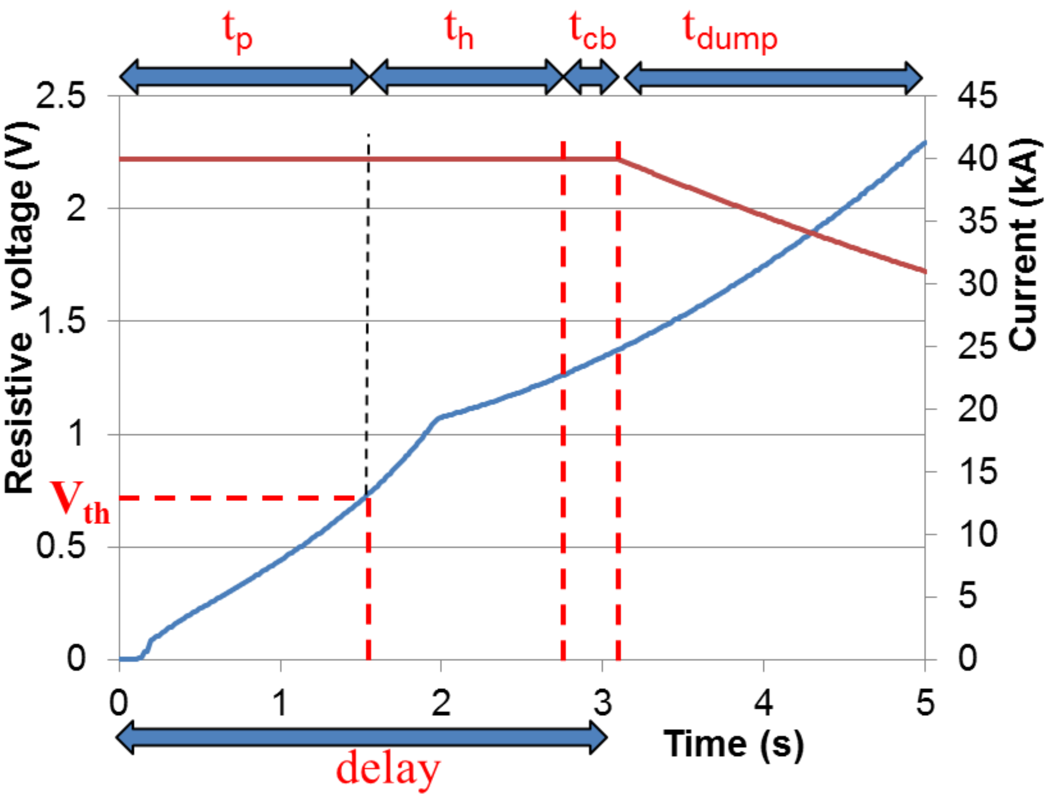

Figure 3.6: Temporal evolution of quench voltage

The time t_{cb} is the current breaker opening time. This is time for a current breaker to bypass the power supply and introduce the dump resistor in the magnet circuit. This time depends on the technology used in the current breaker hardware.

The time t_{dump} is the dump time. At the instant the dump resistor is introduced in the magnet circuit, very high dump voltage appears across it. This voltage is much higher than the threshold voltage and usually the precision electronic circuit used to measure the threshold voltage gets saturated. After the initial peak, the dump voltage will decay along with the magnet current.

The sum of times t_p, t_h and t_{cb} is known as '*delay*' (used in equation 3.11) and it is the minimum time to elapse before magnet current dump is initiated, once a normal zone is detected in the magnet.

4. Design of TF coil Quench detection circuit

Quench detector is one of the most important diagnostics installed on a superconducting magnet system for magnet safety during operation. Its task is to detect quench and initiate quench protection action. Its importance can be judged from the fact that even a single undetected quench can damage the magnet beyond repair. Also the location of TF magnet system within tokamak doesn't allow removal damaged coils without major disassembly of the whole machine, leading to very long downtime for the tokamak. Quench detection (QD) technique specific to the magnet system geometries are needed to design a failsafe QD system [4.1 – 4.4]. This chapter gives details of QD system developed for SST-1 TF magnet system.

4.1 Quench detection of superconducting magnets

Quench causes generation and propagation of resistance in otherwise superconducting magnet, so the voltage measurement across the magnet is the fastest and most direct method of detecting quench. But unfortunately the quench voltage is in range of few 100 mV whereas the inductively couple voltage which are superimposed on this voltage signals are few 100 V. This problem and its solution are schematically shown in figure 4.1.

If we try to measure quench voltage directly as shown in figure 4.1 (a) then the measured voltage will be addition of quench voltage and the inductive component.

$$V_{measured} = V_{quench} + L\frac{di}{dt} \qquad (4.1)$$

To cancel out the inductively coupled voltage, measurement as shown in figure 4.1 (b) is done. The identical sections of same magnet or two identical magnets are compared with each other. So if *L1* = *L2*, the measured voltage will be only the resistive component 'V_{quench}'.

$$V_{measured} = (V_{quench} + L1\,\frac{di}{dt}) - \left(L2\,\frac{di}{dt}\right) = V_{quench} \qquad (4.2)$$

This is the basic principle of inductive noise cancellation. It has to be adapted for the magnet system for which the QD circuit is to be developed. For simple representation, in figure 4.1, induced voltage components from inductively coupled neighbouring coils or from the other sections of the coil itself are not shown. These couplings also influence the measured voltages and are required to be taken in consideration in the noise cancellation scheme. A similar concept has been adopted in the SST-1 TF magnet QD system discussed in next section.

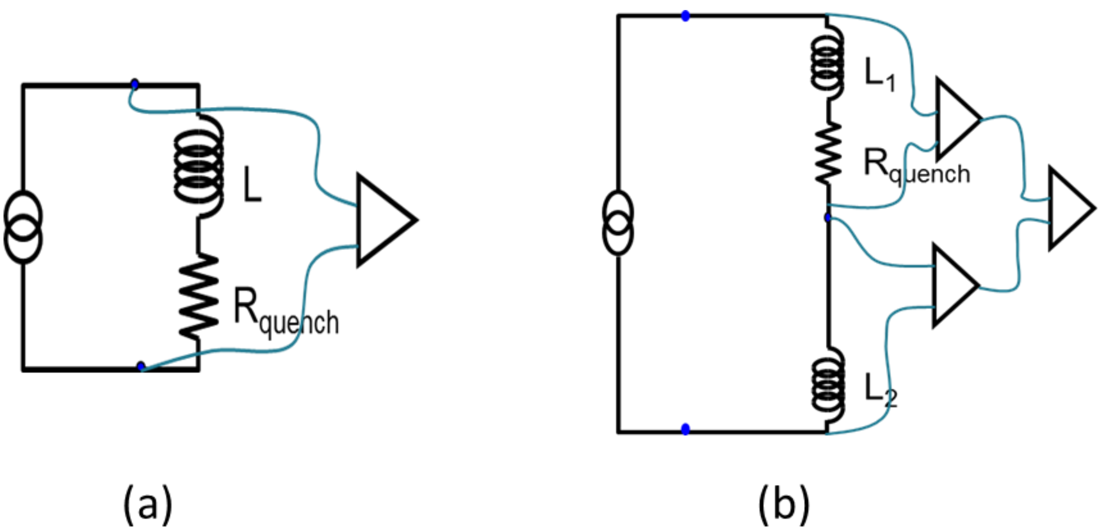

Figure 4.1: Inductive noise cancellation for quench detection

Another option to cancel inductive voltage is to use co-wound tapes [4.5]. In this method, a conducting tape is wound along with the coil winding. In this case, the inductive coupling to this tape is very much similar to voltage coupled to the actual coil. It is shown in figure 4.2

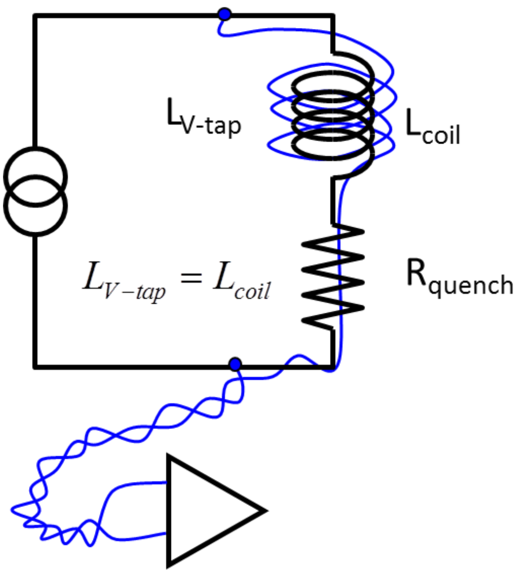

Figure 4.2: Co-wound voltage taps for quench detection

4.2 TF Magnet quench detection system design

4.2.1 Voltage tap locations

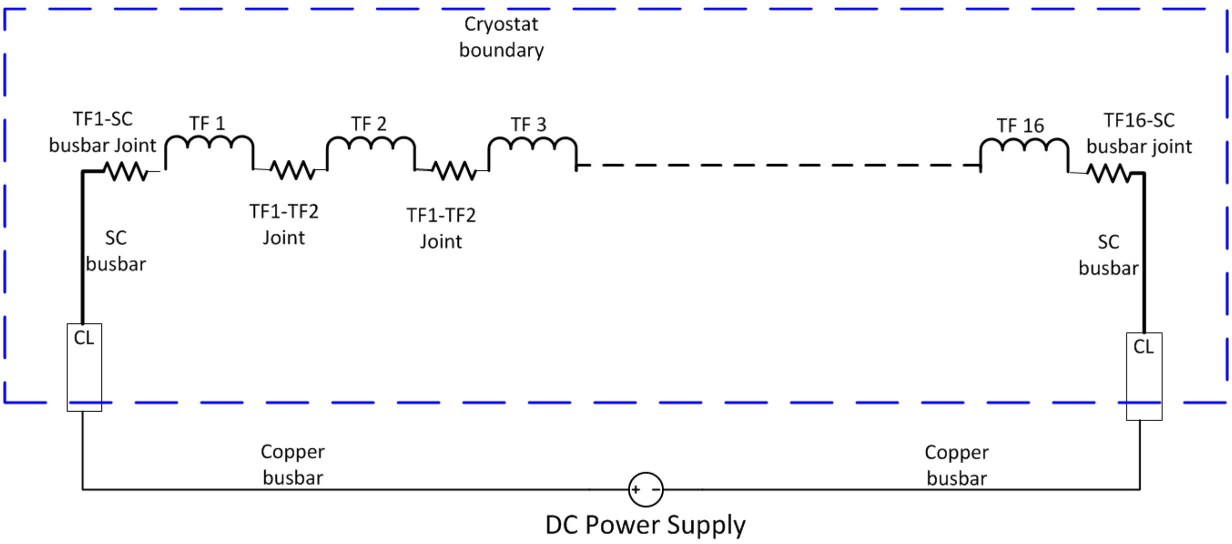

Figure 4.3: SST-1 TF magnet system connection diagram

As described in chapter 2, the SST-1 TF magnet system has 16 TF coils. These coils are connected in series by low resistance inter-coil joints and charged with a 10000 A, 16 V DC power supply, as shown in figure 4.3. The connection between the power supply and the series connected TF coils is made of two distinct parts. The first part is at cryogenic temperature from coils up to the current leads, using superconducting (SC) busbar, which is inside the cryostat. The second part is at room temperature, between the room temperature connection of current leads and the power supply.

Each TF coil has six double pancakes (DPs). Low resistance inter-DP joints have been made outside the coil casing to electrically join these six double pancakes (J1 – J5). Conventional voltage taps have been installed on these joints to measure the voltages across these DPs for QD. The arrangement of voltage taps is schematically shown in figure 4.4 for TF1 coil. This coil is connected to TF2 coil on one side and to the superconducting busbar on other side. Similarly voltage taps are taken from all TF coils.

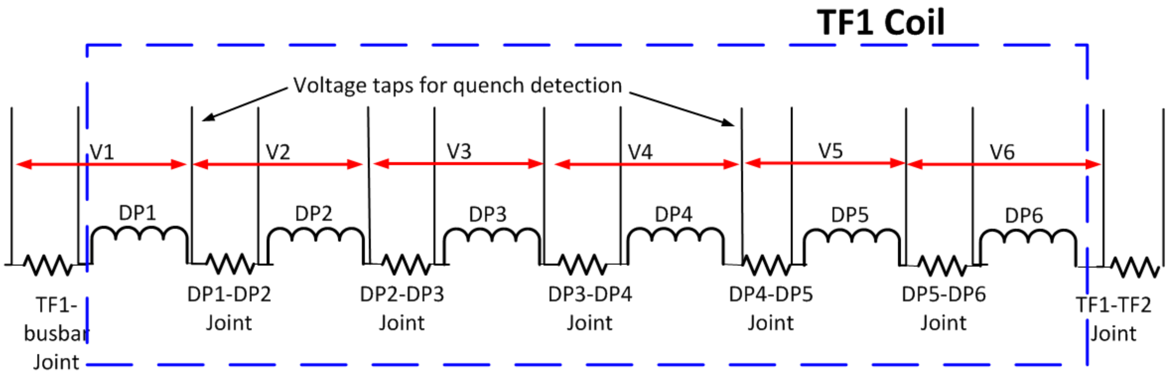

Figure 4.4: Arrangement of voltage taps for TF1 coil

4.2.2 *Inductive noise cancellation scheme*

Two inductive noise cancellation schemes have been tried out on TF magnet QD system. First scheme was modification of so-called central difference averaging [4.6]. The complete scheme for one coil (TF1 coil for example) was as follows:

$$Vquench = \frac{V1 + V3}{2} - V2 \quad (4.3)$$

$$Vquench = \frac{V4 + V6}{2} - V3 \quad (4.4)$$

$$Vquench = (V1 + V2 + V3) - (V4 + V5 + V6) \qquad (4.5)$$

where *V1* to *V6* are voltages across DP1 to DP6 respectively.

As DPs of individual coils are in very close proximity with each other as compared to other coils, the difference between the side pancakes gives very good noise cancellation. These three difference voltages (V_{quench}) were then compared with QD threshold voltage and threshold time. [The experimentally observed difference voltage was maximum up to 10 mV, mainly due to unequal offset voltages present at the output of isolation amplifier of different channels of the quench detection card. This was still in the acceptable limit].

The threshold voltage V_{th} selected for SST-1 TF magnet is 150 mV which is about 4.5 m length of SST-1 CICC getting quenched. This is equal to about 1 turn of TF coil DP. This voltage is well above the expected noise of 10 mV.

The threshold time t_h selected is 100 ms. This time is much higher than the expected time periods of inductively coupled noise voltages from other magnets and other subsystems and the 50 Hz noise. For example, the time constant for induced voltage from plasma disruption will be 15-18 ms due to the presence of vacuum vessel in between the TF coils and the plasma. The inductive noise coupled from ECRH system is found to be about a time period of 5 ms. Other magnets like TR1-4 and PF magnets also have coupling with the TF magnet system but it is not very significant as their magnetic field is in poloidal direction and coupling is mainly due to magnet installation misalignments etc. These couplings are generally measured during the engineering commissioning of the magnet system and the threshold voltage or time is adjusted accordingly. So the SST-1 TF QD cards have been made with adjustable V_{th} and t_h, to tune their values as per the actual experimental observations before actual plasma operation.

The modified central difference averaging scheme ensures that each DP was compared at least two times to give redundancy in case of any electronic component failure in the quench detection card. This scheme was implemented in the QD card and was used during initial SST-1 machine operations and the spare coil test campaigns. This scheme has been reported in [4.7].

During the technology up-gradation of QD card, it was realized that a simple direct comparison scheme may be used to do inductive noise cancellation. This direct comparison scheme had the advantage that apart from TF coils, it could also be used for QD of other components like superconducting busbar, current leads and the PF magnets. This new scheme gave advantages in terms of low inventory requirement as compared to having different QD cards for different components. The simple difference scheme can be expressed as:

$$Vquench = V1 - V2 \qquad (4.6)$$

$$Vquench = V2 - V3 \qquad (4.7)$$

$$Vquench = V3 - V4 \qquad (4.8)$$

$$Vquench = V4 - V5 \qquad (4.9)$$

$$Vquench = V5 - V6 \qquad (4.10)$$

$$Vquench = V6 - V1 \qquad (4.11)$$

This scheme gave similar noise cancellation levels (of less than 10 mV) as the modified central average difference scheme.

4.2.3 Redundancy in voltage taps wiring:

As seen in equations 4.6 to 4.11 each double pancake is compared to its neighbouring DP in at least two channels. Additional redundancy was provided by comparing the entire coil in another quench detection card. Since the joint resistances are less than 1 nΩ, the voltage drop across joints is less than 1 μV [4.8], so voltage taps across joints can be considered as coming from same point for all practical purpose of QD. As shown in figure 4.5, voltage taps 1 and 1´, 2 and 2´, 3 and 3´ coming from joints can be considered as redundant to each other.

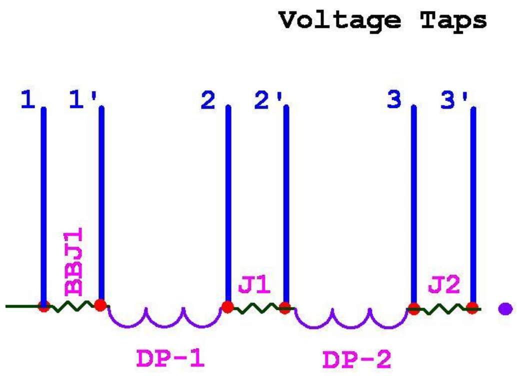

Figure 4.5: Voltage taps across joints used as redundant taps

Using these redundant taps, the simple difference scheme was implemented in a separate redundant QD card as follows

$$Vquench = V1' - V2' \qquad (4.12)$$

$$Vquench = V2' - V3' \qquad (4.13)$$

$$Vquench = V3' - V4' \qquad (4.14)$$

$$Vquench = V4' - V5' \qquad (4.15)$$

$$Vquench = V5' - V6' \qquad (4.16)$$

$$Vquench = V6' - V1' \qquad (4.17)$$

This implementation is shown schematically in figure 4.6, where a single TF coil is wired in two quench detection cards. As seen, each DP is compared in 2 different channels in a QD card and the same DP is compared in 2 different channels of another QD card. The complete wiring of these two cards from coil to the electronic card are done using different cables, feed-troughs and are wired in different instrumentation racks. This has given very high redundancy. This scheme has been implemented in TF coil, busbar and current lead QD cards. This difference scheme has given very good cancellation of inductive voltages during various SST-1 TF magnet system operations. Their performance was also successfully verified in the multiple coil test campaign of SST-1 TF coils [4.8].

4.3 Quench detection system hardware design

Using the design guidelines mentioned in the previous sections, QD cards were developed using the state-of-the-art analog and digital electronic components. Its block diagram is shown in figure 4.6. The functional requirements of major components of this card are as follows:

Voltage taps protection: High voltage and high wattage resistors are installed before the entry of voltage taps into the QD card. This resistor is installed to protect the burnout of voltage tap wires in case of ground faults. Capacitors have been installed across these resistors to get single stage RC filter to bypass high frequency noise.

High voltage surge protection: The next component is for high voltage spike suppression. It’s a combination of metal oxide varistor (MOVs) and back-to-back zener diodes. While MOVs were installed for surge protection, back-to-back zener diodes limit the voltage level to less than ± 5 V which is the input voltage limit of several components of the QD card.

Electrical Isolation: A three-port isolation amplifier AD210 has been selected to provide galvanic isolation between the coils and the QD cards to avoid ground loops. Three port isolation provides isolation between input section, output section and the power supply section. This avoided requirement of separate power supplies for input and output sections of the isolation amplifier. It is rated for 2500 VRMS and 3500 V Peak Continuous voltage. This section also produced a voltage gain of 2, to get better signal-to-noise ratio.

Filter: The next stage was of low pass filter. As the real quench signal is a slow varying signal as compared to inductive noises expected in tokamak magnet systems, a low-pass filter stage was provided by IC MAX292. It is an 8^{th} order, low-pass, switched-capacitor filter. It can be set with cutoff frequencies from 0.1Hz to 25 kHz. The selected cutoff frequency was 10 Hz. The output of the filter stage was sent to the comparison stage and also to the data acquisition system to store the data for post-processing of magnet section voltages to analyse which section of magnet has quenched.

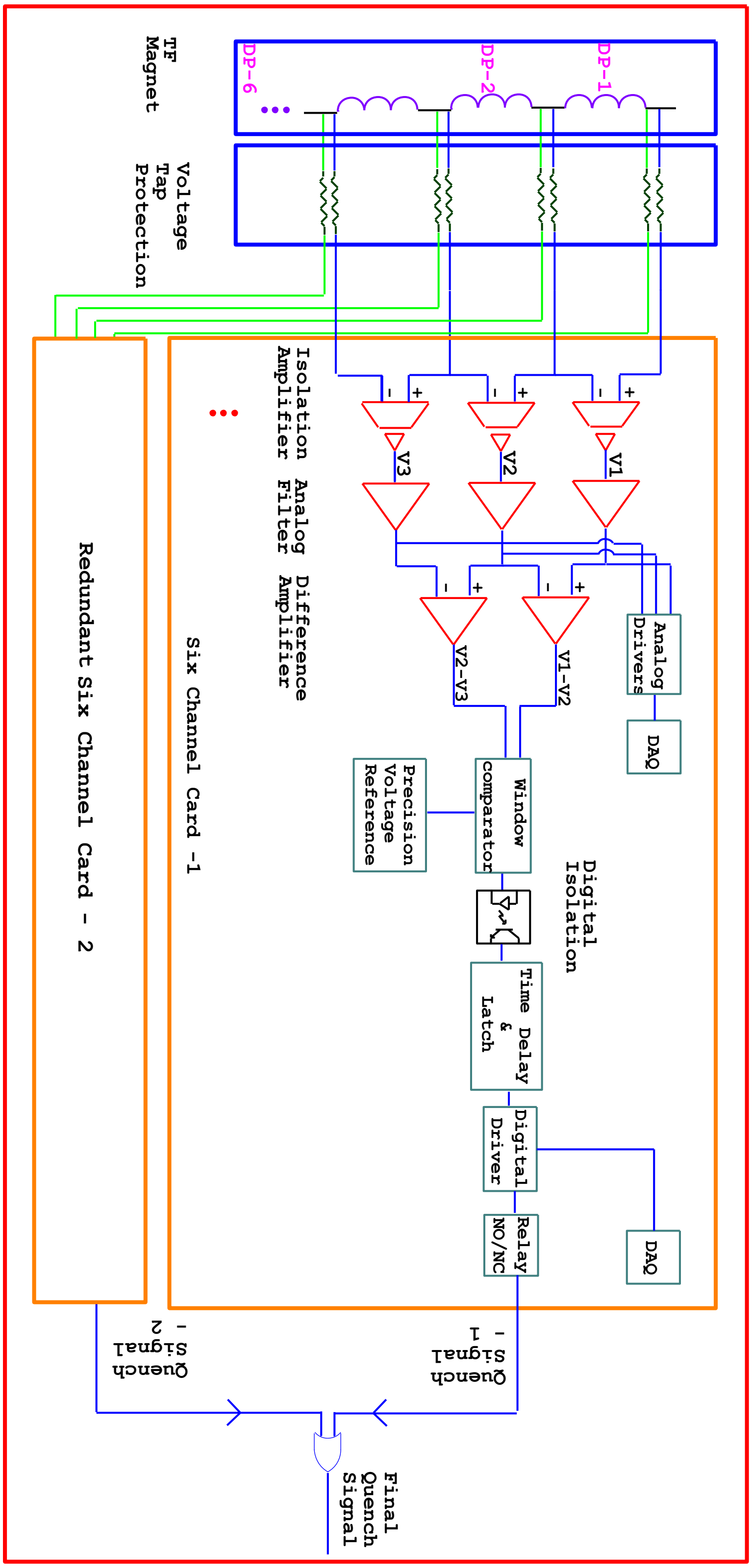

Figure 4.6: Block diagram of SST-1 TF coil quench detection card

Difference module: The function of this module is to compare the different magnet section voltages as per the difference scheme adopted for in the QD card. A unity gain precision differential amplifier INA105 IC has been selected for this module. The INA105 provides differential amplifier without using an expensive precision resistor network and is highly accurate with a maximum offset voltage of 250 µV.

Comparator module: In this module, the voltages from the difference sections are compared with the threshold voltage using a window comparator configuration. Window comparator configuration is chosen as the difference voltage may be either positive or negative, depending on the DP quenched. Window comparator will change its output state for either of the following conditions:

$$Vquench = V1 - V2 > +Vth \qquad or \qquad Vquench = V1 - V2 > -Vth \qquad (4.18)$$

The situation is graphically shown in figure 4.7. The window comparator output changes from low state to high state for the cases of DP1 quench and DP2 quench.

The threshold voltage reference is generated by fixed voltage reference generator giving accuracy of ± 20 ppm. Voltage reference is adjustable manually to enable its tuning as per different operational requirements.

Delay time setting: Once the window comparator output is high, delay time counter monitors its status for the pre-set threshold time. If the output state becomes low in less than the pre-set threshold time, no action is taken and the counter is reset to zero. If output remains high for more than the pre-set threshold time, a high flag is transmitted to the latching circuit. The latch circuit latches the flag and transmits it to the quench trigger generating relay and also to the DAQ system to log the time of quench trigger generation.

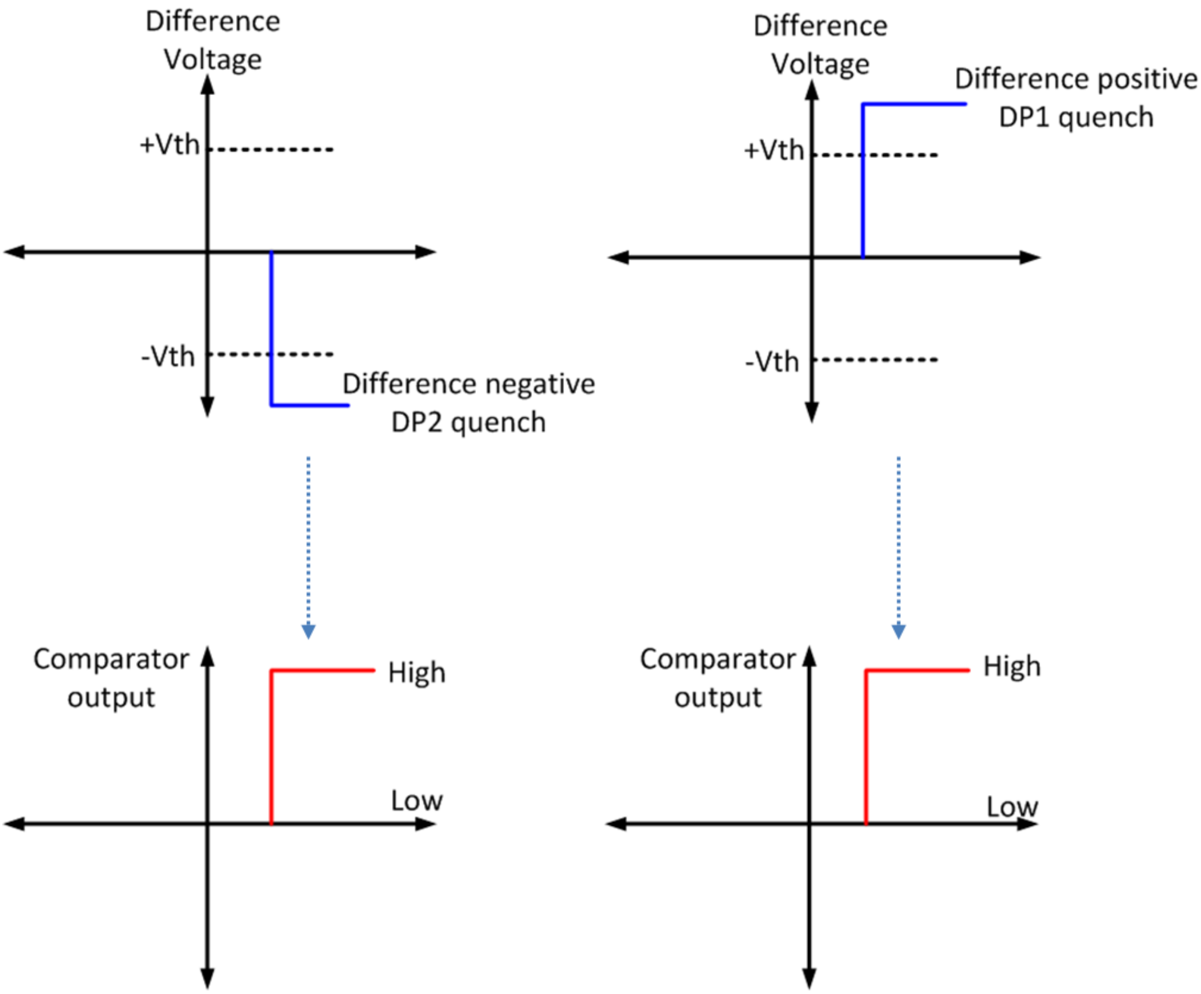

Figure 4.7: Window comparator output for DP1-DP2

Relay: The relay unit triggers the quench protection unit of the magnet power supply to initiate the magnet current dump sequence. A normally open connection type relay is selected for this unit. Under real quench conditions, the relay will open and the quench trigger will be sent to the quench protection unit. In case of no real magnet quench but quench circuit fault conditions like power failure, wire breakage etc., this relay will be open so again the quench protection unit will be triggered. This is acceptable as in the case of absence of a working QD system due to power failure or any other reason, it is safer to initiate current dump. Otherwise an undetected quench event may destroy the magnet.

The photograph of the QD card developed for SST-1 TF coils is shown in figure 4.8.

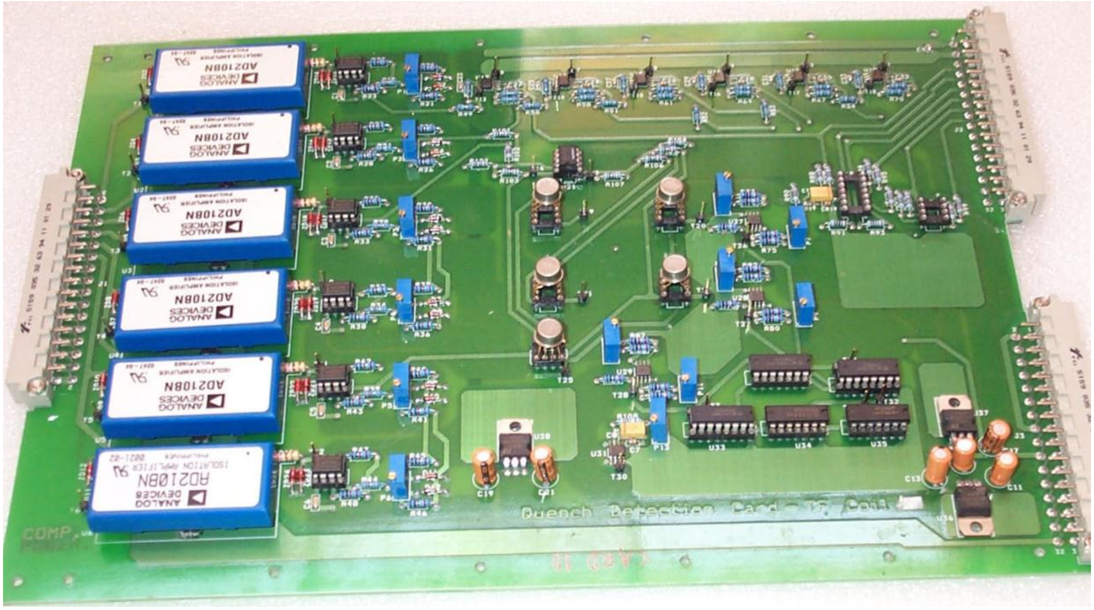

Figure 4.8: Photograph of TF coil quench detection card

4.4 Connection to quench protection system

Once the quench trigger is generated, it has to be transmitted to the quench protection system of the magnet power supply. In SST-1 TF magnet, in the event of quench, the DC current in the power supply is commutated to the controlled bypass, which provides a reliable and stable path. The DC circuit is then opened with on-load mechanical DC breaker and the current is commutated to the dump resistor connected in parallel to the DC breaker. An explosive triggered opening switch (pyro-breaker) is provided as a backup for the mechanical breaker.

The quench triggers from TF1 to TF16 QD cards are put through 'OR' logic in a separate card. The output of this card is transmitted to the DC power supply through a potential free contact using a fibre optic transmitter and receiver unit, which transmits and receives contact open or contact close information to the power supply system. As a system requirement, cryogenic failure and vacuum failure signals should also generate current dump as the magnet operation is not possible with these failures. So the magnet quench potential free contact is interlocked with the fault triggers from vacuum and cryogenics, so that these failures also lead to current dump similar to the magnet quench signal. The schematic of these connections is shown in figure 4.9.

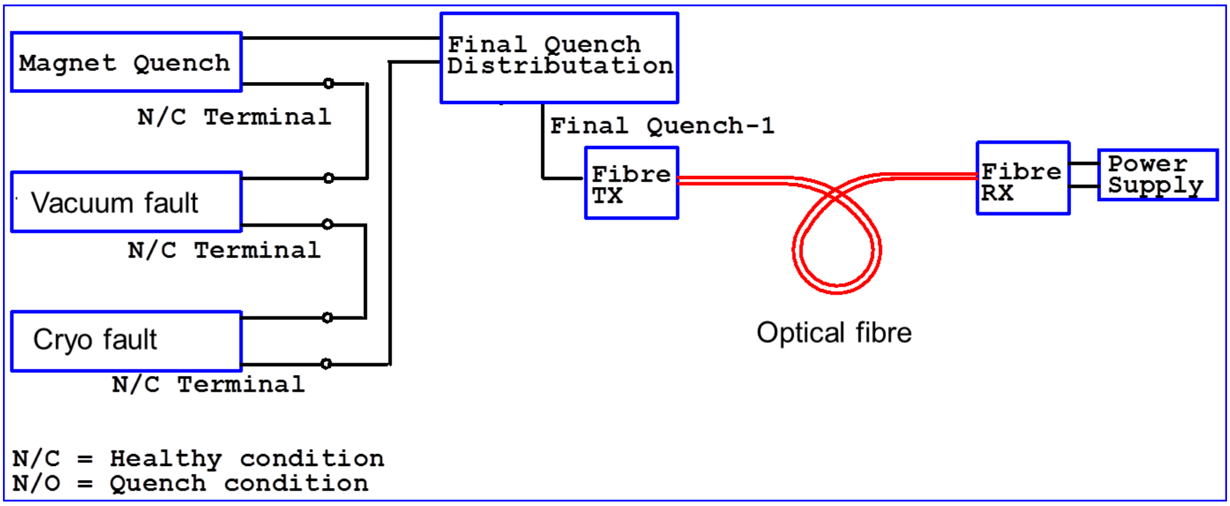

Figure 4.9: Quench interlock with vacuum and cryogenic faults

4.5 Quench detection system results

The quench detection system was tested and validated extensively during the SST-1 TF coil test campaigns. More than 25 TF coil test campaigns were done to validate the TF coil refurbishment and the associated subsystems. Quench detection and protection system worked perfectly during these acceptance tests and not a single quench event was missed. Its performance in one such coil quench event is shown in figure 4.10. As seen, DP6 section of this magnet has quenched. For quench detection, it was compared with DP1 and DP5 in two different cards. As the difference voltage became more than the threshold level of 150 mV for more than 100 ms, quench trigger was generated by both the cards. It was communicated to power supply, which initiated the coil current dump. The total time duration between voltage threshold crossing and PS current breaker opening is 150 ms. Out of these, 100 ms is the pre-set threshold time t_h and 50 ms is time taken for current breaker opening t_{cb}.

Twenty three quench events were observed during the coil test campaigns. Out of these quenches, one was due to the power supply malfunctioning, and two were from current leads quench. All other quenches were attributed to the lack of cryo-stability of the busbar sections or side DPs (DP1 or DP6) of TF coil. In this case, after a few hours of cryo-stabilization, it was possible to charge the magnets to higher current values [4.9 - 4.11].

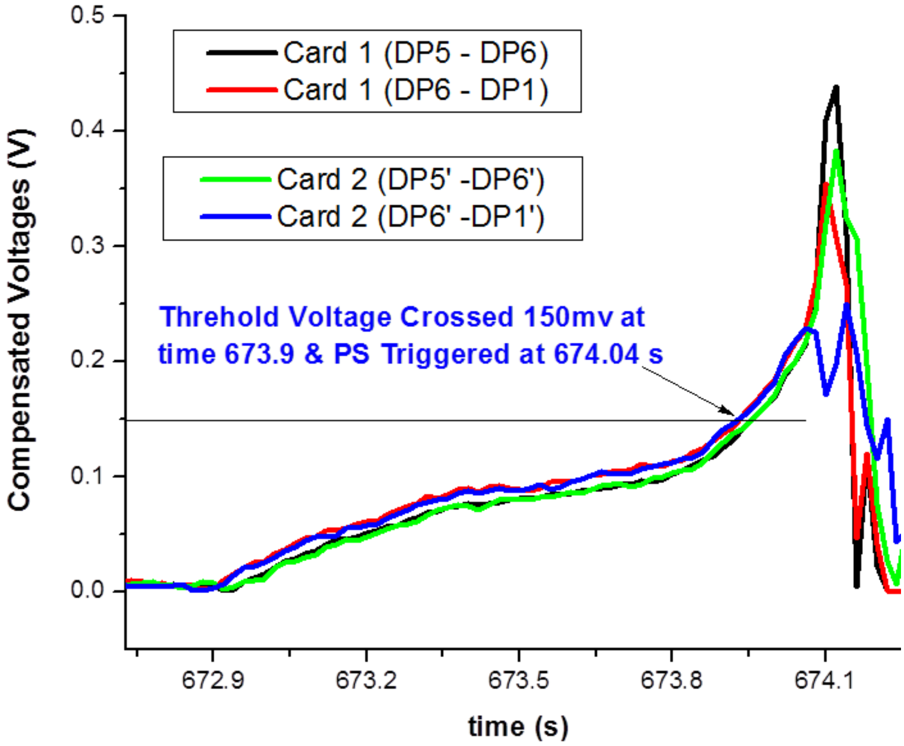

Figure 4.10: Performance of quench detection card in coil test

5. TF coil quench simulation

Understanding the quench behaviour of CICCs is an extremely important issue for reliable superconducting magnet design and operation. The simulation of different aspects of quench like its initiation and propagation are crucial for magnet safety during operation. This is even more important for large magnets for fusion machines due to very high energy content. While analytical tools are handy for adiabatic estimations for the initial design phase; numerical simulation tools are useful in refining the conductor for quench protection and to predict magnet quench in different operating conditions. This knowledge is useful to make required modifications in the magnet system to avoid quench. As a mandate of the SST-1 mission, each TF coil was cold-tested to its full operating conditions for its electromagnetic, thermal hydraulic and mechanical performances at its full operating current. Quenches observed during these single coil test campaigns were analysed in detail and simulated using 1-D code, Gandalf, in order to understand their quench propagation characteristics. This chapter gives some details of TF coil test experiments and details of adaptation of Gandalf code to accurately model TF coil quench observed during these tests. The predictive quench analysis results for fully assembled TF magnet system are also discussed.

5.1 Adaptation of Gandalf code for SST-1 CICC and TF coil

GANDALF code is the numerical implementation of a one dimensional (1-D) model for the simulation of quench initiation and quench propagation in CICC's with cooling channels [5.1] [5.2]. Its 1-D physical model consists of four independent components at different thermodynamic states as follows:

• the strands, consisting of the stabilizer and superconductor materials,

• the conduit, grouping the jacket and the insulation,

• the helium in the bundle, surrounding the strands within the cable, and

• the helium in the hole, flowing in an independent cooling passage.

The temperatures of these components are treated separately and the energy balances are coupled via heat transfer coefficients at the contact (wetted) surfaces. The material properties and boundary conditions can be handled by user routines. It is possible to adapt the code for CICCs like that of SST-1, without additional central cooling channel.

5.1.1 *Friction factor correlation for SST-1 CICC*

Knowledge of friction factor as a function of the Reynolds number is an important parameter required for all thermo-hydraulic simulations. It gives information about pressure drops across the magnet at different mass flow rates. It is also used in convective heat transfer coefficient estimation. Convective heat transfer is an important mechanism of heat transfer during quench in CICC based magnets.

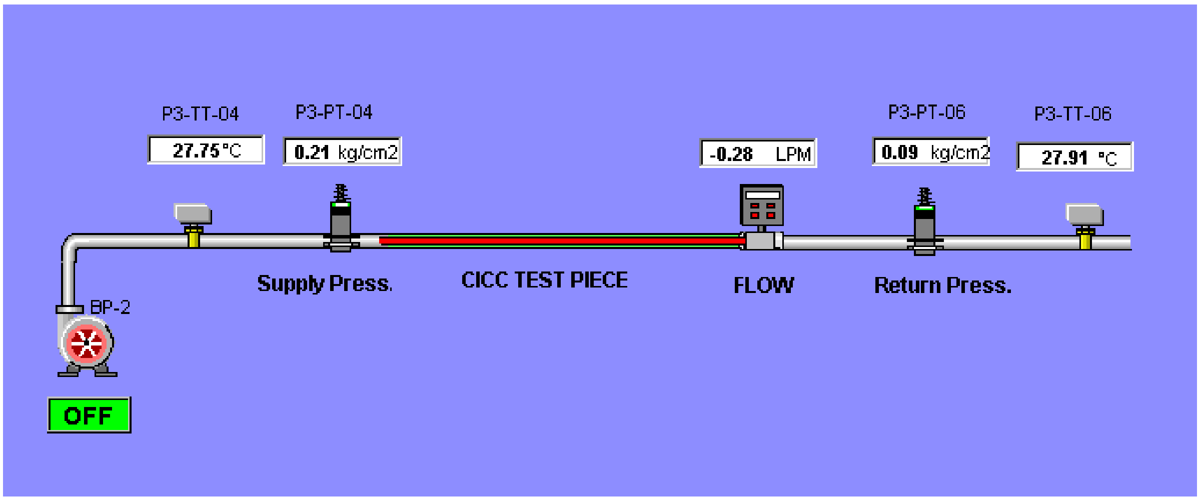

Figure 5.1: Experimental arrangement for friction factor estimation

In the absence of experimental data, the friction factor is estimated from existing co-relations such as that of Katheder and ITER-DC [5.3] [5.4]. Interestingly, these experimental determinations can be done to a fair degree of accuracies at room temperature conditions with pressurized water at constant temperature. This approach has been adopted at CRPP [5.5]. An experiment has been carried out with the Cable-in-Conduit conductor of SST-1 in a similar manner to determine the pressure drop and friction factor characteristics.

The experimental set-up consisted of a closed circuit of demineralized water. Different mass flow rates were generated from a pump at the inlet of the CICC test piece. The inlet and outlet pressure were monitored with IPTX 691 pressure transmitters capable of measuring between 0-25 bar with an accuracy of 0.30% over the entire range. The inlet and outlet temperatures were measured with Pt-100 based Siemens SITRANS-TK-L with an accuracy of 0.10% over the range of 0-100^{o} C. An Orifice flow meter, ABB 2600-T, was installed at the outlet of the test piece to measure the flow rate accurately. The flow-meter can measure flow in a range of 0-35 LPM (litre per minute) with an accuracy of 0.8 %. A schematic of the experimental arrangement is shown in figure 5.1.

The length of the CICC test piece was 1.0 m. Inlet temperature was fixed at 35^{o} C and the maximum outlet temperature is 36^{o} C. So the water density (ρ) and the dynamic viscosity (μ) during the measurement range were constant. The test piece was put in horizontal condition so no hydrostatic correction as a result of gravity was required for the pressure drop. The measurements of inlet and outlet pressure, temperature and mass flow rate in test piece were acquired by a DAQ system. The friction factor 'f' and Reynolds 'R_e' number were calculated from the measurements of the pressure drop and mass flow rates using following equations:

$$f = 2\frac{\Delta P}{L}\rho D_h\left(\frac{A_{he}}{\dot{m}}\right) \qquad (5.1)$$

$$R_e = \frac{\dot{m}}{\eta}\frac{D_h}{A_{he}} \qquad (5.2)$$

Where ΔP = pressure drop, L = length of CICC, ρ = fluid density, η = fluid dynamic viscosity, D_h= hydraulic diameter of the CICC, A_{he} = fluid cross section area, $\dot{m}$ = mass flow rate

The experimentally obtained friction factor for SST-1 CICC (Fexp) was compared with the two other commonly used friction factors of Katheder (Fkath) and ITER-DC (Fiter). These correlations are given by (where V is void fraction):

$$f_{katheder} = \left(\frac{1}{V^{0.72}}\right)\left(0.051 + 19.5\,\frac{1}{Re^{0.88}}\right) \qquad (5.3)$$

$$f_{ITER-DC} = \left(\frac{1}{V^{0.742}}\right)\left(0.0231 + 19.5\,\frac{1}{Re^{0.7953}}\right) \qquad (5.4)$$

The comparison is plotted in figure 5.2.

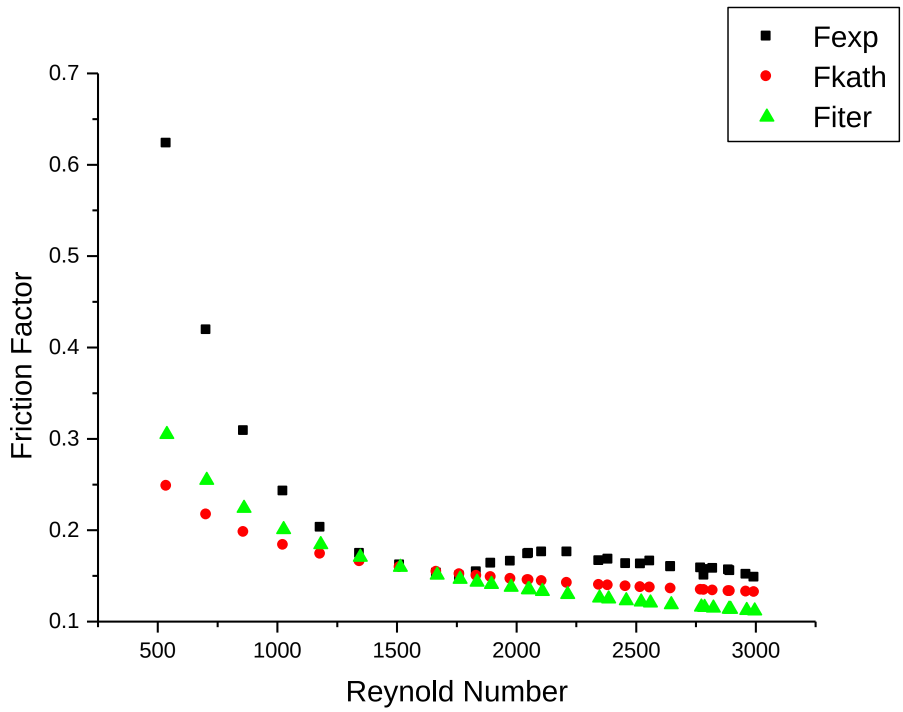

Figure 5.2: Friction factor of SST-1 CICC

It is seen from these results that the Katheder correlation represents the behaviour of SST-1 CICC better than the ITER DC correlation, especially when the Reynolds number of operation is more than 1200. As the Reynolds number during normal operation for SST-1 TF magnet is about 3000, Katheder correlation has been implemented in Gandalf subroutines for estimating friction factor in steady-state operation and transient conditions like quench.

5.1.2 Heat transfer coefficient for quench simulation

The heat flux '$\dot{q}$' the rate of heat transfer per unit area, by a convective process can be expressed as:

$$\dot{q} = h\Delta T \qquad (5.5)$$

where h is called the heat transfer coefficient and ΔT is the temperature difference between the fluid and the surface. In fluid dynamics and heat transfer estimations most of the formulae are empirical. In case of force flow heat transfer processes like in a CICC, it is generally expressed using the dimensionless parameters Prandtl number P_r, Nusselt number and Reynolds number.

$$P_r = \frac{\eta C_p}{K_{He}} \qquad (5.6)$$

$$N_u = \frac{hD_h}{K_{He}} \qquad (5.7)$$

where K_{He} = heat conductivity of the fluid, Cp = Specific heat at constant pressure and other symbols carry usual meaning.

In Cryogenic applications, Dittus-Boetler correlation [5.6] is frequently used for Nusselt number, which is

$$N_u = 0.023 R_e^{0.8} P_r^{0.4} \qquad (5.8)$$

For temperature difference between wall (T_w) and bulk (T_b) higher than 10% of the absolute temperature, Giarrantano et al. [5.7] developed an equation slightly different than Dittus-Boetler as

$$N_u = 0.025 R_e^{0.8} P_r^{0.4} (\frac{T_b}{T_w})^{-0.716} \qquad (5.9)$$

The CICC bundle region is a tortuous medium where turbulence and the Nusselt number are expected to rise and may also be derived from the expression of Nu for fully-developed turbulent flow in rough tubes [5.8], with

$$N_u = \frac{f R_e P_r^{1/3}}{8} \qquad (5.10)$$

This leads to an explicit expression for h proportional to the friction factor f known as Holman correlation. It will be implemented in Gandalf subroutine *exth.f* for steady-state heat transfer coefficient. It is given by

$$h = f \frac{K_{He}\, R_e P_r^{1/3}}{8 D_h} \qquad (5.11)$$

During the initial transient phase of quench initiation following the deposition of external energy, transient heat transfer always involves conductive thermal diffusion in helium around the superconducting strands. The transient components are determined by thermal diffusion in semi-infinite body. In Gandalf, effective heat transfer coefficient during the initial transient phase is a combination of the transient heat transfer coefficient and a Kapitza resistance like

$$\frac{1}{h_{eff}} = \frac{1}{h_{trans}} + \frac{1}{h_k} \qquad (5.12)$$

with

$$h_k = 200 \frac{(T_w^4 - T_h^4)}{(T_w - T_h)} \quad \text{and} \quad h_{transient} = (\frac{K_{He} \rho_{He} C_{He}}{\pi t})^{0.5} \qquad (5.14)$$

T_w is the wall temperature, T_h is the helium temperature

When the transient effect diminishes as time goes on, the steady-state heat transfer coefficient plays a dominant role.

5.1.3 *Critical current density dependence on magnetic* field *for SST-1 CICC*

The critical current density is defined as the current in the strand at which an electric field of 0.1 µV/cm appears at ambient temperature divided by the total area of the strand. For NbTi based conductors, a fitting for critical current dependence on magnetic field is given in [5.9]. This fitting is given by the following equations

$$J_c = \frac{C_0 b^{\alpha}(1-b)^{\beta}(1-t^{n'})^{\gamma}}{B} \qquad (5.16)$$

$$T_c = T_{c0}\left(1 - \frac{B}{B_{c20}}\right)^{1/n'} \qquad (5.17)$$

$$b = \frac{B}{B_{c20}(T)} \qquad (5.18)$$

$$t = \frac{T}{T_{c0}} \qquad (5.19)$$

Above equations make use of four free parameters: C_0 = normalization constant, α and β describing the dependence on the reduced field 'b' and γ describing the dependence on the reduced temperature 't'.

T_{c0} = critical temperature at $B = 0$, $n' = 1.7$ while other symbols carry usual meaning.

These equations were incorporated in Gandalf subroutine "*exts.f*" for implementing the SST-1 CICC J_c-B relation. It was also used to calculate T_c and T_{cs}. Coefficients used to match the experimentally reported data for SST-1 CICC [3.1] are:

$C_0 = 1.2 \times 10^{11}$ A T/m^2, $B_{c20} = 14.93$ T, $T_{c0} = 8.7$ K, $\alpha = 0.9$, $\beta = 1.2$, $\gamma = 1.94$

The *Jc-B* curve obtained with these coefficients matches with the experimentally reported curve, as shown in figure 5.3 [3.1]. As can be seen, the extrapolation beyond the experimental data is also available for using in different operating conditions.

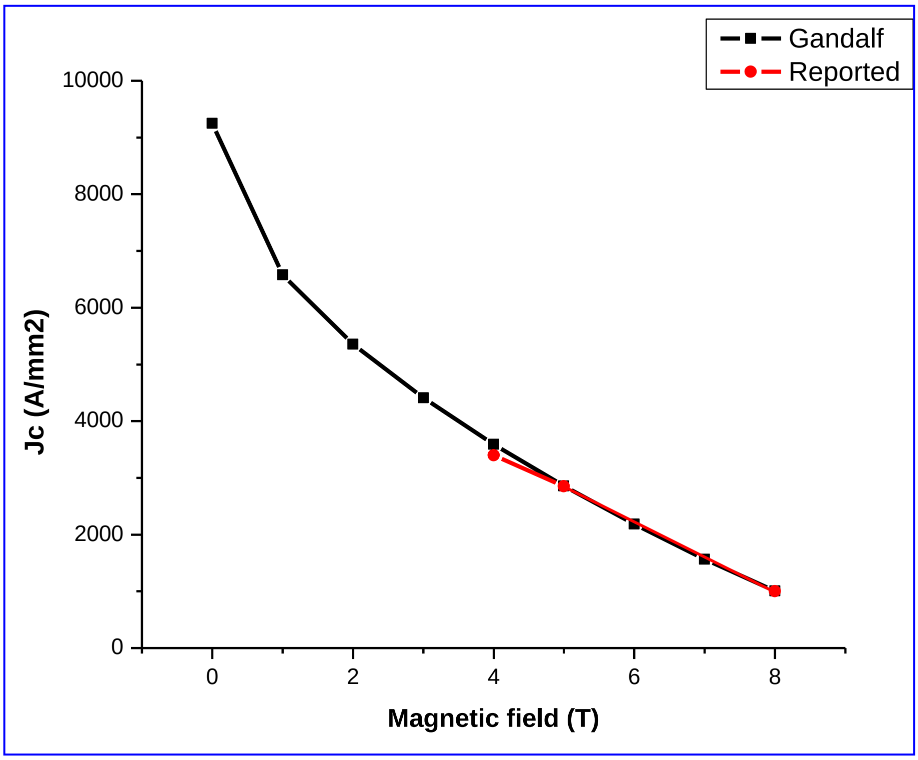

Figure 5.3: J_c-B fitting for Gandalf subroutine

5.1.4 *Cryogenic plant model for quench simulation*

Gandalf version 2.1 is coupled with flower version 2.1. Flower subroutine is useful in describing the cryogenic plant used for the cooling of magnets. This enables putting realistic initial boundary conditions in Gandalf, and it also couples with Gandalf the changes in mass flow, pressure and temperature during the execution of the program. The hydraulic model developed was a simplified model of the cryogenic plant associated with the SST-1 TF coil tests and it is shown in figure 5.4. It consisted mainly of a volumetric pump (Jun 2), inlet and outlet manifold volumes (vol 1 and 2 respectively) and the conductor length equal to the single hydraulic path length of TF coil DP. This model provided the initial condition of mass flow rate, pressure and temperature at the inlet and outlet of busbar as per the operating conditions in the coil test. The model also had the possibility to bypass helium to the quench recovery system (vol 3) by the opening of pressure relief valves (Jun 3 and Jun 4), in case the pressure rise at inlet or outlet of conductor crosses the threshold limit of 1.2 MPa.

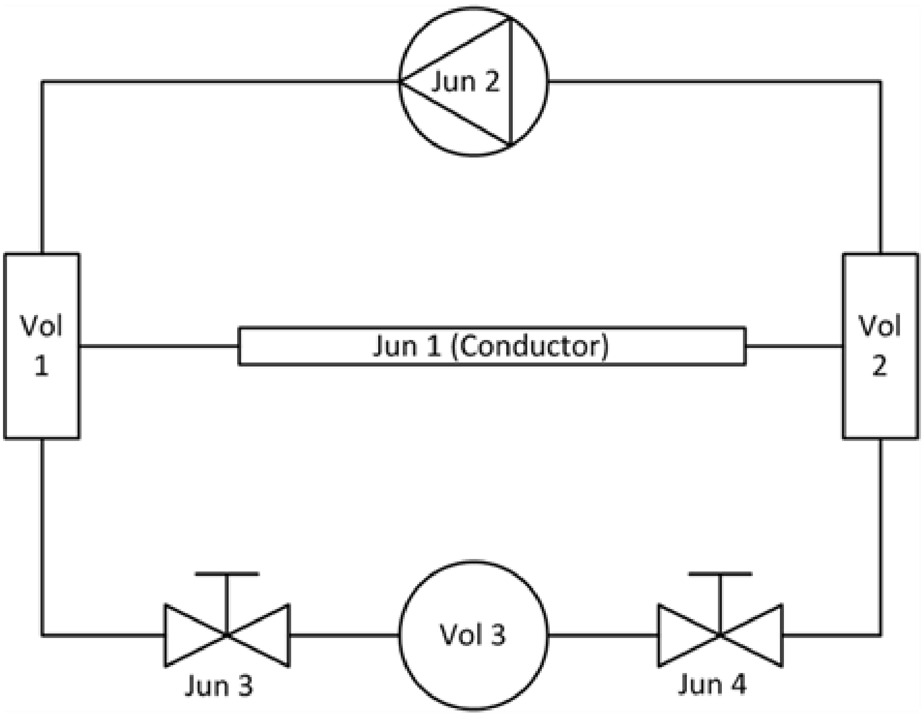

Figure 5.4: Cryogenic plant model implemented in Gandalf subroutine

5.1.5 Magnetic field variation along the conductor

The magnetic field profile is not uniform along the conductor in the winding pack. For example, in SST-1 TF magnet system the field variation on conductor is from 5.1 T maximum to less than 1 T. So there is variation of current sharing temperature along the conductor. In order to accurately model quench, it is desirable to implement in code the magnetic field variation along the conductor. Magnetic field '*B*' variation along the DP6 length was calculated using MAC code [5.10]. This spatial variation of magnetic field was implemented using '*extb.f*' subroutine of Gandalf. The Gandalf implemented magnetic field along the DP6 pancake with TF coil operating at 8960 A is plotted in figure 5.5.

It is the typical magnetic field profile obtained in Double pancake winding of D shape TF coil, where it is combination of 1/R variation along major radius R and the fact that each turn of double pancake of experiences magnetic field from Peak field at inboard side and minimum field at the outboard side.

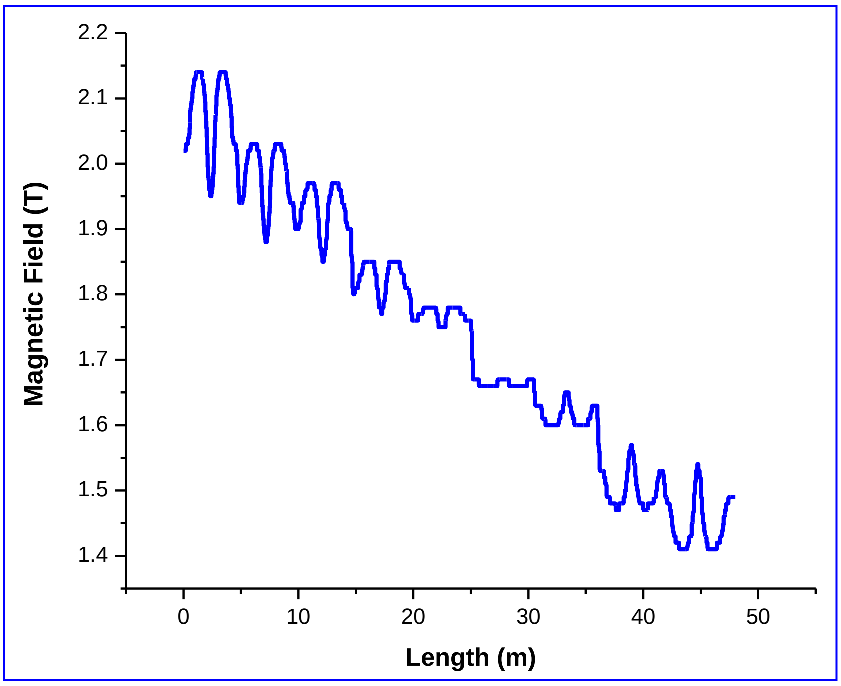

Figure 5.5: Magnetic field profile along DP6 at 8960 A during single coil test

5.1.6 *Time and space discretization*

Also, a detailed convergence study was done to gain the confidence in the numerical solutions of quench studies, which is a complex and highly non-linear problem [5.11]. The aim was to determine the time and space discretization steps such that the results are not then changed by the further refinement of these parameters. Time step of 1ms and minimum node size of 7 mm with adaptive mesh size were used in all the simulations.

5.2 TF coils test program

In a tokamak configuration, access to TF magnets for repair is very limited and its replacement may involve the partial or full dismantling of machine. So in SST-1 tokamak, before integration into machine shell, each TF magnet was cold tested for its electromagnetic, thermal-hydraulic and mechanical performances at its full operating current in either two-phase or supercritical cooling conditions. SST-1 TF coil test has the following primary objectives:

- To demonstrate the ability to carry transport current of 10,000 A in either supercritical helium cooling or two-phase helium cooling modes.
- Demonstration of joint resistances < 5 nΩ at 5 K and 10 kA of transport current for all inter-double pancake joints.
- Demonstration of the helium leak tightness of integrated magnet with leak acceptance limit of less than 1×10^{-6} Pa m^3s^{-1} at 0.4 MPa, 4.5 K supercritical helium. The integrated magnet means a TF coil with 5 inter-pancake joints, 2 busbar joints, 12 electrical breaks of inlet and outlet manifolds and all the hydraulic connections that exist inside the experimental cryostat.
- Demonstration of ground insulation resistance (between the winding pack and that of the grounded structure) greater than 1 MΩ at 4.5 K with 1 kV DC voltage.
- To study the normal zone related thermo-hydraulic aspects in supercritical helium cooling or two-phase helium cooling modes.

All 16 TF magnets have been individually tested during June 10, 2010 to January 24, 2011 in a dedicated coil test cryostat [4.4] [4.7]. All magnets have successfully demonstrated the above mentioned test objectives. During the current charging experiments of these coils, few quenches have been observed near nominal operating current of TF coils. Origin of these quenches was linked to the heat loads from coil casings and coil support structures inside the cryostat. No quenches were observed, if coil case temperature was maintained to less than 30 K during current charging.

5.3 TF coil hydraulics, sensors and diagnostics

TF coil hydraulic scheme and sensor and diagnostics during the coil test are shown in figure 5.6. As shown, helium from inlet manifold enters middle of each double pancake (DP1 to DP6). Helium exits are on inter-double pancake joints (not shown in figure). This helium is then collected in the outlet manifold (except half of DP1 and DP6). Helium of the first half of DP1 and the second half of DP6 flows through positive busbar and current lead and negative busbar and current leads respectively. Helium of these two sections is collected and fed to the radiation shield of coil casing. Helium from the outlet manifold and the TF thermal shield outlet flows back to 1.3 kW at 4.5 K helium refrigerator/liquefier system via the outlet header. Electrical isolators are used at appropriate locations to avoid electrical shorting. So when the nominal flow of 15 g/s is given at inlet header, each DP will receive 2.5 g/s and each pancake will have 1.25 g/s flow. Since TF thermal shield is fed with outlet of 2 single pancakes, it will a have mass flow rate of 2.5 g/s.

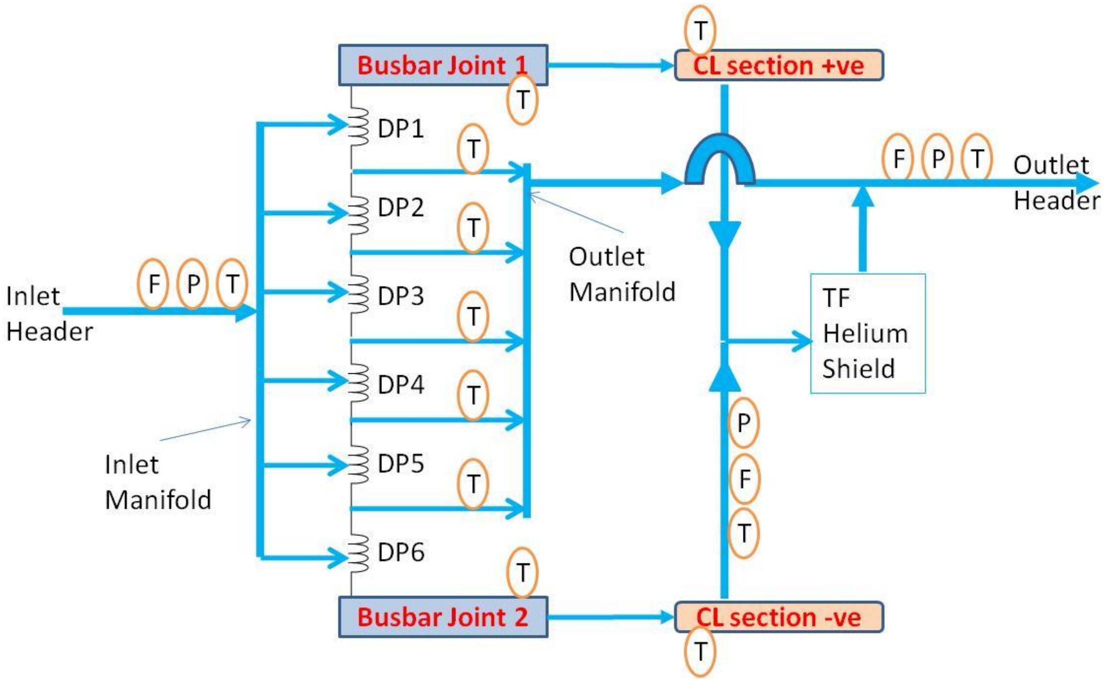

Figure 5.6: Hydraulic connections and instrumentation during TF coil test

Calibrated cernox and carbon ceramic temperature sensors were installed at inlet and outlet headers, outlet of inter-double pancake joints, busbar joints, current lead section and TF thermal shield inlet [5.12]. Calibrated pressure transmitters were placed at inlet and outlet header and TF thermal shield inlet. Calibrated venturi flow meters were placed at main inlet, main outlet and outlet of negative current lead section. Calibrated cryogenic hall probes were installed at inner straight section of TF coil to measure the magnetic field generated by the coil. For measurements of all these sensors, modular signal conditioning electronics with very high accuracy, stability and with isolation had been developed in-house [5.13]. Measurement accuracy for temperature sensors, hall probes, pressure sensors and flow meters was, respectively, ±0.1 K for 4.5 K to 80 K temperature range, 0.1%, 0.1% and ~2%.

The signals from all voltage taps, temperature sensors, mass flowmeters, hall probes and pressure transmitters were continuously acquired during the current charging experiments to study the coil behaviour under electromagnetic loads. PXI-based DAQ system was developed for coil test experiments. Its flexible GUI based application program allowed to monitor and store the data in slow rates during cool-down and warm-up and at faster rates during current charging experiments [5.14].

5.4 **TF coil #15 quench details**

SST-1 TF coil #15 was cooled using supercritical helium with inlet temperature at 5.7 K and inlet pressure of 0.386 MPa. Total mass flow rate measured at coil inlet was 27 g/s. Outlet temperature was 6.1 K and pressure was 0.338 MPa. During the current charging experiment, coil quenched during the ramp-up phase when the current was about 8960 A. When voltage tap signals were analysed, it was observed that the DP6 section of the coil had quenched. The voltage tap signals of all pancakes along with the coil current are shown in figure 5.7 (a). Changes in temperature, flow and pressure signals are shown in figure 5.7 (c) – (d), respectively.

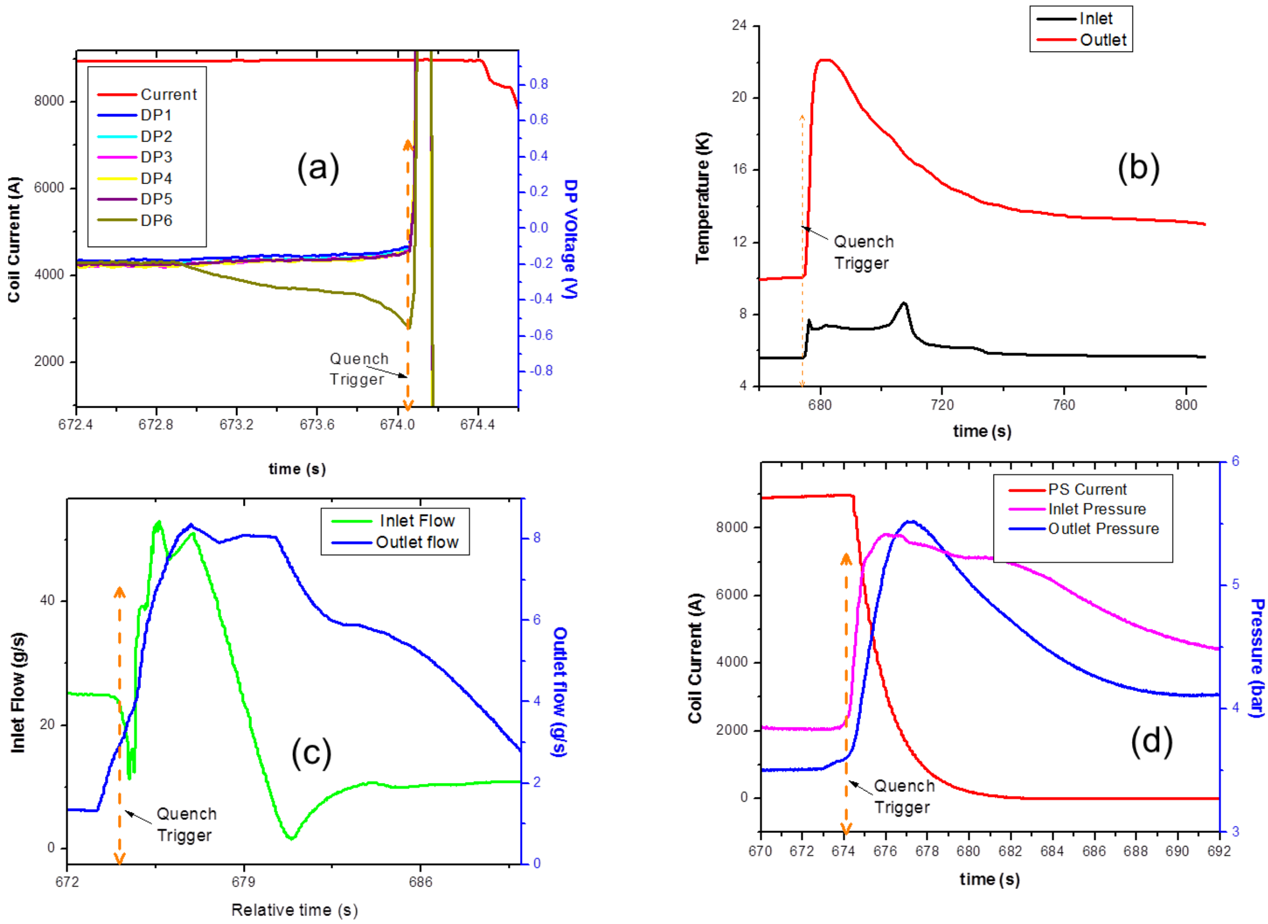

Figure 5.7: Experimental observations during TF coil #15 quench

5.5 Normal zone propagation speed estimation

As the quench was generated in the coil during the ramp-up phase, raw acquired voltage across DP6 has an inductive component in addition to the normal zone voltage (cancelled in QD hardware). This voltage will be proportional to self and mutual inductances of the double pancakes and the current ramp rate of the coil.

Total voltage developed across DP6 up to the triggering of quench protection = 556 mV

Quench detection card gain = 2

Actual voltage developed across the DP6 = 278 mV

Inductive voltage developed across each DP = 94 mV

So normal zone voltage (quench voltage) developed across DP6 = 184 mV

As the coil current ramp rate is only 20 A/s, the operating current of 8960 A is considered constant during the quench development time.

Normal zone resistance developed across DP6 = 20.53 μΩ

SST-1 CICC resistance was calculated using copper resistivity value at 15 K (RRR 100, magnetic field 2.2 T) which is 0.23 nΩ-m. SST-1 CICC resistance at above operating conditions is = 3.46 μΩ/m. So total quenched length of CICC in DP6 = 5.93 m

The quench-development time from figure 5.3 is about 1.17 s, so the average normal zone propagation speed comes out to be about 5.07 m/s.

5.6 Simulation results

As during the experiment, major temperature rise was observed at the outlet of the coil as compared to inlet, so it was expected that quench occurred near to outlet on the outermost turns of DP6. Also CICC of this turn and the innermost turn are in contact on 2 sides with the coil casings. Rests of the turns of last DP have only one side in contact with the coil casing. Since the exact location of quench initiation was not known, a parametric study was done by initiating quench in different locations of last turn of DP6. As the quench was initiated from the heat load coming from the coil casing, in Gandalf, the heat load was distributed over long lengths. The amount of heat load was taken at just the minimum required to initiate a non-recoverable normal zone. After the parametric study, by varying amount of heat load, location of heat load and length of heated zone a good match was found with the experimental results when quench was initiated by heating 1 m length between 43 m and 44 m distance from inlet. Linear heat flux of 1200 W/m with time duration of 50 ms was used in this trial. Other parameters like helium temperature, pressure, mass flow rate and operating current were as per the experimental conditions described earlier. Quench development time during the experiment was about 1.17 s after which the threshold voltage of quench detection circuit was reached and dump was initiated after a 100 ms delay time. So in Gandalf also, current was maintained at 8960-A for 1.17 s and after which current is dumped with experimental dump time constant.

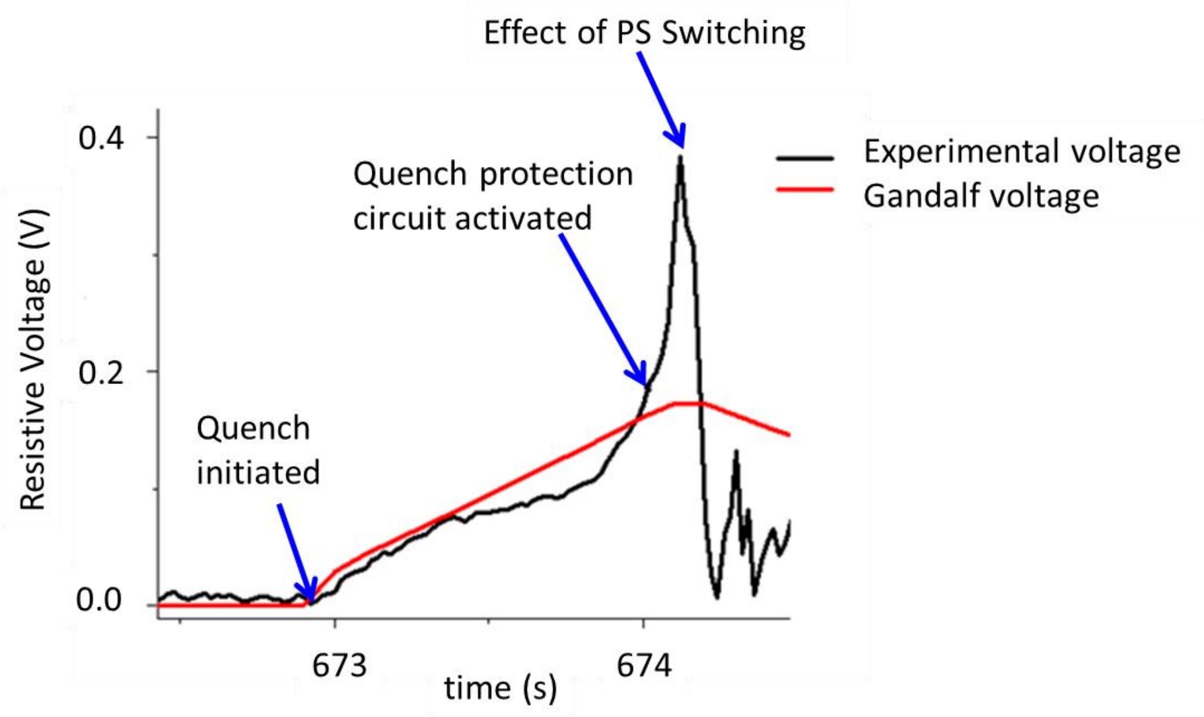

Figure 5.8: comparison of normal zone voltage during TF coil #15 quench with the Gandalf simulation results

To compare the experimental plot and Gandalf plots of normal zone voltage development, zero in the time-line of the Gandalf plot was shifted by 672.9 s. This is the time at which quench was initiated as per the experiment data. Also gain component and the inductive voltage component is removed from the experimental data. The comparison is shown in figure 5.8. The figure shows a good matching till the point marked as ‘quench protection circuit activated’. This is the point at which in the experiment, quench dump was initiated. So the rapid rise in experimental quench voltage is due to generation of large dump voltage from the switching of power supply. It is not the actual normal zone voltage, which decreases with the decaying current. In the simulation this dump voltage component is missing and current decay initiates smoothly as programmed in the Gandalf input file. So Gandalf normal zone voltage shows a reducing trend after this point.

The experimentally-observed temperature rise at the DP6 inlet and outlet during the quench was also compared with the temperature rise from simulation results. The comparison is shown in figure 5.9. Temperature is represented in terms of difference between the initial operating temperature and the observed temperatures during quench. This was done to avoid the influence of absolute error in the temperature measurement system from the experimentally measured temperature. As seen in figure 5.9, the temperature difference was initially zero and increased during the quench development. Experimentally-observed temperature difference at DP6 inlet and outlet shows similar peak values and trends to that obtained from Gandalf simulation within ±1 K. The observed differences in simulation results with experimental results are mainly because heating due to AC losses during magnet current dump are not included in simulation.

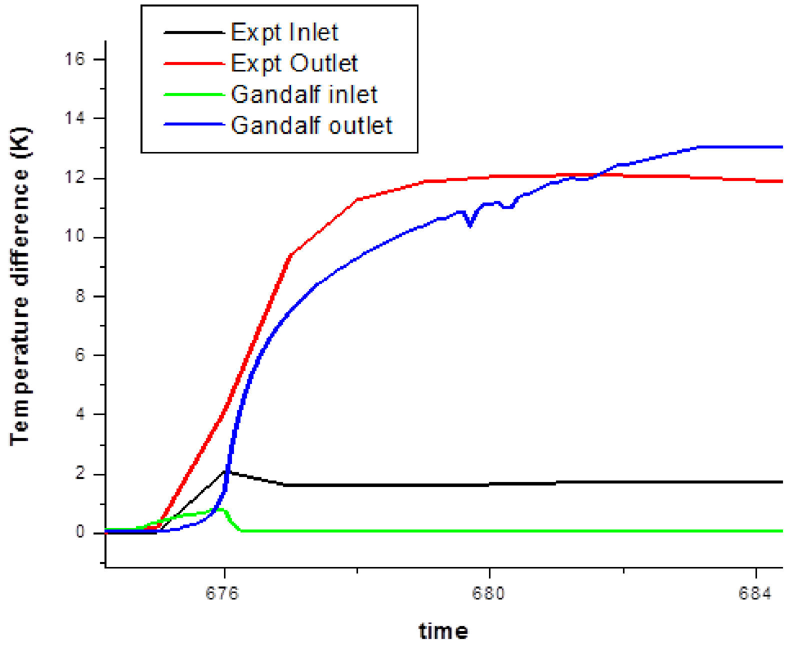

Figure 5.9: comparison of temperature changes during TF coil #15 quench with the Gandalf simulation results

The matching of inlet and outlet temperatures is an important and useful result proving the validity of the simulation. Using the results from this simulation, Gandalf post processor can be used to find out the maximum temperature reached inside the DP6, the so-called hotspot temperature.

The maximum hotspot temperature from Gandalf simulation was found to be 37 K. Since the temperature at the outlet and inlet could be simulated within ±1 K, value of hotspot temperature inside DP6 is also expected to match within similar error margin. As actual hotspot temperature cannot be physically measured by sensors in big size actual magnets like TF coil of a Tokamak, such simulation results are useful for its accurate prediction.

5.7 **Inlet flow increase following the quench**

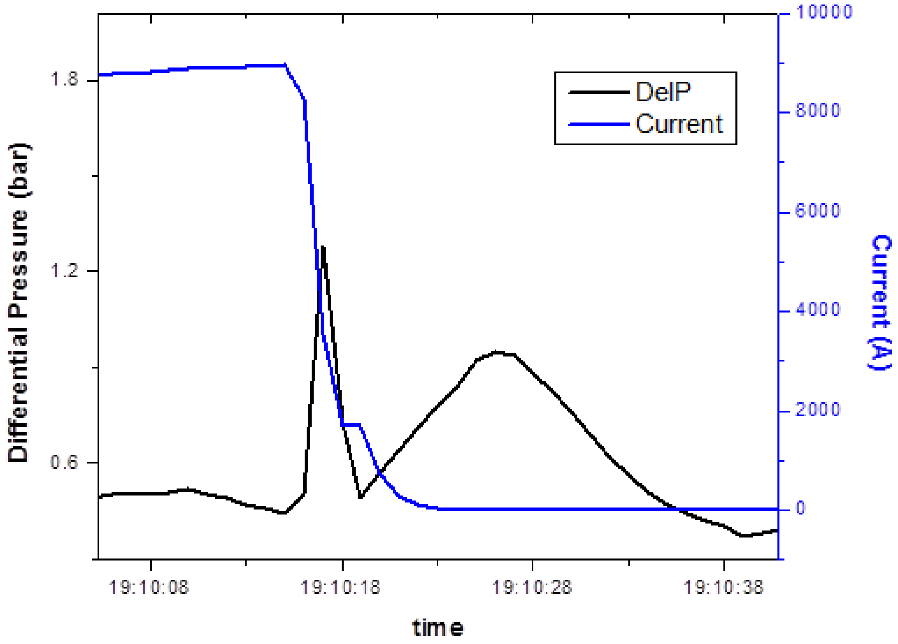

Figure 5.10: Observation of differential pressure increase after TF15 quench

A rather unexpected result of increase in inlet mass flow rate was observed in TF coil #15 quench as shown in figure 5.7 (b). This is a new observation, as in general flow reduction following quench have been reported or the results of simulations have predicted it [5.15–5.17]. Following the quench, initially inlet flow decreased slightly, and then it increased substantially. We tried to find the reason for this. When data from the cryogenic plant was analysed it was found that during quench propagation period, difference between inlet and outlet pressure of the coil initially decreased slightly, and then it increased substantially. Probably due to quench which occurred near the outlet, as explained in later sections, the outlet pressure started increasing. In order to maintain the pressure difference across the load constant, the plant also started increasing the inlet pressure. This response of the plant along with the thermal hydraulic effects of quench led to pressure fluctuations across the coil. As the pressure difference is closely linked to the mass flow rate in the coil, increased pressure drop as plotted in figure 5.10, led to increase in mass flow rate of coil initially and then it returned to its normal value after about 20 s. This behaviour was observed in a few other coils as well during the coil test. A database has been generated of the level of these fluctuations and the time taken by these fluctuations to reach the inlet/outlet sensors. It will be used to generate the threshold limits for secondary quench detection and will be discussed in detail in chapter 8.

5.8 **Predictive quench simulation for assembled TF magnet system in SST-1**

The code modified for TF coil #15 quench simulation has been used to do the predictive quench simulation with all 16 TF coils assembled in series in SST-1 machine shell. It was done to find out the hotspot temperature within the TF coil following a quench with the TF magnet system under operation. The main difference between a stand-alone coil operation and assembled TF magnet system operation will be in the background magnetic field. In single-coil operation, at the operating current of 10,000 A, the expected peak magnetic field is 2.2 T whereas in assembled magnet system it will be 5.1 T at the same operating current. This is due to superposition of magnetic field from neighbouring TF coils. Also dump time constant for assembled TF magnet system will be 12 s as opposed to the 1.7 s dump time constant used for single coil test.

So keeping all other input parameters and subroutines of Gandalf similar to that used for TF coil #15 quench simulations, the magnetic field distribution and dump time constant for assembled magnet system was implemented in the code. The temperature profile across the quenched coil was obtained from Gandalf post processor and it is plotted in figure 5.11. As observed, the maximum hotspot temperature is found to be about 118 K. This is under the design temperature limit of 150 K. This result has confirmed the suitability of SST-1 TF coil quench detection and protection system design parameters like threshold voltage, delay time and dump time constant.

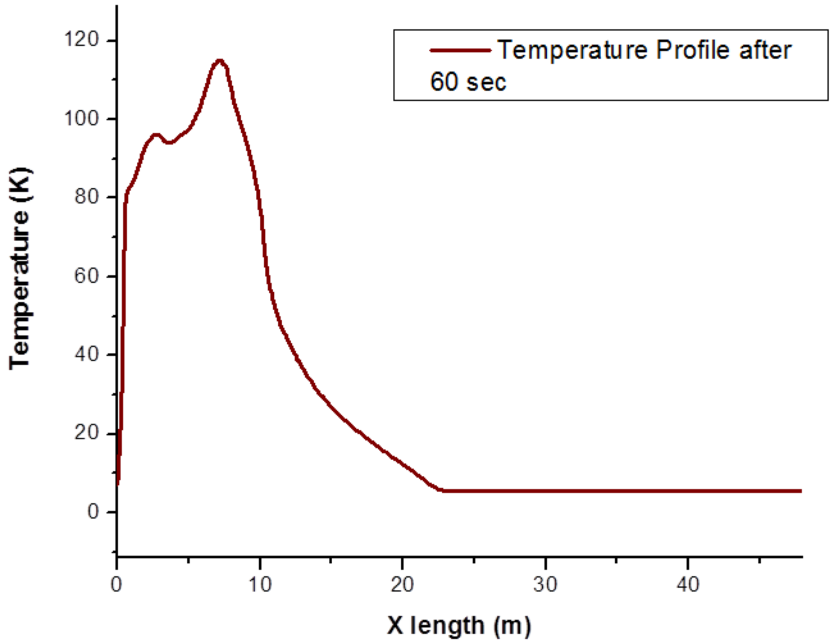

Figure 5.11: Temperature profile within a quenched TF coil pancake with the assembled TF magnet system operating at 10000 A

5.9 Conclusion

Quench observed in TF coil #15 coil was analysed to estimate the normal zone propagation speed. This quench was simulated using 1-D code, after suitably modifying its subroutines for SST-1 CICC. Simulation results have given detailed information about the hotspot temperature and the normal zone propagation speed. Reasonably good agreement with the experimental data has been found in the simulated temperature development. The normal zone propagation speed estimated from the normal zone voltage development time in simulation and in the experiment also showed good agreement. These results were used to make predictive analysis for the assembled TF magnet. These results are reported in [5.18]. Results of these analyses confirm the suitability of the quench detection and protection algorithms of SST-1 TF magnets.

6. Quench characterization and thermo-hydraulic simulation of TF magnet busbar

During the coil test campaigns TF magnets were connected to a pair of conventional vapour-cooled current leads through a pair of CICC busbar of about 1.8 m lengths inside the test cryostat. Quenches observed in these busbar sections have been experimentally found to have different thermo-hydraulic behaviour as compared to quenches in double pancake windings of TF magnets. One such quench has been analysed in detail and analysis results have been used to predict the safe operation regime of TF magnet system busbar during actual tokamak operation. Steady-state thermo-hydraulic analysis of busbar has also been carried out to investigate the optimum helium mass flow rate and operational temperature margins during SST-1 tokamak operations. Details of these analyses are given in this chapter.

6.1 TF Magnet Busbar in TF coil test cryostat

The test cryostat was made of three parts; the bottom-dish end, middle cylindrical section and top-dish end. The current leads were permanently integrated with the top dish end. During test preparation, each TF coil was integrated with the top dish end. Current leads were connected to magnet ends with busbar of about 1.8 m length. Demountable supports were designed using SS304 angles and glass fibre plates to support the busbar against electro-magnetic forces during coil current charging experiments as shown in figure 6.1.

Demountable supports were designed to facilitate the repeated installation and removal of supports after coil test completion. Due to limited space inside the cryostat, lengths of supports were short, leading to a constant heat load onto the busbar. The amount of this heat load was directly dependent on the coil casing temperature; which leads to quench of busbar in some current charging experiment. So later on, coil casing temperatures near busbar supports were ensured to be less than 30 K before initiating the current charging experiments.

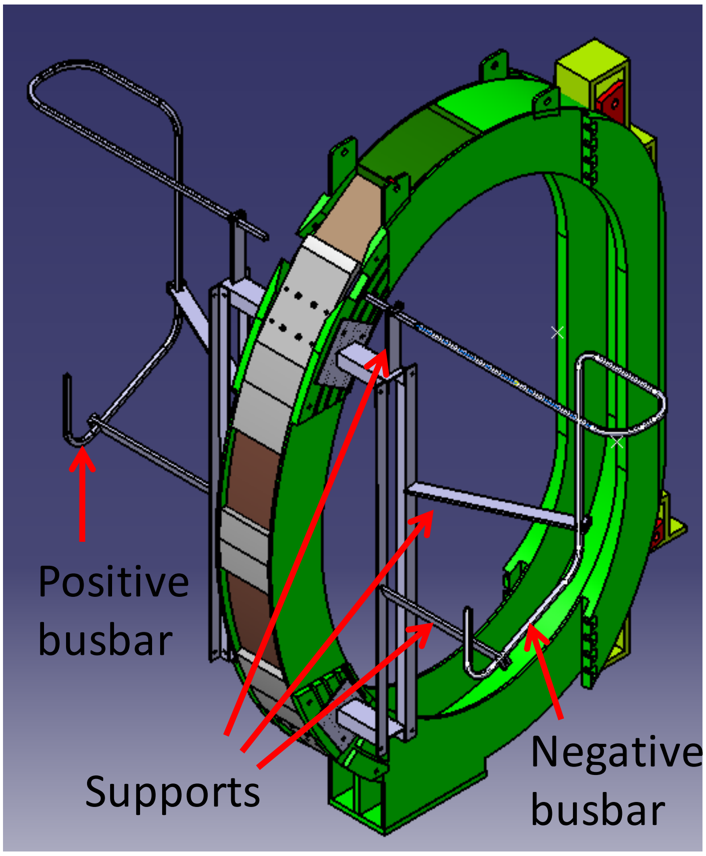

Figure 6.1: TF Coil busbar and supports in test cryostat

6.2 **Magnetic field on current busbar**

In general in a tokamak environment, the magnetic field outside the torus is low. So busbars are usually in a low self-magnetic field. In single coil tests, the magnetic field at the busbar location was higher than the self-field. This magnetic field was estimated by using the MAC code. The plane of measurement for the magnetic field near the busbar region and its results are shown in figure 6.2. The estimations showed that a peak magnetic field of 1 T was acting on both positive and negative busbars.

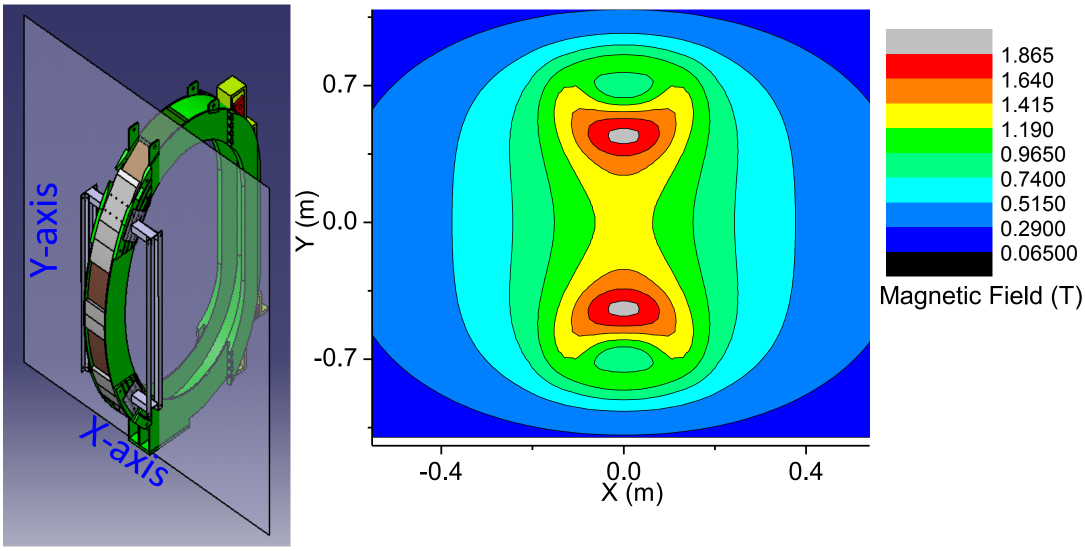

Figure 6.2: Magnetic field profile in the busbar region during single coil test

6.3 Quench detection of busbar in coil test campaigns

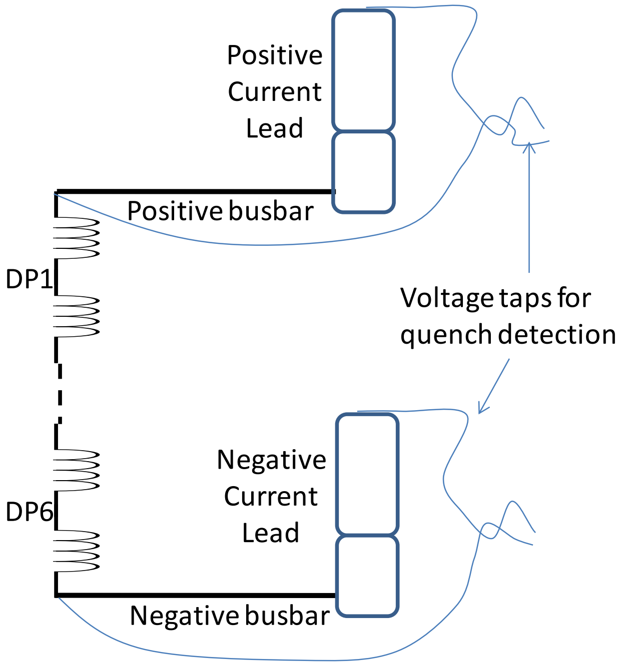

Figure 6.3: Location of voltage taps for quench detection during single-coil test

The voltage taps installed across the busbar coil joints and across the current leads were used for quench detection in the single coil test program. This is shown schematically in figure 6.3.

As shown in this figure, combined voltage drop across positive busbar and positive current lead section was compared with the voltage drop across negative busbar and current lead section. This ensured the cancellation of inductive voltages across the busbar during magnet charging and also the cancellation of the resistive drops across the two current leads. As the quench detection card had the gain of 2, when the difference voltage between compared sections became greater than ± 300 mV for more than 100 ms then the quench trigger was generated by the quench detection hardware system.

6.4 TF coil #4 busbar quench analysis

SST-1 TF coil #4 was cooled using supercritical helium with inlet temperature at 5.1 K and Inlet pressure of 0.4 MPa. Total mass flow rate measured at inlet of coil was 23 g/s. Outlet temperature was 6.5 K and pressure was 0.345 MPa. During the 8 kA current charging shot, in the current flat top, quench detection system triggered the quench protection system.

When the voltage tap signals were analysed it was observed that negative busbar section of the coil had got quenched. The difference of voltage between two busbars and current lead section is shown in figure 6.4 along with operating current of the coil. As the difference signal crossed the 300 mV level the quench detection circuit had generated the quench trigger. The difference voltage has DC offset of about -185 mV, due to the non-symmetric voltage drops across the positive and negative current leads. During the 8 kA flat-top operation, negative busbar voltage was found to increase, which increased the difference quench voltage beyond the quench threshold voltage leading to the triggering of quench detection circuits. The quench protection system activated the DC current breaker which dumped the coil current across a dump resistor of 16 mΩ.

It can be deduced from this voltage development that a normal voltage of 61 mV was generated in this quench (deduced from observed voltage is 122 mV divided by electronic card gain of 2) in about 5.3 s. Considering the SST-1 CICC resistance at about 15 K, the total busbar length of 1.8 m was quenched. This gives an average normal zone propagation speed in the range of 0.34 – 0.4 m/s. This is found to be quite low as compared to about 5 m/s observed in TF coil double pancakes. In order to understand the reason of this quench initiation and its relatively slow normal zone propagation mechanism, it was simulated using the Gandalf code. This code has been bench marked earlier to simulate SST-1 TF coil in chapter 5. The input parameters for Gandalf such as mass flow rate, pressure, temperature, operating current and background magnetic field etc. were taken from experimental details of TF coil #4 provided earlier. SST-1 CICC specifications, friction factor and heat transfer correlations, hydraulic model used in the code are similar to that used earlier in chapter 5.

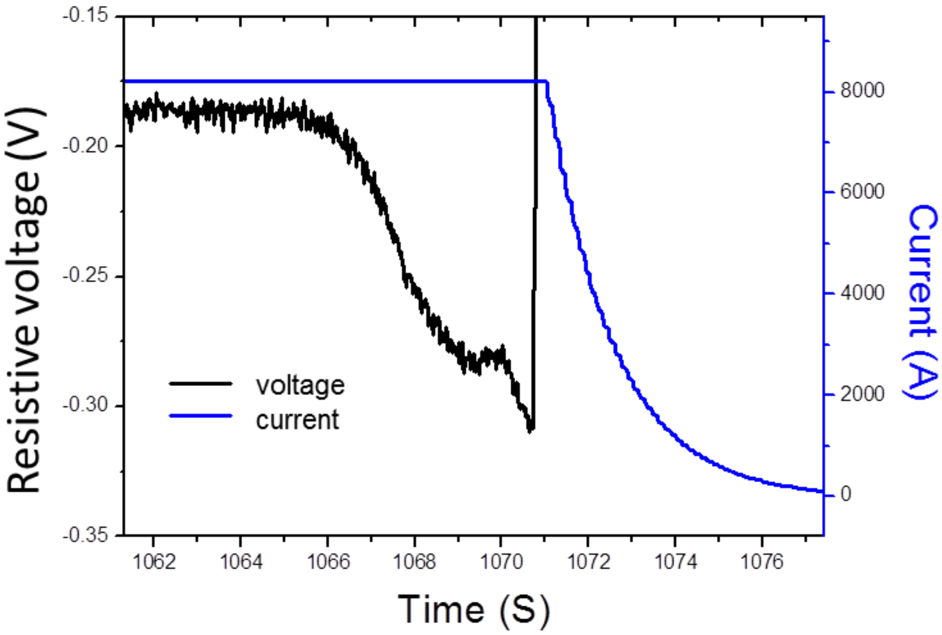

Figure 6.4: Resistive voltage development during TF coil #4 busbar quench

6.5 Simulation results

In simulation trials, the quench was generated in the busbar section by applying a square wave-shaped heat pulse of varying magnitudes and varying lengths as well as on different locations along the entire length of conductor. The normal zone voltage development was then compared with the experimental observations of normal zone voltage shown in figure 6.4. After several iterations, it was found that when a heat pulse is applied in a very small section of 10 mm at the beginning of conductor, the experimental and simulation voltage profiles match well. This position corresponds to a short support location of the busbar just after the coil to busbar joint. For comparison of two plots, the DC offset of -185 mV was added to the simulation voltage. Its time reference also matched with the experimental time. This comparison is shown in figure 6.5 and its matching is found to be acceptable. The distinct changes in slopes observed in Gandalf simulation plot coincides with the entire 1.8 m of busbar being quenched. Since the total voltage across busbar has not reached the quench threshold voltage level of quench detection card, continuous joule heating increased the conductor temperature and hence its resistance, till the voltage level across busbar crossed the threshold voltage limit.

During the experiment, no significant change in temperature was recorded. This is because at the busbar outlet, helium was fed to the current lead section, which had large supercritical helium volume. Temperature sensor was installed on outer stainless steel can of supercritical helium section of current lead. This section is also thermally shorted to LHe section of current lead which is continuously filled with fresh liquid helium from the plant during current charging experiments. Similarly mass flow rate and pressure changes experimentally observed during this quench were found to be small.

One reason for observations of lower normal zone propagation speed as compared to those in the DPs of TF coils is presence of lower background magnetic fields on busbar. Lower magneto-resistance of copper stabilizer then generates lower joule heating. Another reason is the absence of transverse quench propagation mechanisms in a single-turn busbar compared to that in tightly wound double pancakes inside of TF coil. Incidentally, in the Gandalf code simulation, the transverse conduction of heat is not modelled which contributed to a good matching of the experimental observations and the simulation results. Good matching of these results have additionally validated the predictions of SST-1 coil test team that the heat load coming from short length supports can lead to quench during coil test experiments.

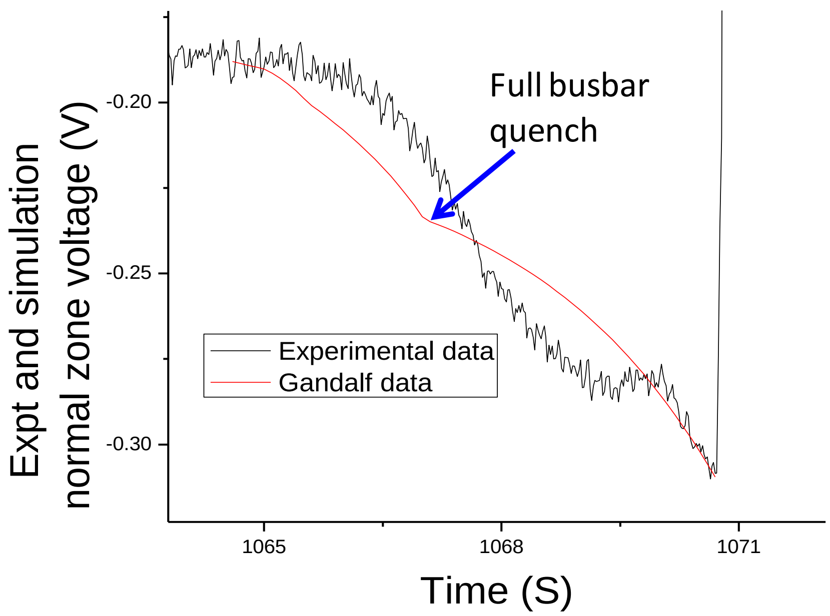

Figure 6.5: The comparison of experimental and simulation normal zone voltage

6.6 Recommendation for SST-1 TF magnet feeder quench detection

It was realized from the experimental observations that the quench propagation speed in busbar can be very low as compared to the TF coils. Thus, in the case of quench threshold voltage being similar to that set for the TF coils, it would take longer to reach the threshold voltage level, which would lead to higher hotspot temperature and probable insulation degradations. So quench threshold voltage levels must be set to lower values for the busbar. A threshold voltage level of 52 mV is recommended, which corresponds to 2 m of quenched length of SST-1 CICC at 0.44 T, for 10 kA operations. Total length of the SST-1 TF magnet busbar is about 10 m.

Another recommendation was related to the locations of voltage taps. If the voltage taps are installed as shown in figure 6.3, then current lead DC voltage drop will always be present in busbar voltage signals. This, in the case of unequal current lead voltage drops, would give non-zero difference voltage even with no quench in the busbar. Thus separate measurements of current lead and busbar voltages were recommended and it has been subsequently implemented in SST-1. This new scheme is shown in figure 6.6.

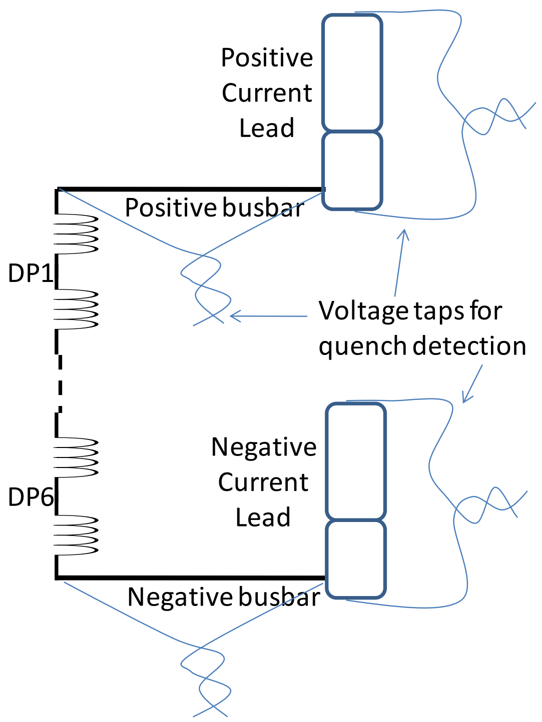

Figure 6.6: New voltage tap locations for current leads and busbar

During the engineering validation phase of the assembled SST-1 TF magnets, a quench was observed in the TF busbar section. This quench was triggered by a vacuum failure event in the TF busbar duct, leading to quenching of both positive and negative busbars. The voltage signals acquired from the new voltage tap scheme of figure 6.6 have given an unambiguous quench trigger for this event. These voltage signals are shown in figure 6.7. Once the difference voltage between busbar reached the threshold value, the quench trigger was generated after the threshold time delay.

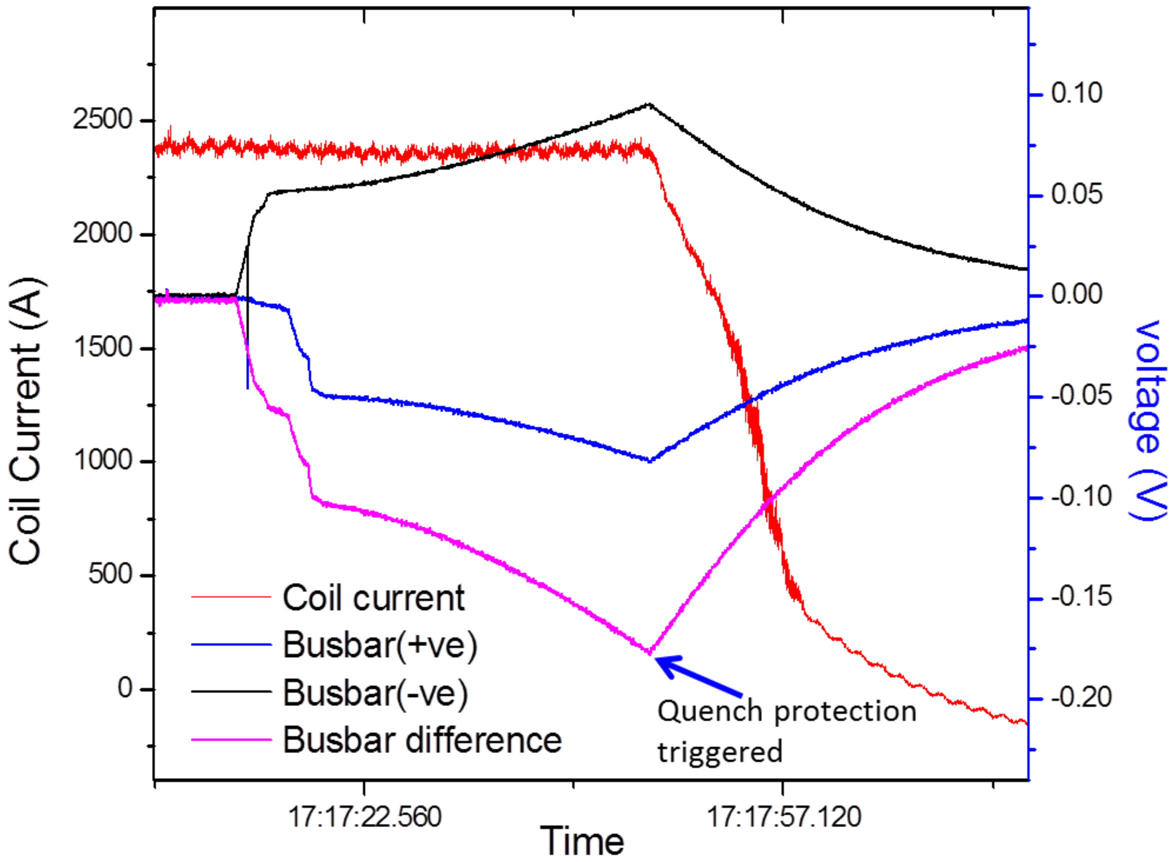

Figure 6.7: SST-1: Detection of quench in TF magnet busbar

6.7 Thermo-hydraulic simulation of Busbar in assembled TF magnet system

SST-1 TF magnet current feeder system’s main components are shown schematically in figure 6.8. TF magnet busbars terminate in a chamber known as current lead assembly chamber (CLAC). CLAC and cryostat are connected to each other with stainless steel ducts known as TF duct. The TF duct has liquid nitrogen-cooled thermal shields to reduce the radiation heat load on to the superconducting busbar. All throughout the length, busbar are supported on the thermal shield by using several glass fibre supports (G 10 CR) at a spacing of 600 mm. CICC of the busbar is similar to that used in SST-1 TF and PF magnets. Both positive and negative TF busbars are about 10 m in length and have two joints each. One joint is between the Current lead and busbar and the other is between the busbar and the magnet. Joint with current lead is a bolted lap joint and joint with magnet terminal is a soldered lap joint. Vacuum barrier with ceramic isolator and stainless steel bellows are installed closer to magnet side to isolate the cryostat vacuum with CLAC vacuum. Busbars are cooled from current lead side joint location. The steady-state heat loads acting on the TF magnet system busbars mainly comprised of conduction from supports and vacuum barriers, radiation, residual gas conduction (RGC) and joule heating from joints. Actual values of these heat loads have been calculated. For radiation heat load calculation, the entire busbar is considered at 4.5 K and thermal shield temperature is considered as 85 K. Emissivity of cold and warm surface is assumed as 0.2 and 0.3 respectively. Interspace vacuum pressure of 2 x 10-5 mbar is used for residual gas conduction heat load. For estimating conduction heat load from supports and vacuum barriers, thermal conductivity integral values between 4.5 K and 85 K of glass fibre and ceramic and actual geometrical dimensions have been used. Joule heat load estimations have been done using the joint resistance value of 5 nΩ for the bolted joint between current lead and busbar and 1 nΩ for the soldered joint between magnet terminals and busbar. The heat load estimations are summarized in table 6.1.

It is found that the heat loads from supports, vacuum barrier and joints are dominant as compared to other heat loads. A total heat of 6.46 W is estimated to be acting on each busbar during 10000 A current operations of TF magnets. In order to compensate for uncertainty in actual contacts from supports etc. and other simplifications or errors in estimations, a safety factor (SF) of 1.5 is used and the total heat load is taken to 9.7 W for all calculations.

Table 6.1: Steady-state heat load acting of TF busbar

Radiation (W)	RGC (W)	Supports (W)	Vacuum barrier (W)	Bolted joint (W)	Soldered Joint (W)	Total (W)	Total with SF of 1.5 (W)
0.003	0.025	3.89	2	0.5	0.05	6.468	9.7

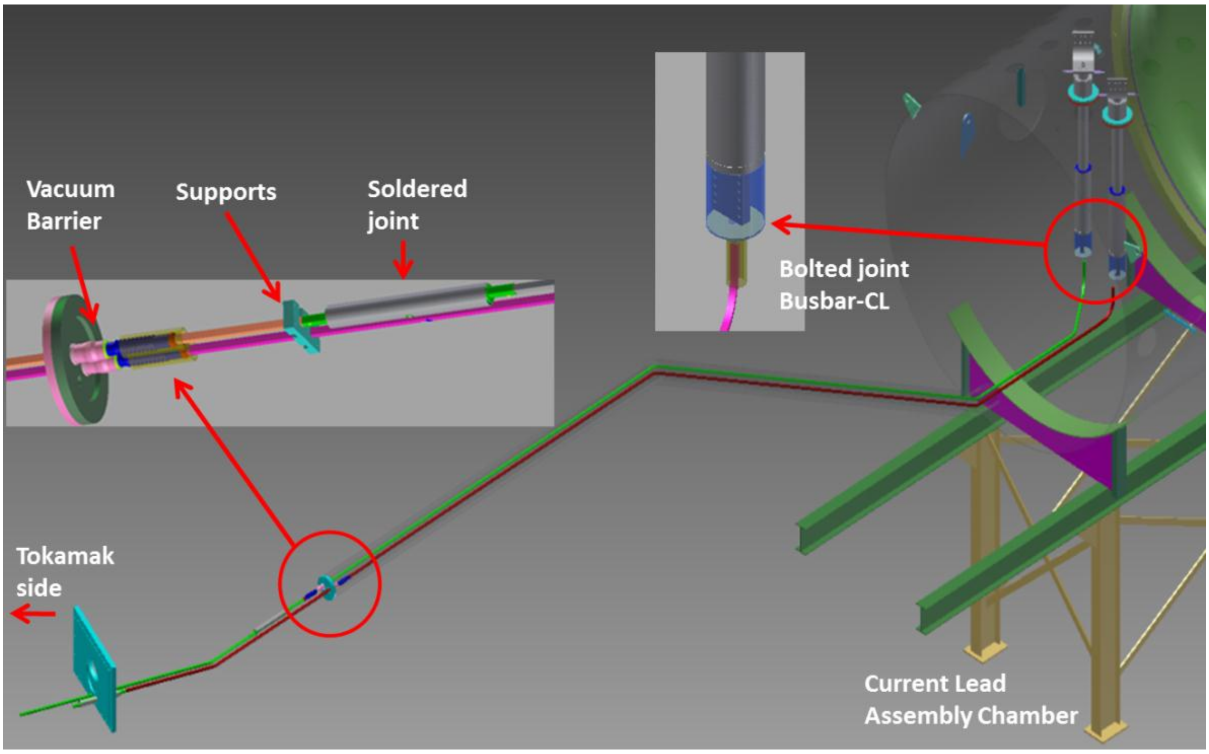

Figure 6.8: SST-1 TF current feeder schematic

Thermo-hydraulic analysis of busbar has been done using code HESS [6.1]. It is a code for steady-state analysis of helium cooled conductors. Heat load from different components as per table 6.1 were mapped at different locations on the 10 m length of busbar conductor as per the actual locations of these components in the current feeder system. Under the action of these heat loads, busbar pressure drop and its outlet temperature were estimated for different mass flow rates under steady-state conditions using HESS. The results are shown in Fig. 6.9. As seen, the pressure drop is in the acceptable range for the entire flow range of 0.4 g/s to 1.5 g/s. Thus a suitable mass flow rate can be selected purely on the basis of required temperature margin during SST-1 operation.

The maximum field acting on TF busbar, with all TF and PF magnets fully charged, is estimated to be about 0.44 T near the tokamak side. At other locations, busbar will be in the self-field of 0.22 T. Near the current lead side, where busbar bends at an angle of 135 degrees, self-field is enhanced to 0.28 T. Considering the worst case scenario, the entire busbar is considered in a background magnetic field of 0.44 T. At this magnetic field and 10000 A operating current, current sharing temperature of SST-1 CICC is calculated to be about 7.7 K [6.2]. As seen in figure 6.9, outlet temperature is 5.83 K at the mass flow rate of 1 g/s which gives a temperature margin of 1.9 K. This is acceptable and so this mass flow rate is recommended for TF busbar. Two dedicated Venturi mass flow meters have been installed on these paths to monitor the flow and provide necessary feedback to the helium plant for controlling the flow rate close to 1 g/s.

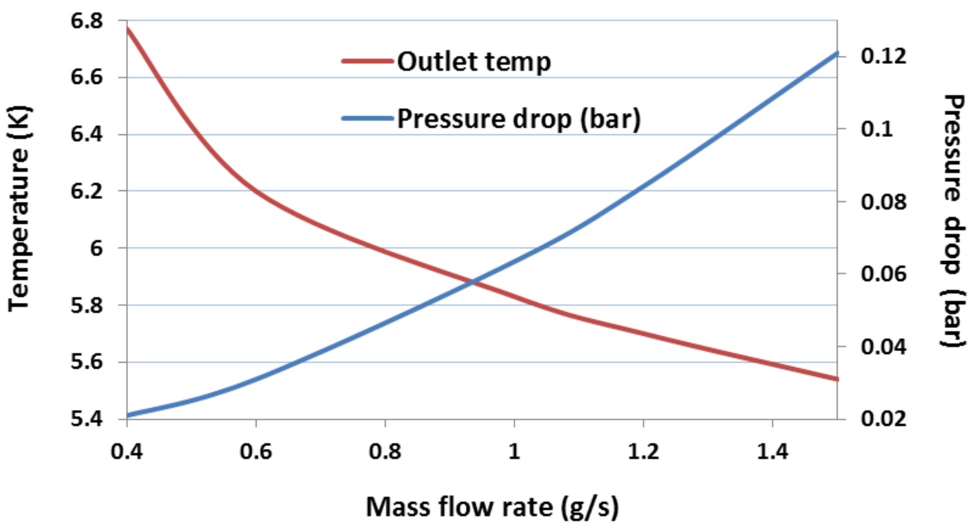

Figure 6.9: Pressure drop and outlet temperature for different mass flow rates

6.8 Conclusion

Quench observed in busbar during the single coil tests of SST-1 TF magnet has been analyzed in detail and quench propagation speed has been estimated. A propagation speed in the range of 0.34 – 0.4 m/s has been observed. This speed is quite low when compared to those observed during TF coil quenches involving DPs. These fundamentally different characteristics are primarily attributed to a lower acting background field on busbar and absence of transverse thermal conduction like in double pancake windings. Such slow quench propagation has been successfully simulated with the Gandalf code. A steady-state thermal load of about 10 W has been calculated to be acting on actual SST-1 TF magnet busbars. A mass flow rate of 1 g/s will be sufficient to compensate this heat load and will give a temperature margin of 1.9 K, which ensures a safe and cryo-stable operation of SST-1 TF magnets. These analyses results have been reported in [6.3].

7. CICC Design study

Design of CICC for fusion magnet application involves optimization of several parameters like strand design, conductor sizing, void fraction, jacket material and jacket thickness [7.1 - 7.3]. These parameters in turn depend on operating magnetic field and current requirements, plasma operation scenarios and magnet current ramp rate requirements, etc. The objective is to get an optimized design of a CICC such that the magnet should not quench during any planned tokamak operational scenarios. And if quench occurs, CICC should be able to bear the effects of quench. While CICC design is a very vast topic for the scope of this work, optimization of stabilizer area in strands of CICC is discussed in this chapter. It has a direct impact on the stability and the quench characteristics of CICC [7.4]. Generally, a high RRR copper and aluminium are the preferred choice for stabilizer. A NbTi/Cu based, high current and high field virtual conductor is used for this case study using Gandalf.

7.1 Copper to Superconductor ratio in Strands of CICC

7.1.1 The virtual conductor

A virtual conductor was considered for this case study. Its operating current is 26.5 kA and operating peak magnetic field is 6.5 T. The CICC cross-sectional area, void fraction (helium area), inlet temperature mass flow rate and jacket thickness are fixed for this CICC. The aim is to find the suitable copper to superconductor NbTi ratio (Cu: SC) in the area allotted for strands in the CICC. This ratio decides the quench behaviour (from copper stabilizer area) and the stability margin (discussed later) of the CICC. Gandalf code is used as a tool to study this critical optimization.

It is a square conductor of side 29.1 mm (including 3.5mm thick SS304L jacket) with following allocated space for different components and major operating conditions:

Helium section = 161.3 mm^2

Composite section (NbTi + Copper): 287 mm^2

Strand diameter: 0.712 mm

Inlet pressure = 0.6 MPa

Mass flow rate = 1 g/s

Inlet temperature = 4.6 K

Insulation thickness = 2 mm

7.1.2 Stability

Superconducting magnets experience a wide spectrum of disturbance (external energy deposition) during tokamak operations. Mechanical energy release by wire movement, insulation de-bonding or epoxy cracking, AC losses and plasma disruptions are some examples of disturbances of different magnitude, timescale and spatial distribution [3.2]. The maximum energy which could be absorbed by strands without getting quenched is known as stability margin 'E_c'. In this study using Gandalf, heat will be deposited on different conductor lengths and for different time scales. Stability margin will be calculated from the maximum heat energy absorbed by CICC without getting quenched, using equation 7.1. It is generally expressed in mJ/cc of the composite. The disturbances selected for stability study should represent the typical disturbance expected on the magnets.

$$E_c = \frac{Q}{A_{cu}+A_{SC}} \times \Delta t \qquad (7.1)$$

where Q = total heat deposited in Watt

A_{Cu} = Copper Cross section in NbTi strands (m^2)

A_{SC} = Superconductor cross section (m^2)

Δt = time duration of disturbance of square shape (s)

7.1.3 *Classical model of stability*

Insufficient stability margin and large disturbances were the main reasons of failure of earlier magnets. In 1965 Stekly and Zar gave the concept of cryostability [7.5]. Cryostability was achieved when the composite temperature with the full operating current flowing in the stabilizer was below the critical temperature of the superconductor. It was represented in terms of Stekly criterion $\alpha < 1$ and

$$\alpha = \frac{\rho I^2}{h P_w A (T_c - T_{op})} < 1 \qquad (7.2)$$

Where

h = steady-state heat transfer coefficient, P_w = wetted parameter of conductor, A = Stabilizer cross-section, I = current in the conductor, ρ = matrix resistivity, T_c = critical temperature, T_{op} = operating temperature

This concept of cryostability is not applicable for CICC as the helium available as heat sink is not infinite, rather it is limited and its temperature increases during the disturbance. Application of this criteria leads to requirement of very high copper area in the CICC strands.

Numerical code Gandalf is more suitable for estimating the stability of CICC as exact helium volume is used in calculation and it treats the temperatures of helium, strands and jacket separately and the energy balances are coupled via heat transfer coefficients at the contact (wetted) surfaces. CICC are designed as metastable with ability to operate at specified nominal current density with an ability to withstand the specified spectrum of external disturbances.

7.1.4 *Copper to superconductor ratio*

The subject of ratio of copper stabilizer and superconductor in CICC strands, known as Cu: SC ratio is an important design parameter of CICC. It has a direct impact on the stability and the quench protection characteristics of the CICC. As discussed in chapter 3 of this thesis, if external disturbance raises the strand temperature above current sharing temperature T_{cs}, joule heat generation is initiated. The available temperature margin for operation is the difference between the operating temperature and T_{cs}. Also, as described in equation 3.3, T_{cs} depends directly on the section of superconductor in the strand, so available temperature margin depends on the section of superconductor.

It is known that copper in the conductor plays an important role in reducing the maximum hotspot temperature. If copper area is more, a higher discharge time τ_{dis} can be allowed for the similar maximum hotspot temperature. Higher discharge time helps in reducing the dump voltage as lower value dump resistor could be selected.

In the study of the virtual conductor with a fixed conductor cross-section and a fixed load line we will study the effect of variation of copper and superconductor ratio using Gandalf.

7.2 Different cases studied using Gandalf

In this section, a virtual conductor is studied with the total NbTi and copper composite section fixed to 287 mm^2. Stability and protection aspects were studied for four Cu:SC ratios to cover the wide range from less than 1 to about 7. The specific ratios studied are given in table 7.1.

Table 7.1: Different Cu: SC ratio used for stability studies

Sr. No.	S_{Cu} (mm^2)	S_{NbTi} (mm^2)	Cu:SC ratio
1	252.1	34.6	7.28
2	239.2	47.5	5.03
3	212.2	74.5	2.84
4	127	160	0.79

The time step and mesh size were finalized after detailed convergence studies. Table 7.2 gives the exact details of different parameters used in Gandalf.

Table 7.2: time and mesh sizes used in Gandalf

Parameter	100 ms on 1m	10 ms on 1 m	1 ms on 0.01 m
Total conductor length in simulation	4 m	4 m	1.2 m
Time step	0.1 ms	0.01 ms	0.001 ms
Mesh size (length)	1 mm	1 mm	0.03 mm

7.3 **Results of the stability study**

Three disturbances of 100 ms on 1 m, 10 ms on 1 m and 1 ms on 10 mm were selected for stability study as these represent the typical disturbances related to plasma disruption, AC losses and wire movements in tokamak magnets. The total conductor lengths for simulation were chosen to be sufficiently longer to avoid the cable end effects. SST-1 CICC *Jc-B* relationship was implemented in Gandalf. The magnetic field was uniform over the conductor length. The input data for the Gandalf code was generated from the details of the virtual conductor provided earlier. Different amount of heat energy were put on the heated lengths of the conductor and iteratively the maximum allowable heat deposition was calculated for all the three cases seen earlier. The available temperature margins for these cases were also found out from the code. These results for three cases are given in table 7.3 to 7.5.

Table 7.3: Results of 100ms disturbance on 1 m length

T Margin (K)	A_{NbTi} (mm^2)	A_{Cu} (mm^2)	Cu:SC	Stekly Parameter	Stability margin (mJ/cm^3)
0.8	34.6	252.1	7.28	0.59	166
1	47.5	239.2	5.03	0.62	209
1.2	74.5	212.2	2.84	0.70	237
1.4	160	127	0.79	1.18	261

Table 7.4: Results of 10 ms disturbance on 1 m length

T Margin (K)	A_{NbTi} (mm^2)	A_{Cu} (mm^2)	Cu:SC	Stekly Parameter	Stability margin (mJ/cm^3)
0.8	34.6	252.1	7.28	0.59	211
1	47.5	239.2	5.03	0.62	238
1.2	74.5	212.2	2.84	0.70	249
1.4	160	127	0.79	1.18	91

Table 7.5: Results of 1 ms disturbance on 0.01 m length

T Margin (K)	A_{NbTi} (mm^2)	A_{Cu} (mm^2)	Cu:SC	Stekly Parameter	Stability margin (mJ/cm^3)
0.8	34.6	252.1	7.28	0.59	1414
1	47.5	239.2	5.03	0.62	1625
1.2	74.5	212.2	2.84	0.70	1606
1.4	160	127	0.79	1.18	750

As seen from these tables, Cu: SC ratio of 2.84 corresponding to temperature margins of 1.2 K is the most suitable to get high stability margin for all disturbance scenarios. This option was then further investigated for the protection studies.

Also, it is observed that the critical energy in some cases decreases when the Stekly parameter decreases which is contrary to the Stekly criterion. A larger critical energy was found associated with the higher Stekly parameter. This is because the helium volume available to remove joule heating in CICC is not infinite, as assumed in this criterion. Additionally, for disturbances on small lengths like 0.01 m, heat conduction can also play a role which is not considered in the Stekly criterion. This justifies the use of numerical codes like Gandalf rather than the classical analytical tools for designing CICCs with a specified minimum stability margin and for a spectrum of expected disturbance.

7.4 Results of protection studies

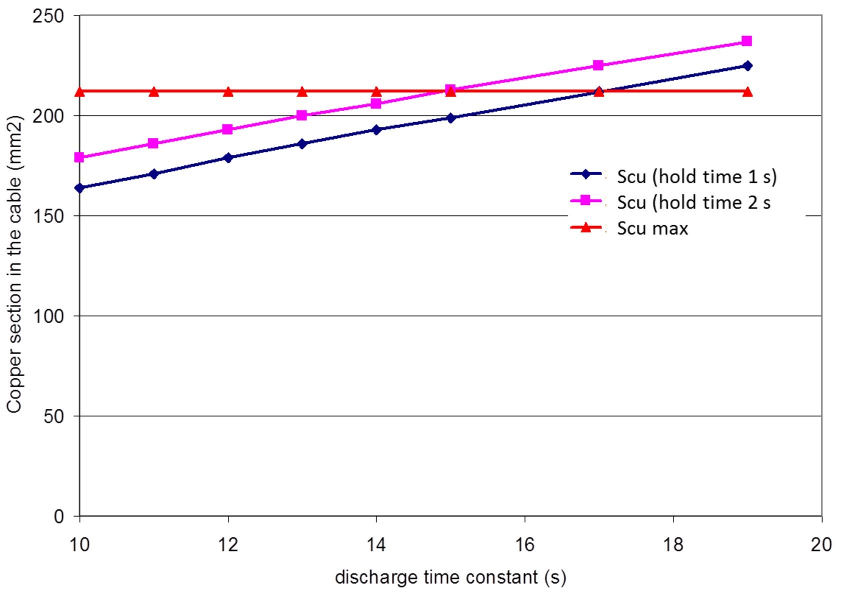

Figure 7.1: Copper section needed for protection as a function of τ_{delay} and τ_{dump}

The copper section (S_{cu}) is a direct function of allowable dump time constant to limit the hotspot temperature below the prescribed limit. For the virtual conductor, with Cu:SC ratio of 2.84, we can find by the classical approach of total adiabaticity, the dump time constant limiting the hotspot temperature to 250 K. Two cases of 1 s and 2 s hold time are considered to see if the copper area is sufficient. The result is shown in figure 7.1. As observed, dump time constant of maximum 15 s is allowed for the case of 2 s hold time (τ_{delay}) to limit the hotspot temperature to less than 250 K.

7.5 Conclusion

The virtual conductor example was used to show the possibility of use of Gandalf code to design CICC for a specific stability margin. The conductor version with the temperature margin of 1.2 K is preferable for higher stability margin. The total copper section is such that a time constant as large as 15 s can be considered for the safety discharge associated with a detection delay of 2 s.

8. Quench detection of SST-1 TF coils by helium flow and pressure measurement

TF magnets of SST-1 are cooled by supercritical helium at 4.5 K and 0.4 MPa. Two types of Venturi meters (VM) are used for measuring helium mass flow rates in these magnets. Signal conditioning for temperature, absolute pressure and differential pressure sensors and a suitable data acquisition system have also been developed for these flow meters. These flow meters were extensively qualified during single-coil test campaigns of SST-1 TF coils. Mass flow and pressure signals behaviour during quench events of TF coil tests were analysed and a quench detection system using these signals has been proposed for TF coils. This secondary quench detection methodology and its hardware development are discussed in this chapter. VM design, fabrication, installation and the flow measurement system are also described in this chapter.

8.1 Cryogenic flow distribution system

SST-1 TF magnets will be cooled by SST-1 cryogenic plant comprising a 1.3 kW at 4.5 K Helium Refrigerator/Liquefier (HRL) system, which is the largest He cryogenic plant in India. The operation features of HRL include controlled cooling down and warming up of the magnet system from 300 K to 4.5 K and vice versa, operation in double-phase mode and supercritical mode, absorption of transients from SST-1 during ramp-up/down of the magnets, plasma operations and handling abnormal events like magnet quench. The cold circulator provides 300 g/s supercritical helium at 4.5K, 0.4 MPa. The Integrated flow distribution and control (IFDC) system, divides this flow in three major hydraulic paths: the TF system, the PF coils and the case cum support structure. A separate path for TF and PF busbar also exists. Its schematic is shown in figure 8.1. An accurate measurement of helium flow is required over a wide range of operating parameters to ensure efficient operation and control of cryogenic plants and to characterize the superconducting magnets [8.1]. Flow measurement of individual sections is done with venturi mass flow meters.

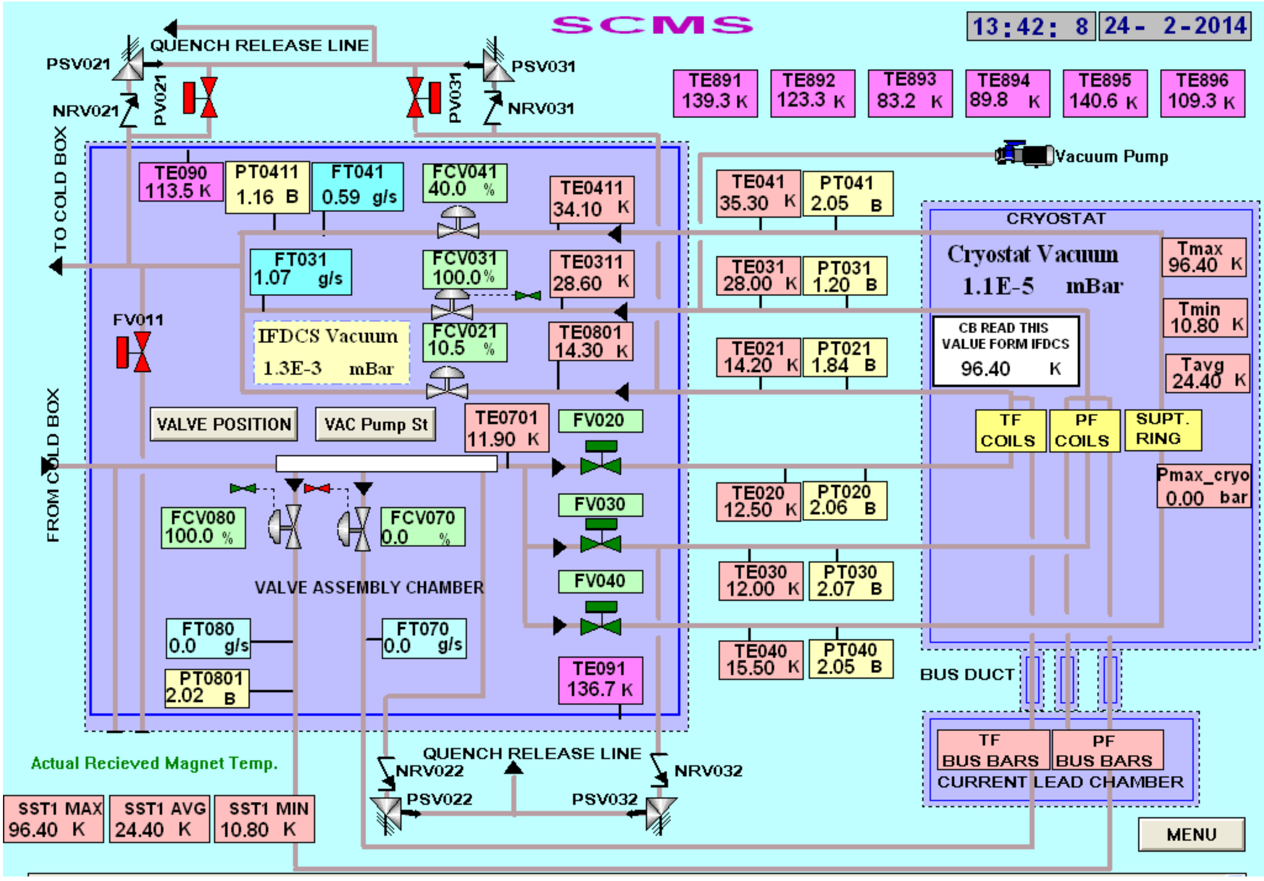

Figure 8.1: Block diagram of IFDC system and its interface with SST-1

8.2 Design of Venturi meters

VM was selected for flow measurement because of its inherently low pressure drop, easy fabrication, high repeatability of measurement and no wear and tear over long-term operation. The supercritical helium mass flow rate design values for individual superconducting magnet of SST-1 Magnet system are given in table 8.1.

Table 8.1: Supercritical helium mass flow rates of SST-1 Magnets

Coil	Number of flow paths, average path lengths	Design mass flow rate in each flow path (g/s)	Total mass flow rate in one coil (g/s)
TF (16 coils)	12 paths, 48 m	1.25	15
PF1 (1 coil)	2 paths, 113 m	0.9	1.8
PF2 (2 coils)	1 path, 113 m	0.9	0.9
PF3 (2 coils)	8 paths, 75 m	1.1	8.8
PF4 (2 coils)	4 paths, 113 m	0.9	3.6
PF5 (2 coils)	4 paths, 130 m	0.8	3.2

VMs are generally designed and manufactured according to the standards ISO-5167. These flow meters rely on the differential pressure measurement through the constricted section and the density estimation at the inlet of the VM with dedicated pressure and temperature measurements. When designing a VM for LHe service, its main dimensions can be derived by scaling down those which are advised by the ISO -5167 standard [8.2].

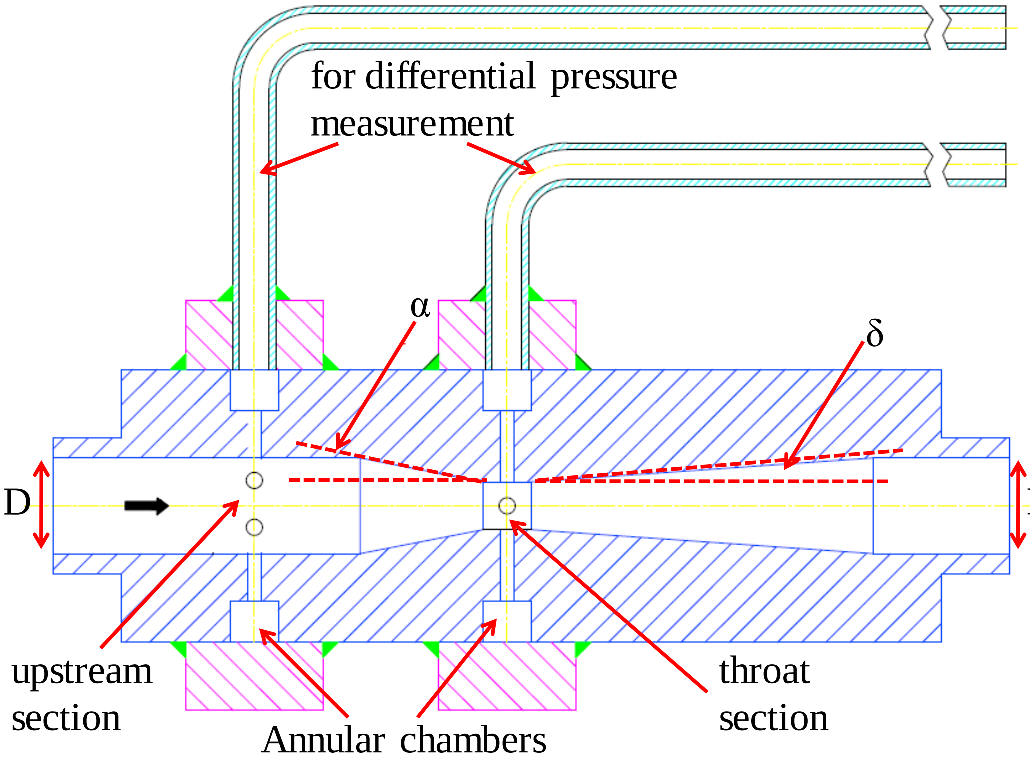

Figure 8.2: typical inner profile of VM

The VM inner profile can be divided into four main parts shown in figure 8.2:

- upstream section: cylindrical, with diameter *D* equal to that of the upstream pipe and length at least equal to *D*
- throat section: cylindrical, with diameter and length equal to *d*
- converging section: conical, connecting the upstream and the throat sections with semi-angle aperture 'α' of (10.5 ± 0.5)°
- diverging section: conical, with initial diameter *d* and final diameter *D*, here the semi-angle aperture δ is (4 ± 0.5) °

Using these guidelines two VMs were designed to meet the wide range of SST-1 flow measurement requirements. One is for TF coil and the other for PF coil flow measurement.

The VMs were designed to give an easily measurable range of differential pressure across its upstream and downstream section [8.3]. The details of both types of VM are given in table 8.2. VMs were fabricated by precision machining of SS304L metal bars. The tapered structures were made by wire cut with a 2-delta finish. After fabrication of these, the dimensions were measured by using custom made dies. Six radial holes were made in the upstream and throat section each. These holes connected to annular chambers with tubing welded for differential pressure measurements as shown in figure 8.2. After final fabrication VMs were ultrasonically cleaned, electro-polished and helium leak-tested with an acceptable leak rate of ≤ 1 x10^{-8} mbar l/s.

Table 8.2: Details of venturi meter construction

Type	Throat diameter, length (mm)	Upstream, Downstream diameter (mm)	Downstream semi-angle (degrees)	Upstream semi-angle (degrees)	Total length (mm)
TF	6	12	10.5	4	120
PF	4	8	10.5	4	90

8.3 Calibration of venturi meter

Mass flow rate through a VM is given by

$$G = C_d A_t \sqrt{\frac{2\rho P_d}{1-\beta^4}} \qquad (8.1)$$

Where:

G = mass flow rate [kg/s]

A_t = throat section area [m^2]

P_d = pressure difference across upstream and throat [Pa]

C_d = discharge coefficient

ρ = fluid density [kg/m^3]

β = throat to upstream diameter ratio

As per equation (8.1), all quantities required for estimating flow rate can be directly measured except C_d which needs to be obtained experimentally by calibration. Both TF and PF VM were calibrated using a standard mass flow meter connected in series with the VM. Using the mass flow rate values from standard mass flow meter and the measured ΔP across the VM, C_d has been estimated for both these flow meters over a range of mass flow rates applicable for SST-1. The discharge coefficient of VM tube with a machined convergent entrance varies slightly with the Reynolds number [8.4]. Since in our case the highest accuracy was desired at low-temperature conditions, constant discharge coefficient equal to 1 was considered for both these VMs. This simplification introduced an inaccuracy of about 3% in the flow measurement. The total accuracy of flow measurement can be calculated by simplified root mean square method after considering additional inaccuracies of differential pressure, absolute pressure and temperature measurement [8.5]. For TF and PF VMs it is estimated to be about 3.18 %.

8.4 **Venturi meter installation on SST-1 Magnets**

Twenty seven VMs are installed on SST-1 magnets namely on the outlet side of each TF magnet, inlet of all 9 PF coils and on 2 CICC busbar inlets of TF magnets. Locations of VM installation were made on the basis of available space inside the SST-1 machine shell. Figure 8.3 shows the schematic of VM installed on TF magnet outlet side. VMs were installed in the system by welding the units into the process piping. In order to ensure that the velocity of the fluid at the VM is primarily axial and swirl free, a straight pipe of 350 mm was kept at the upstream of the VM [8.6]. Stainless steel tubings of 6 mm O.D. and 1 mm thickness were welded into the pressure tap sockets of the VM (not shown). These tubing were extended outside the cryostat through vacuum flanges. The possible heat load from these tubing onto the magnet was estimated to be 6 mW per tube and 12 mW per VM. This was calculated using the integrated thermal conductivity of SS from 4.5 K to 300 K. Each tubing length was minimum 6 m inside the cryostat and was anchored to liquid nitrogen header to reduce the heat load onto the magnets. As VMs were welded after the electrical break the possibility of electrical shootings due to long SS tubing could be avoided.

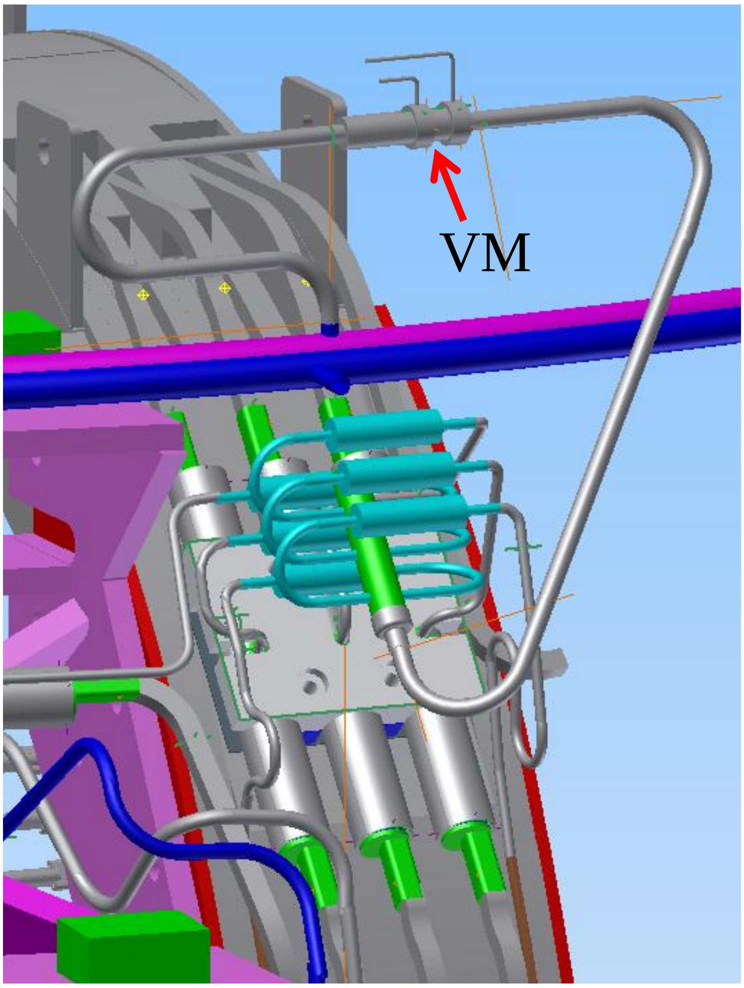

Figure 8.3: TF coil VM installed on the outlet manifold of TF coil

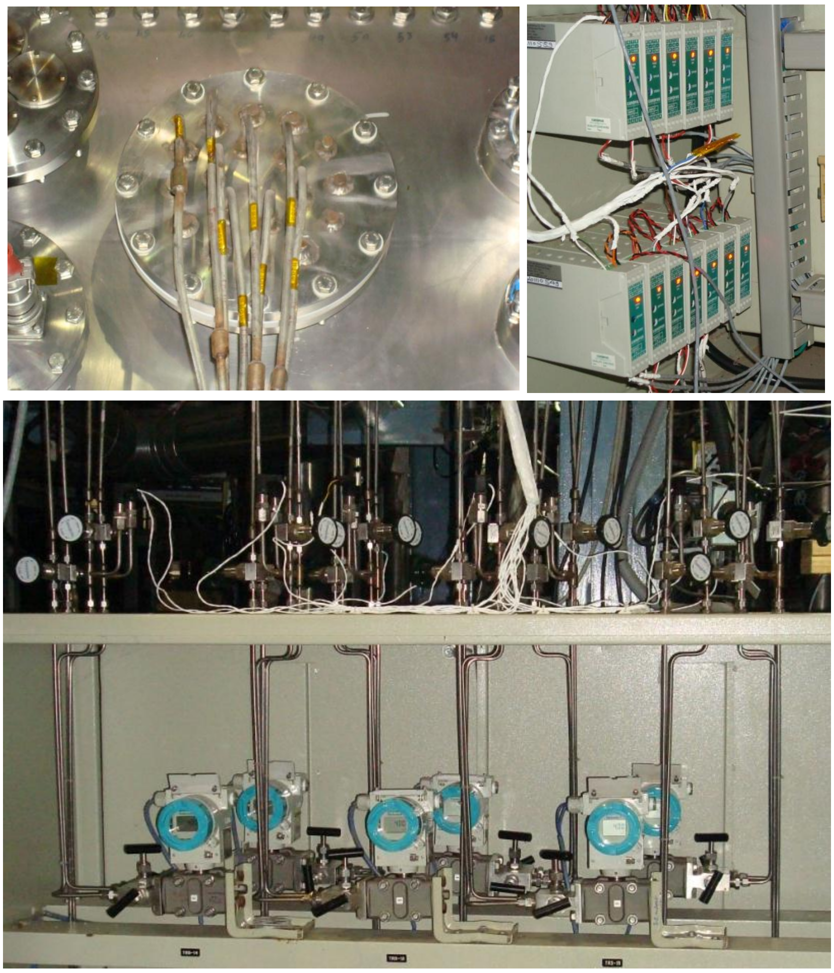

Figure 8.4: Differential pressure tubing of VM welded onto vacuum flange of cryostat (top left), valve fittings before the pressure transducers, current to voltage convertors with isolation for connection of transducer output to VME (top right)

The temperature measurements were available from the temperature sensors already installed on individual coil outlets. Absolute pressure was measured by a Keller PR-21Y transducer and differential pressure was measured using a Siemens 7MF4433 transducer. There was concern about the possibility of helium leak in tubing connections from VM up to these transducers. To take care of this issue, all the connections inside the cryostat from VM to vacuum flanges were welded connections. Outside the cryostat, Swagelok make SS below sealed valves were installed between the cryostat vacuum flange and the transducers. Tubings with high quality surface finish were used to avoid leaks from the Swagelok connectors. In the case of leak or transducer malfunction, online repair could be done by isolating the transducers from the process line by using valves, whenever required.

VME-based data acquisition system was used to acquire signal from all the transducers [8.7]. The 4-20 mA output of pressure transducers was electrically isolated and converted to 1–5 V before connection to the VME. Mass flow rate was calculated using the relevant sensor data and helium property database for density estimations.

These flow meters have been extensively used to measure the helium mass flow rates at operating conditions, during several SST-1 campaigns, single TF coil test experiments and lab scale experiments [4.4][8.8]. Several component of these flow meters installation set-ups are shown in figure 8.4. Mass flow rate measured using different VMs at different temperatures during the SST-1 cool down is shown in figure 8.5.

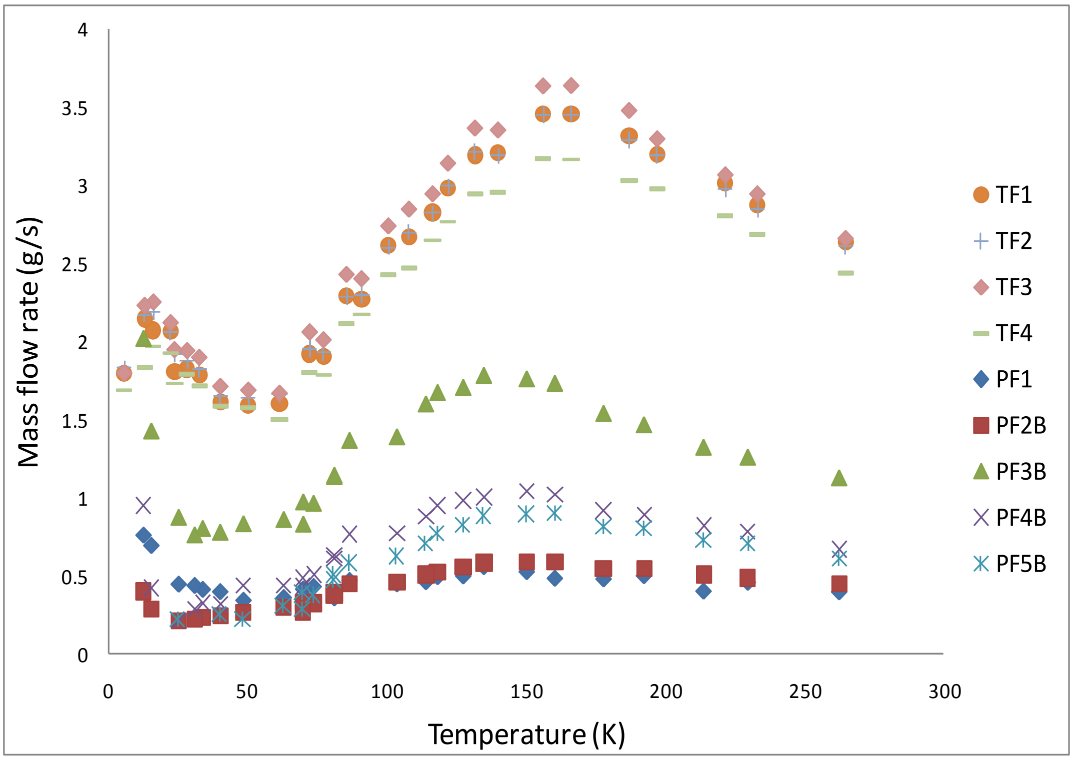

Fig. 8.5 Mass flow rate during cool down of SST-1 magnets

8.5 Quench detection methods

Superconducting magnets operating in high magnetic field, with high current density and limited operational stability margins, like that of tokamaks or stellarators, always have finite probability of getting quenched during operations. Quench is an off normal event, wherein a resistive zone (also called normal zone) develops along a superconducting conductor. The joule heating of the initial resistive zone heats the additional conductor lengths, as well as the coolant being the vector of further propagation of normal zone. If protection actions are not taken in time, extensive damages like conductor melting, arcing, coolant pressure increase and expulsion etc. can occur and damage the magnet system beyond repairs. Therefore quench must be detected at the earliest possible to insert external resistors in the circuit and dump the magnetic energy into this resistor and protect the magnet from thermal damage. So reliable quench detection and protection aspects must be incorporated in the design of every superconducting magnet system.

Voltage measurement is one of the fastest and widely used methods of quench detection [3.4]. In this method, voltages across different identical sections of magnets are compared. When a section of magnet is quenched, it develops additional voltage and when it crosses a certain threshold voltage level and stays above this level for a certain threshold time, a quench trigger is generated by quench detection hardware and magnet energy extraction process is initiated. This method has also been successfully implemented for SST-1 TF coils [4.5, 4.6].

Quench can also be detected by monitoring non-electrical signals from like mass flow rate and pressure [8.9 - 8.11]. Any significant change in the steady-state operational values of these signals can indicate a fault condition like quench inside the magnet. These are inherently slow signals and are expected to give slow response to the quench process, but can be used as a secondary quench detector. This redundancy could be very useful in case of major malfunction or failure of the primary quench detector. Following this philosophy, a hydraulic signal-based secondary quench detection system has been proposed for SST-1 TF magnet.

8.6 **Hydraulic quench detection**

A quench detection method has been proposed based on monitoring the changes in nominal flow and pressure values rather than crossing above or below a certain value and based on the venturi meters described in the preceding section. This has been done to accommodate for measurement uncertainty in mass flow and pressure signals and to avoid requirement of flow path dependent threshold settings. Also drawing analogy from voltage measurement-based quench detection methods, thresholds for time and levels are proposed after review of coil test data.

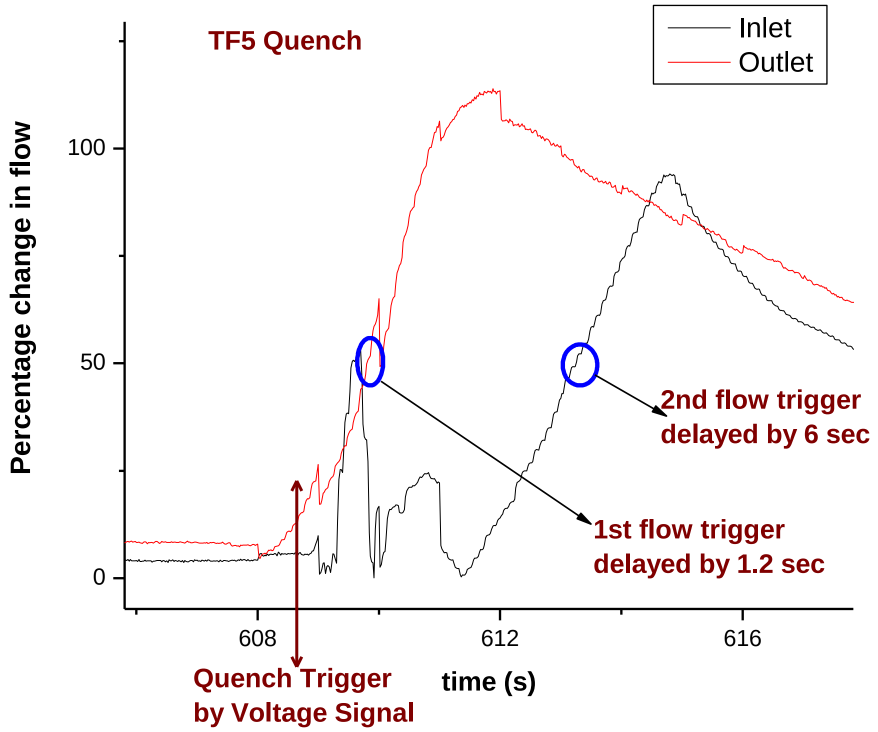

Figure 8.6: mass flow change during TF5 coil quench

It is proposed that if mass flow/pressure data register more than 50 % change in its nominal value (similar to threshold voltage) and if this change continues for more than 500 ms (threshold time) quench trigger will be generated.

The TF5 flow data trends during quench are shown in figure 8.6. The difference between the time taken for reaching flow/pressure thresholds and for reaching the voltage-based quench detection threshold are shown as delay. As seen for TF5, the mass flow change at outlet crossed the threshold with a delay of 1.2 s and at inlet with a delay of 6 s. For TF2 coil as seen from figure 8.7, the mass flow change at outlet crossed the threshold without any delay and at inlet with a delay of 5 s. The study of signal from other coils revealed that always at least one of the inlet or outlet mass flow rate always crossed the threshold with delay less than 2 s.

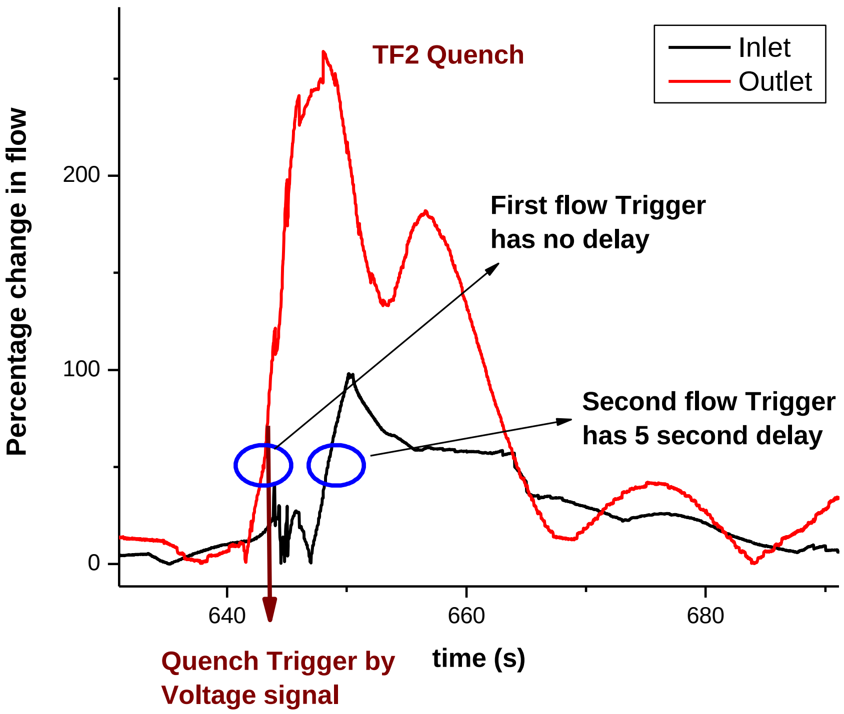

Fig. 8.7 mass flow change during TF5 coil quench

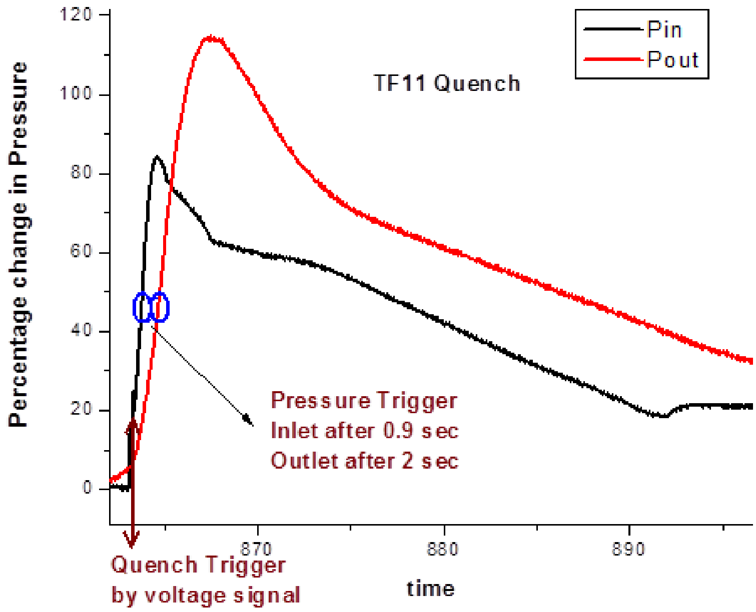

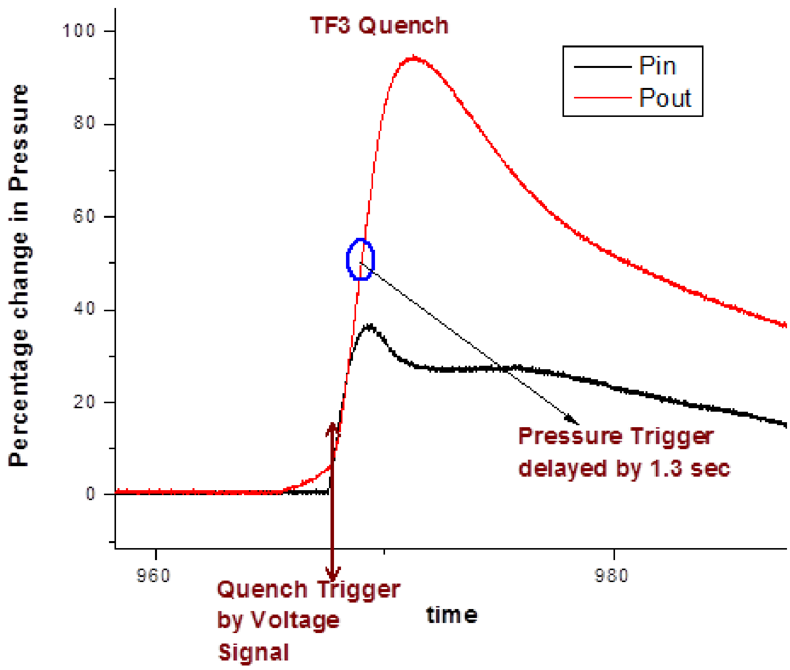

Figure 8.8: Pressure changes during TF11 and TF3 coil quench

Similarly the pressure data trend for all quench cases has been studied. Fig. 8.8 shows the pressure trends for coil TF11 and TF3 at coil inlet and outlet with delay times with respect to voltage based quench detection. As observed, the minimum delay time for reaching the pressure threshold is 1.3 s. The study of pressure signals from other coils revealed that always at least one of the inlet or outlet mass flow rate always crossed the threshold with a delay of less than 2 s.

These observations of flow and pressure signals have confirmed that use of hydraulic-based quench detection system for SST-1 TF magnet system is feasible. As in SST-1 tokamak the quench-induced flow and pressure changes will be higher than in single coil test, due to higher joule heating. The peak magnetic field on TF conductor is 5.1 T as compared to peak field of 2.2 T in coil test environment, giving rise to higher magneto-resistance of copper stabilizer resulting in higher joule heating.

Thermo-hydraulic simulation of TF magnet is SST-1 tokamak assembly was done to simulate the possible effects of failure of voltage-based quench detection system and quench detection by hydraulic means with a delay of 3 s. This time was conservatively chosen higher than the maximum delay of either flow or pressure-based first triggers observed in TF coil test campaigns. Gandalf was used for these simulations. The input parameters for Gandalf such as mass flow rate, pressure, temperature, operating current and background magnetic field etc., were obtained from SST-1 TF magnet system nominal operating values. SST-1 CICC specifications, friction factor and heat transfer correlations and the hydraulic model used in the code are similar to that used earlier in chapters. This simulation was done to estimate the maximum hotspot temperature and maximum pressure rise observed if quench detection is delayed by 3 s. The results are shown in figure 8.9 and 8.10. As seen the peak temperature reached within the conductor length is about 178 K and the peak pressure is 9.5 bar. This is still within the safe limits of SST-1 CICC design.

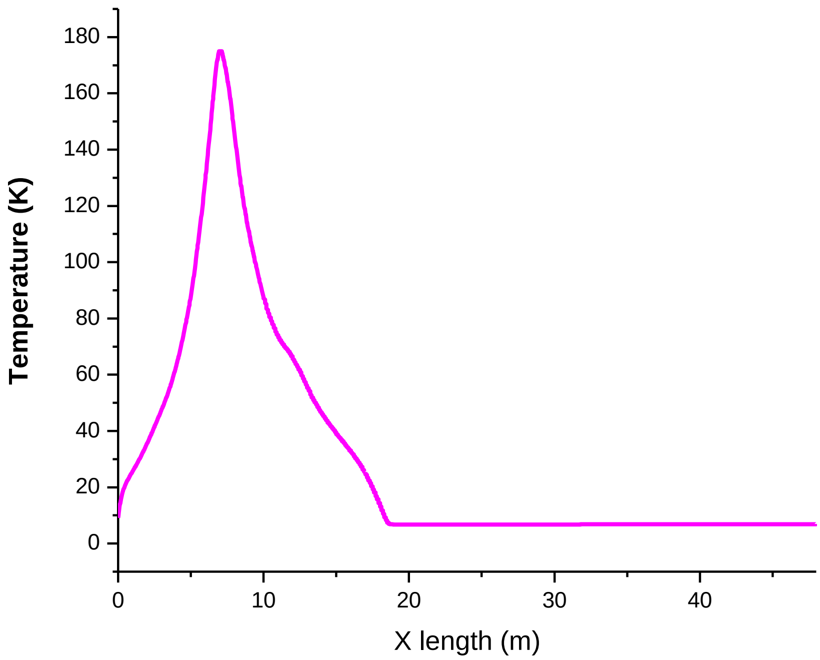

Figure 8.9: Temperature rise from Gandalf simulation in case of delayed quench detection

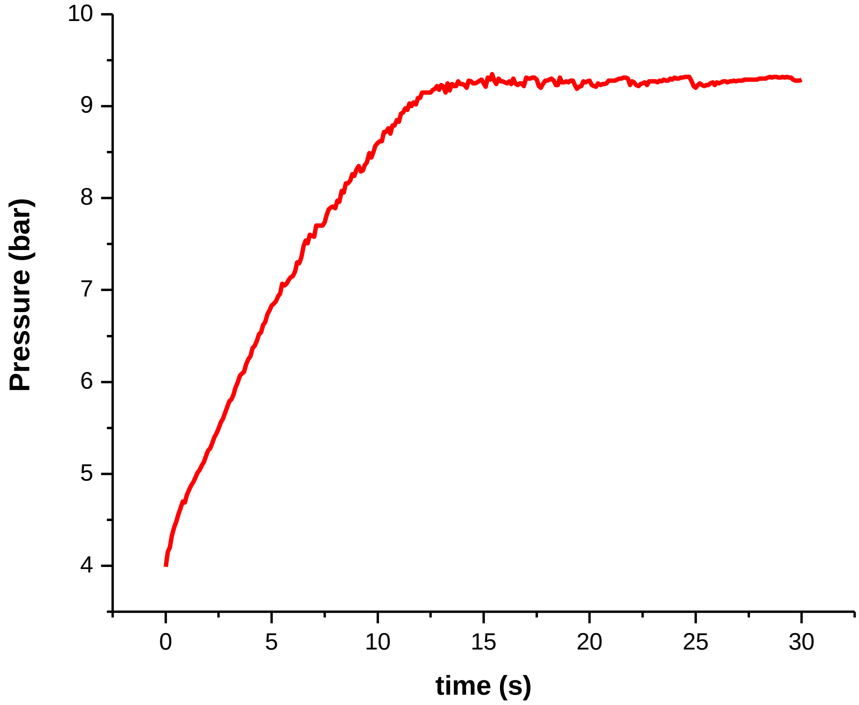

Figure 8.10: Pressure rise at the hotspot from Gandalf simulation

8.7 Proposal for quench detection hardware

A quench detection hardware schematic is also proposed for flow-based secondary quench detection system. It is shown in figure 8.11. As shown the voltage value corresponding to the actual flow during operation in TF1 coil to TF16 coils is taken from corresponding differential pressure transmitters (DPT) of venturi flow meter installed at outlet. These are compared with the voltage reference value corresponding to the nominal operating flow of 16 g/s. The window comparator continuously compares these two voltages. In normal operational scenarios of no quench, the difference between DPT and the voltage reference will be zero or some small values due to possible flow variation between coils from the nominal 15 g/s.

The window comparator output will become high (+5 V) from low (0 V) if the difference becomes higher than the voltage corresponding to 24 g/s or lower than the voltage corresponding to 8 g/s. This high signal will be transmitted to OR circuit only if it remains high for more than the delay time of 500 ms. After this, the ORing circuit will generate a quench trigger. Similar circuits can also be implemented for pressure-based quench detection.

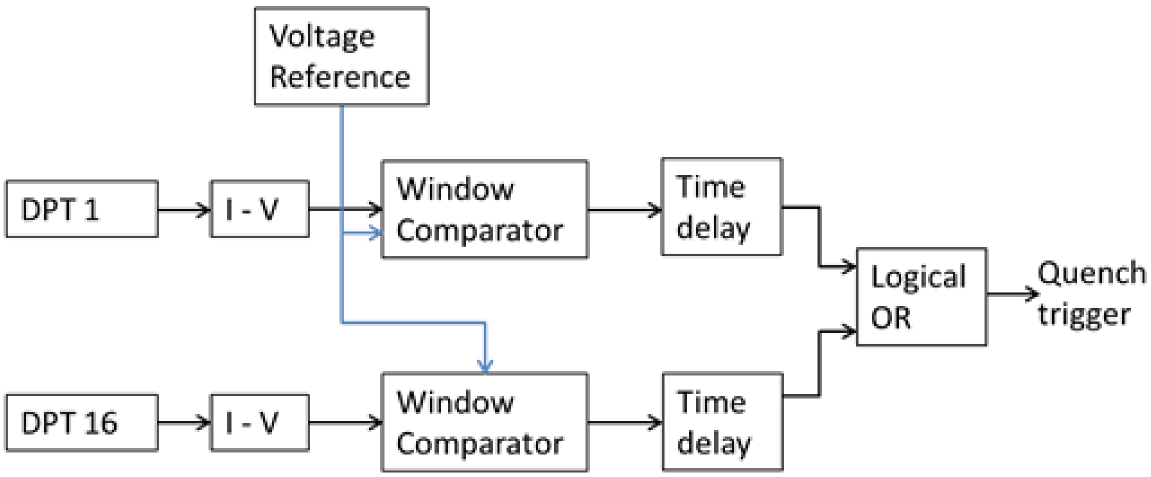

Figure 8.11: Schematic of flow based quench detection hardware

8.8 Conclusion

Venturi meter-based flow measurement system has been designed and developed for SST-1 magnet system. This system has been successfully used for helium flow measurement during the TF coil test experiments and on the assembled TF magnet system during engineering commissioning and plasma experiment phase of SST-1. A secondary quench detection system based on flow and pressure measurement has been conceptualized for the SST-1 TF magnet system. The flow and pressure trends during quenches observed in single coil test experiments have been used to quantify the quench detection system logic. A schematic is also proposed for development of suitable hardware for this secondary quench detection system. Work is reported in [8.12].

9. Summary and future scope of work

9.1 Summary

Analytical model of SST-1 CICC for estimation of hotspot temperature was developed assuming complete adiabatic conditions during quench development. This model was used to design the quench protection system of the SST-1 TF magnet system. The dump resistor was selected to limit the temperature to less than 115 K and voltage to less than 1 kV. This method is found to be very useful for quick first order estimation of maximum temperature in CICC after quench initiation and current dumping.

A simple direct difference algorithm was selected to cancel inductively-coupled voltages on the coils for accurate quench voltage measurement on TF coils. State-of-the-art, fail safe quench detection cards were developed using this algorithm. Its main features are precise and tuneable voltage and time thresholds, and inbuilt complete redundancy. These cards were successfully tested in several TF coil test campaigns and during the TF magnet system engineering validations and SST-1 plasma experiments. No failure leading to undetected quench has been observed with these cards. The card architecture was kept flexible to allow its use for quench detection of busbar and current leads. These cards will also be also used for PF magnet quench detection.

SST-1 Toroidal Field coils were individually cold-tested in a dedicated campaign spanning from June 10, 2010 till January 24, 2011. The electromagnetic, thermal hydraulic and mechanical performances of each TF magnet was qualified at its nominal operating current of 10000 A in either two-phase or supercritical helium cooling conditions. During the current charging experiments, few quenches were observed in some of the TF magnets.

A commercially available 1-D Gandalf code is a popular code to study the quench characteristics of CICC-based magnets. This code was adapted to correctly represent SST-1 CICC. Friction factor is an important input parameter in simulation of quench of CICCs. It is different for each CICC. An experiment was done using pressurized water to determine SST-1 CICC friction factor as a function of pressure drop. Holman correlation was used to model the steady-state heat transfer coefficient. This correlation which has direct dependence on friction factor was adapted in the code subroutine. Critical current density as a function of magnetic field was also implemented in the code so as to accurately reproduce experimental results from the SST-1 CICC test.

A variety of possible hydraulic models were studied. Results of these different models were studied and a suitable model was proposed and implemented in the code to generate accurate flow conditions as observed during coil test.

Magnetic field on individual DPs was calculated using MAC code. The spatial variation of magnetic field was implemented in the subroutine of Gandalf for use in quench simulation.

Detailed convergence study was done to gain the confidence in the numerical solutions of quench studies, which is a complex and highly non-linear problem. The minimum required time and space discretization steps were determined such that the results were then not changed by the further refinement of these parameters. Suitable time steps and mesh sizes were then used in the quench simulation.

The quench observed in TF coil #15 at 8960 A current was simulated using this code and the developed subroutines. The simulated temperature rise and the quench propagation were found to be in good agreement with the experimental data.

Observation of flow increase at inlet, following quench, was reported from the TF coil test experimental observation. This was investigated and found to be linked with the dynamic behaviour of the cryogenic plant.

The CICC model and subroutines developed for TF coil #15 were also used for predictive quench simulation of the SST-1 TF magnet system.

During the coil test campaigns, TF magnets were connected to a pair of conventional vapour-cooled current leads through a pair of CICC busbars of about 1.8 m length inside the test cryostat. Quench observed in the busbar section was experimentally found to have a very low propagation velocity of 0.34 – 0.4 m/s, as compared to about 5 m/s observed in double pancake windings of TF magnets. This slow propagating quench was analysed and simulated successfully using Gandalf. These fundamentally different quench propagation characteristics were attributed to the lower background magnetic field on the busbar and the absence of transverse thermal conduction in the busbar which exists in double pancake windings. Recommendation for low threshold voltage of 52 mV was made for busbar quench detection. The rearrangement of voltage taps was also proposed for busbar quench detection.

Heat loads were estimated for TF magnet system busbar in the SST-1 tokamak. Steady-state thermo-hydraulic analyses of the busbars were carried out to find the optimum helium mass flow rate and for the required operational temperature margin of more than 1.5 K during SST-1 tokamak operations. A mass flow rate of 1 g/s is found to be sufficient to compensate the estimated heat load and to give a temperature margin of 1.9 K, which ensured safe and cryo-stable operation of the SST-1 TF magnets.

The virtual conductor example was used to show the possibility of use of Gandalf code to design CICC. The stability of this conductor was studied for the disturbance of 100 ms on 1 m, 10 ms on 1 m and 1 ms on 10 mm as these represent the typical disturbance related to plasma disruption, AC losses and wire movements in tokamak magnets. The conductor version with the Cu: SC ratio of 2.84 was found to be preferable with higher stability margin for all three disturbances. Using the classical adiabatic approach of hotspot temperature it was found that for this Cu: SC ratio, maximum dump time constant of 15 s is allowed with a detection delay of 2s.

Venturi meter-based flow measurement system was designed and developed for SST-1 magnet system. This system was successfully used for helium flow measurement during the TF coil test experiments and on the assembled TF magnet system during engineering commissioning and plasma experiment phase of SST-1. A secondary quench detection system based on flow and pressure measurement was conceptualized for SST-1 TF magnet system. The flow and pressure trends during quenches observed in single-coil test experiments were used to quantify thresholds limits for this secondary quench detector system. A schematic was also proposed for development of suitable hardware for this secondary quench detection system.

These works have led to successful development of quench detection and protection system of the first superconducting tokamak of India, SST-1. The quench simulation results were found to be in good agreement with the experimental observations.

9.2 **Future Scope of work**

The quench detection circuits developed as a part of this work, could be utilized to develop advanced noise-cancellation schemes to cancel out inductively-coupled voltages. For example, the voltages after the isolation and filter stages of the quench detection card could be acquired in fast DAQ system and noise cancellation schemes could be implemented in software program. This will make this system more versatile, allowing flexibility in cancellation logics, channels to be compared and in selection of the threshold limits.

These quench detection circuits can also be used to test the use of co-wound tapes for quench detection of future magnets of IPR.

The quench simulation models developed could be extended and modified to study quench behaviour of the proposed Nb3Sn based central solenoid of SST-1 tokamak. This will be useful, as the future fusion reactor magnets in India are expected to be made with Nb3Sn conductors.

With the generation of additional experimental data from the hydraulic-based quench detectors, its suitability for use with fast current changing magnets like PF coils and central solenoid could be verified. This technique, along with voltage-based quench detection technique, can ensure more reliable quench detection of these magnets.

10. References

[1.1] www.iter.org

[1.2] D. Maisonnier, “DEMO and fusion power plant conceptual studies in Europe”, Fusion Engineering and Design Volume 81, Issues 8–14, February 2006, Pages 1123–1130

[1.3] Weston Stacey, “Fusion”, WILEY VCH, Verlag GmbH & Co. KGaA, Weinheim, 2010

[1.4] WESSON J., "Tokamaks", Oxford University Press, USA; 4 edition (August 1, 2011)

[1.5] P.N. Haubenreich et al., “Superconducting magnets for fusion”, Nuclear fusion, Vol 22, No. 9, (1982), 1209-1236

[1.6] SERIO L., “Challenges for cryogenics at ITER”, Advance in Cryogenic Engineering, 45, 2010, page 651

[1.7] B. Seeber, “Handbook of Applied Superconductivity”, IOP publishing limited, Bristol and Philadelphia, 1998

[2.1] S. Pradhan et al. “Status of SST-1 refurbishment”, J. Fusion Res. Series, vol. 9, pp. 650–657, 2010

[2.2] S. Pradhan et al. “Superconducting Magnets of SST-1 Tokamak”, 20th IAEA Fusion Energy Conference (2004), FT3-4Rb

[2.3] S. Pradhan et al. “Superconducting cable-in-conduit-conductor for SST-1 magnets”, in Proc. 2nd IAEA TCM on Steady-state Operation of fusion devices, Fukuoka, Japan, 1999, vol. II, p. 482.

[2.4] S. Pradhan et al. “SST-1 poloidal field magnets”, in Proc. 17th IEEE/ NPSS Symposium on Fusion Eng., San Diego, CA, USA, 1997, pp. 665–668.

[2.5] V. L. Tanna et al. "Recent progress and development of cryogenics system towards Refurbishment of SST-1", Indian J. Cryogenics, vol. 38, no. 1–4, pp. 87–92, Jan. 2013.

[2.6] Sarkar B et al. "1 KW class Helium Refrigerator/Liquefier system for SST-1", ICEC-18, Narosa Publication, New Delhi, pp. 123-126, 2000

[2.7] Z. Khan et al. "Vacuum system of SST-1 Tokamak", Fusion Eng. Design, vol. 88, no. 6–8, pp. 692–695

[2.8] S. Jacob et al. "Plasma facing component design for steady-state tokamak SST-1", Journal of Nuclear Materials, 233–237 (1996), pp. 655–659

[2.9] D. Bora and SST-1 Team "Test results on systems developed for SST-1 Tokamak", Nuclear Fusion, 43 (2003) 1748.

[2.10] S. Pradhan et al. "SST-1 Status and Plans", IEEE Trans. Plasma Science, 40 (2012), pp. 614–621

[3.1] "Performance of Cable-in-Conduit-Conductors for SST-1 at IPR", Hitachi cable review, 2001, No.20, 101

[3.2] L. Dresner, "The growth of normal zones in cable-in-conduit superconductors", Proceedings 10th symposium on fusion engineering, Philadelphia, PA, 1983, 2040-2043

[3.3] M. N. Wilson, "Superconducting Magnets", Oxford Science Publication, 2002

[3.4] Y. Iwasa, "Case studies in superconducting magnets: design and operational issues", Springer 2009

[3.5] B. J. Maddock et al., "Protection and stabilisation of large superconducting coils", Proceeding IEE Control & Science, 115 (4) 1968, 543

[3.6] A.N. Sharma et al., “Quench detection and Protection system for superconducting magnet of SST-1 tokamak”, in 4th IAEA TCM on Steady-state Operation of magnetic Fusion Devices, Feb 1-5, 2005, Ahmedabad, India

[4.1] M. Coatanea et.al “Quench Detection in the ITER Magnet System”, IEEE Trans. on Applied Superconductivity, vol.20, no.3, pp.427-430, June 2010

[4.2] Y Chu, et al., "Quench detection based on voltage measurement for the KSTAR superconducting coils", IEEE Trans. on Appl. Superconductivity 20, (2008) 1568

[4.3] J.L. Duchateau et al., “Quench detection in ITER superconducting magnet systems”, Fusion Science and Technology, Vol 64, No. 4, Nov 2013, 705-710

[4.4] R.G. Benson, et al., “Quench circuit for electronic instruments used with superconducting magnets”, Cryogenics 26 (1986) 482–483

[4.5] L. Bottura, “Quench 101”, Workshop on Accelerator Magnets, Superconductors, Design and Optimization WAMSDO 2013, January 15th-16th, 2013

[4.6] Chaplin, M.R.et.al., “Quench detection & instrumentation for the Tokamak Physics Experiment magnets”, Fusion Engineering, 1993., 15th IEEE/NPSS Symposium on , vol.2, pp. 802-805, 11-15 Oct 1993

[4.7] A.N. Sharma, et al., “Quench detection and data acquisition system for SST-1 superconducting magnets”, Fusion Engineering and Design 74 (November (1–4)) (2005) 819–823

[4.8] A. N. Sharma, et al., “Cryogenic Acceptance Tests of SST-1 Superconducting Coils”, IEEE Trans. on Applied Superconductivity, 04/2015, 25(2), 420010

[4.9] Y. Khristi, A.N. Sharma, et al., “Quench Detection System for TF Coil-Test Campaigns of SST-1”, IEEE Trans. on Applied superconductivity 22, (April (2)) (2012) 4200108.

[4.10] Y. Khristi, A.N. Sharma et al., “Design and implementation of quench detection instrumentation for TF magnet system of SST-1”, Fusion Engineering and Design 89 (2014) 623–627

[4.11] Pradhan, S., "SST-1 Toroidal Field Magnet Tests: Some Results and Lessons Learnt", IEEE Transactions on Applied Superconductivity, vol.22, no.3, 9501804, June 2012

[5.1] L. Bottura, “A Numerical Model for the Simulation of Quench in the ITER Magnets”, J. Comp. Phys., Volume 125, (1996) 26-41

[5.2] Gandalf user manual, version 2.1

[5.3] H. Katheder, “Optimum thermo-hydraulic operation regime for cable-in-conduit superconductors (CICS)”, Cryogenics, 1994, 34, 595–598

[5.4] ITER Final Design Report 2001: DRG1 Annex ‘Magnet Superconducting and Electrical Design Criteria’, IAEA, Vienna, 2001.

[5.5] P. Bruzzone, “Pressure drop and helium inlet in ITER CS1 conductor”, Fusion Engineering and Design, 2001, 58–59, 211–215

[5.6] F. W. Dittus et al., “Heat Transfer in Automobile Radiators of the Tubular Type”, Publications in Engineering, University of California, Berkeley 1930, Vol. 2, p. 443

[5.7] P. J. Giarratano et al., “Forced convection heat transfer to supercritical helium”, Cryogenics 11, 385-393

[5.8] J. Holman “Heat transfer”, Ninth edition, McGraw Higher Education, International edition

[5.9] L. Bottura, “A Practical Fit for the Critical Surface of NbTi”, IEEE Transactions on Applied Superconductivity, 2010, 10 (1), 1054

[5.10] L. Bottura, “Analytical Calculation of Magnetic Field in an Isoparametric Brick”, CryoSoft Internal Note CRYO-97-2, 1997

[5.11] L. Bottura, “Criteria for the numerical convergence of quench simulations in CICC’s”, Cryogenics, 2006, 46(7–8), 556–562

[5.12] D. Patel et al., “Thermal anchoring of wires in large scale superconducting coil test experiment”, Fusion Engineering and Design 2013, 88 (5), 374–379.

[5.13] K. Doshi et al., “Precision signal conditioning electronics for cryogenic temperature and magnetic field measurements in SST-1”, IEEE Transactions on Plasma Science, 2012, 40, 641–645

[5.14] P. Varmora et al., “PXI based data acquisition system for SST-1 TF test program”, Indian Journal of Cryogenics 2013, 38, 104– 109.

[5.15] M. Sugimoto et al., “An evaluation of the inlet flow reduction for a cable-in-conduit conductor in pulsed operation”, Cryogenics, 1998, 10, 989–994

[5.16] M. Sugimoto et al., “Test results of the DPC-TJ: thermal and hydraulic performance”, Cryogenics1993, 33(6), 597–602.

[5.17] S. Nicollet et al., “Thermal-hydraulic behaviour of the ITER TF system during a quench development”, Fusion Engineering and Design, 2011 86 (6–8), 1497–1500

[5.18] A.N. Sharma et al., “Thermo-hydraulic and quench propagation characteristics of SST-1 TF coil”, Fusion Engineering and Design, Volume 89, Issue 2, (2014) 115–121

[6.1] HESS code, “a computer program for steady-state analysis of helium cooled conductors”, L. Bottura and NET team, NET/IN/87-62, 1987

[6.2] M.S. Lubell, “Empirical Scaling Formulas for Critical Current and Critical Field for commercial NbTi”, IEEE Transactions on Magnetics, 1983, 19, 754

[6.3] A. N. Sharma et al., “Quench characterization and thermo-hydraulic analysis of SST-1 TF Magnet Busbar”, accepted for publication in Fusion Engineering & Design (2014)

[7.1] M. Ghate et al., “Design, development and fabrication of indigenous 30 kA NbTi CICC for fusion relevant superconducting magnet”, Cryogenics, Vol. 63, 166–173

[7.2] J. Huawei et al., “Optimization model of a structural simulation design for a CICC”, Chinese science bulletin, 2011, 56(27) 2978 – 2983

[7.3] H.W. Jiang, “Optimization Design Model of a CICC Based on Energy Margin”, IEEE Transactions on Applied Superconductivity 24(1), 4800105

[7.4] J. L. Duchateau, “New considerations about stability margins of NbTi cable in conduit conductors”, IEEE Transactions on Applied Superconductivity, 2009, 19(2), 55 - 62

[7.5] Z. J. J. Stekly and J. L. Zar, “Stable superconducting coils”, IEEE trans. on nuclear science NS-12, 367-72

[8.1] S. Das et al., “Supercritical helium flow requirement and cooling scheme for SST-1 SCMS”, Proceedings ICEC 18, Mumbai, 2000 pp 443-446

[8.2] A. Rivetti et al., “LHe Venturi Flowmeters: Practical Design Criteria and Calibration Method”, Cryogenics 1994, Vol, 34, 449-452

[8.3] G. Bansal et al. “Design of venturi flow meter for sst-1 superconducting magnets”, 17th National symposium on Cryogenics, Nagpur, India, 19 – 21 February 1999

[8.4] H. Katheder and M. Susser, “Discharge coefficient of a classical venturi tube for measuring liquid helium flow”, Cryogenics, 1989 Vol 29, 1067-1069

[8.5] R. W. Miller, “Flow Measurement Engineering Handbook”, McGraw-Hill, New York, 1983, Chapter 9

[8.6] L. R. Baylor, “Helium mass flow measurement in the international fusion superconducting magnet test facility”, ORNL/TM-9992

[8.7] K. Doshi et al. “A Large Channel Count Multi Client Data Acquisition System for Superconducting Magnet System of SST-1”, Proceedings of the 9th International Workshop on Personal Computers and Particle Accelerator Controls, ISBN 978-3-95450-124-3, p.p.26-28

[8.8] S. Kedia et al. “Effect of Temperature on Hydraulic Parameters of Cable-In-Conduit-Conductor of SST-1”, Journal of Superconductivity Novel Magnetism (2013) 26:1289–1296

[8.9] L. Dresner, “Quench Detection by Fluid Dynamic Means in Cable-In-Conduit Superconductors”, Volume 33 1988, Advances in Cryogenic Engineering, Pages 167-174

[8.10] S. Nicollet et al., “Thermal behaviour and quench of the ITER TF system during a fast discharge and possibility of a secondary quench detection”, IEEE Transactions on Applied Superconductivity, 2012, 22(3) 4704304

[8.11] S. Nicollet et al., “Secondary thermos-hydraulic quench detection for the ITER Correction Coils”, IEEE Transactions on Applied Superconductivity, 2013, 23(3), 4201004

[8.12] A. N. Sharma et al., “Quench detection of SST-1 TF coils by helium flow and pressure measurement”, accepted for publication in Journal of fusion energy (2014)